Technische Universität München
Fakultät für Medizin

Signalling and metabolic requirements in early pancreatic carcinogenesis

Thorsten Stefan Neuß

Vollständiger Abdruck der von der Fakultät für Medizin der Technischen Universität München zur Erlangung eines

Doktors der Naturwissenschaften (Dr. rer. nat.)

genehmigten Dissertation.

Vorsitz: Prof Dr. Maximilian Reichert

Prüfer*innen der Dissertation:

1. Prof. Dr Roland M. Schmid
2. Prof. Angelika Schnieke, Ph.D.

Die Dissertation wurde am 21.11.2022 bei der Technischen Universität München eingereicht und durch die Fakultät für Medizin am 21.03.2023 angenommen.

Parts of this thesis have been presented at the following conference:

Cancer and Metabolism 2022, London, UK:
T Neuß, N Wirges, W Schmitz, M-C Chen, S Usluer, R Oellinger, S Lier, M Dudek, P Knolle, R Rad, M Jastroch, T Madl, K Steiger, R M Schmid, H Einwächter; *Metabolic reprogramming is required for acinar to ductal metaplasia in the pancreas*

Parts of the thesis have been published as pre-print on BioRxiv:

T Neuß, N Wirges, M-C Chen, S Usluer, R Oellinger, S Lier, M Dudek, T Madl, M Jastroch, K Steiger, W Schmitz, H Einwächter, R M Schmid; *Acinar-ductal metaplasia in the pancreas requires a glycolytic switch and functional mitochondria* [1]

Contents

List of Abbreviations

2-DG	2-desoxyglucose
3-PHP	3-phosphohydroxypyruvate
3-PG	3-phosphoglycerate
Abs	absorbance
ACC	acetyl-CoA carboxylase
ACC	acinar cell carcinoma
ADM	acinar to ductal metaplasia
AKT	protein kinase B
AMPK	AMP-activated protein kinase
AMY2A	amylase 2a
AP	acute pancreatitis
BPE	bovine pituitary gland extract
Braf	v-raf murine sarcoma viral oncogene homolog B
Brca2	breast cancer type 2 susceptibility protein
BrdU	5-bromo-2-deoxyuridine
BSA	bovine serum albumin
CCK	cholecystakinin
CCK1R	cholecystakinin-1 receptor
CCCP	carbonyl cyanide m-chlorophenylhydrazone
CDKN2a	cyclin dependent kinase inhibitor 2A
CD	cluster of differentiation
CDK4/6	cyclin dependent kinase 4/6
CP	chronic pancreatitis
CPA	carboxypeptidase A
CPB	carboxypeptidase B
c-MYC	myc proto-oncogene
DAPI	4’,6-diamidino-2-phenylindole
DHIDH	mitochondrial dihydroorotate dehydrogenase
DMSO	dimethyl sulfoxide
DNA	deoxyribonucleic acid
ER	endoplasmatic reticulum
EGF	epithelial growth factor
EGFR	epithelial growth factor receptor

ERK	mitogen-activated protein kinase 1
ERRB	erb-b2 receptor tyrosine kinase 2
FCS	fetal calf serum
FFPE	formalin-fixed, paraffin-embedded tissue blocks
FOXO1	forkhead box O1
GDP	guanosine diphosphate
GLS	glutaminase
GLUT1	glucose transporter 1
GSK3β	glycogen synthase kinase 3 β
GTP	guanosine triphosphate
H&E	hemalaun-eosin
HEPES	4-(2-hydroxyethyl)-1-piperazineethanesulfonic acid
HIF1α	hypoxia induced factor 1 α
HRP	horse radish peroxidase
HSP90	heatshock protein 90
IgG	imunoglobulin G
IκBα	inhibitor of NFκBα
IKK	inhibitor of nuclear factor κB kinase subunit β
IL	interleukin
IPMN	intraductal mucinous neoplasm
JNK	mitogen-activated protein kinase 8
KI67	marker of proliferation Ki-67
KLF5	krüppel-like factor 5
KRAS	kirsten rat sarcoma
KRT19	cytokeratine 19
LC-MS	liquid chromatography–mass spectrometry
LDHA	lactate dehydrogenase A
MAPK	mitogen activated protein kinase
MCN	muscinous cystic neoplasia
MEK	mitogen-activated protein kinase kinase
MIST1	basic helix-loop-helix family member a15
mTOR	mammalian target of rapamycin
NAD	nicotinamide adenine dinucleotide
NADP	nicotinamide adenine dinucleotide phosphate
NFκB	nuclear factor κ B

NMR	nuclear magnetic resonance
OxPhos	oxidative phosphorylation
p38-MAPK	mitogen-activated protein kinase 14
PanIN	pancreatic intraepithelial neoplasia
PBS	phosphate buffered saline
PDAC	pancreatic ductal adenocarcinoma
PDH	pyruvate dehydrogenase
PDX1	pancreatic and duodenal homeobox 1
PFA	paraformaldehyde
PGC-1α	peroxisome proliferator-activated receptor γ coactivator 1 α
PHGDH	phosphoglycerate dehydrogenase
PI3K	phosphoinositide 3-kinase
PKM2	pyruvate kinase isozymes M2
PPP	pentose phosphate pathway
Prss1	trypsin-1
PTEN	phosphatase and tensin homolog
RAF	rapidly accelerated fibrosarcoma
RAS	rat sarcoma
RNA	ribonucleic acid
ROS	reactive oxygen species
RPIA	ribose 5-phosphate isomerase A
SDS	sodium dodecyl sulfate
SMAD4/DPC4	mothers against decapentaplegic homolog 4/deleted in pancreatic cancer 4
SPINK1	serine peptidase inhibitor kazal type 1
STAT3	signal transducer and activator of transcription 3
TCA cycle	tricarboxylic acid cycle
TGFβ	tissue transforming growth factor β
TIGAR	tp53 induced glycolysis regulatory phosphatase
TNFα	tumour necrosis factor α
TP53	tumor protein p53
WNT	proto-oncogene wnt
WT	wild-type

Abstract

Pancreatic cancer is one of the most lethal cancers worldwide. Due to the typically late diagnosis, there are often only limited treatment options resulting in a 5-year-survival rate of below 10%. Therefore, it is important to understand the early steps of carcinogenesis to develop new screening and prevention approaches.

Acinar to ductal metaplasia (ADM) initiates carcinogenesis and occurs in response to inflammation. To reveal common metabolic and signalling patterns in oncogenic and inflammatory ADM formation, three different oncogenes and two inflammatory ligands were used to induce ADM.

Glycolytic markers were upregulated in both human and murine ADM *in vitro* and *in vivo*. Accordingly, inhibition of glycolysis blocked ADM formation. In addition, a functional electron transport chain (ETC), but not mitochondrial ATP, was essential for ADM formation. On the other hand, NAD^+ provided by the ETC was needed for *de novo* synthesis of serine from glycolysis intermediates.

Signalling pathways required for ADM were investigated using pharmacological inhibitors. Two kinases, PI3K and MEK, were essential for ADM formation by all inducers tested. In addition, the transcription factor MYC was indispensable for ADM formation.

In summary, essential signalling hubs as well as metabolic requirements for ADM development were identified. These findings can pave the way to develop new interventional strategies to prevent pancreatic carcinogenesis.

Zusammenfassung

Das Pankreaskarzinom zählt zu den tödlichsten Tumorerkrankungen weltweit. Durch die häufig recht späte Diagnose in einem bereits fortgeschrittenen Stadium verbleiben meist nur wenige Behandlungsmöglichkeiten. Dies führt zu einer 5-Jahres-Überlebensrate von unter 10%. Um dem entgegenzuwirken, ist es notwendig vor allem die frühen Stadien der Karzinogenese besser zu verstehen. Die gewonnenen Erkenntnisse können dann zu einer Verbesserung in der Früherkennung und der Prävention genutzt werden.

Die azinoductale Metaplasie (ADM) tritt sowohl zu Beginn der Karzinogenese als auch während einer Pankreatitis auf. Um die Gemeinsamkeiten in den Signalkaskaden und im Zellmetabolismus der onkogenen und inflammatorischen ADM zu erforschen, wurden 3 unterschiedliche Onkogene und 2 inflammatorische Liganden verwendet.

Die Expression glykolytischer Proteine und der Durchsatz der Glykolyse waren während der ADM von humanen und murinen Azini sowohl *in vitro* als auch *in vivo* erhöht. Durch die Inhibition der Glykolyse hingegen, wurde die ADM gehemmt. Zusätzlich wurde eine funktionale Atmungskette, jedoch nicht das mitochondriale ATP, benötigt. Vielmehr war es das durch die Atmungskette bereitgestellte NAD^+, das essentiell für die Biosynthese von Serin war.

Mittels einer Reihe pharmakologischer Inhibitoren wurde ermittelt, welche Signalkaskaden für die ADM benötigt werden. Die Kinasen PI3K und MEK waren essentiell für alle Induktoren. Das gleiche galt für den Transkriptionsfaktor MYC.

Zusammenfassend konnten zentrale Signalkaskaden und metabolische Voraussetzungen für die ADM identifiziert werden. Diese Erkenntnisse können den Weg für neue Präventionsstrategien gegen das Pankreaskarzinom ebnen.

1 Introduction

1.1 Anatomy and Physiology of the Pancreas

The pancreas is one of the accessory glands of the gastrointestinal tract. It is situated in the abdominal cavity between the stomach and the spleen. Functionally, it can be divided into the endocrine and the exocrine compartment [2].
The endocrine compartment is built by the islets of Langerhans which can be subdivided into α-, β- and δ-cells. Although the islets make up only 1-2% of the pancreatic cell mass, they are better known than the exocrine compartment due to their prominent function [3]. The major function of the islets is the regulation of the energy metabolism. The α-cells secret the peptide hormone glucagon upon low blood sugar levels to increase it. Upon high blood sugar levels, the peptide hormone insulin is released by the β-cells so that glucose is taken up from the blood. The δ-cells produce somatostatin. Somatostatin regulates the insulin and glucagon production within the other islet cells but also acts on the hypothalamus. The islet cells are arranged in small groups within the pancreas [4].
The majority of the pancreatic cell mass belongs to the exocrine compartment. This part covers the enzyme producing acinar cells and the duct cells delivering the pancreatic juice to the duodenum. The acinar cells are organised in grape-like structures around a central acinar cell (Figure 1). From there the digestive enzymes are secreted into small ducts which are joining all together into the main duct connecting the pancreas and the duodenum. The digestive enzymes include amylase, proteases and lipases. To protect the duct, the proteases are stored as inactive proenzymes in zymogen granules and are also released as zymogenes. Upon entering the duodenum, protrypsin is cleaved by the duodenum standing enteropeptidase into trypsin. With trypsin activated, it cleaves further peptidases, thus starting an activation cascade of the proenzymes [5]. In addition, the secretion of bicarbonate by the exocrine compartment neutralises the gastric acid [6].

1.2 Pathology of the Pancreas

1.2.1 Diabetes

Diabetes mellitus is a collective term for diseases of the insulin controlled blood sugar regulation. Type 1 diabetes, or juvenile diabetes, describes the impairment of insulin secretion. This can be caused by either damaged or non-functional β-cells. In contrast to type 1, the β-cells

in type 2 diabetes are still functional. In this form, which is also called adult or new onset diabetes, there is an insulin resistance within the target tissues. This is mostly thought to be caused by obesity and high caloric intake [8].

Recently, diabetes has also been discussed in the context of pancreatic cancer. High fasting blood sugar levels and reduced oral glucose tolerance of cancer patients have been reported not only during the course of pancreatic cancer but also before the diagnosis. So far, it has not been understood if this is a cause or a consequence. It was already demonstrated that diabetic conditions are promoting cancer development, listing diabetes as a risk factor of pancreatic cancer [9]. On the other hand, the growing cancer itself interferes with the blood sugar regulation, making it an interesting parameter for either the detection or the monitoring of pancreatic cancer [10]. In recent publications, two additional aspects have been brought up: Increased body weight, often associated with diabetes type 2, leads to an altered signalling in β-cells which in turn promotes an inflammatory setting within the pancreas [11]. This inflammatory environment is a risk factor for PDAC development. On the other hand, high levels of blood glucose are suspected to elevate the risk of kirsten rat sarcoma (Kras) mutations [12]. Both findings support the idea that diabetes is a risk factor in pancreatic tumour development.

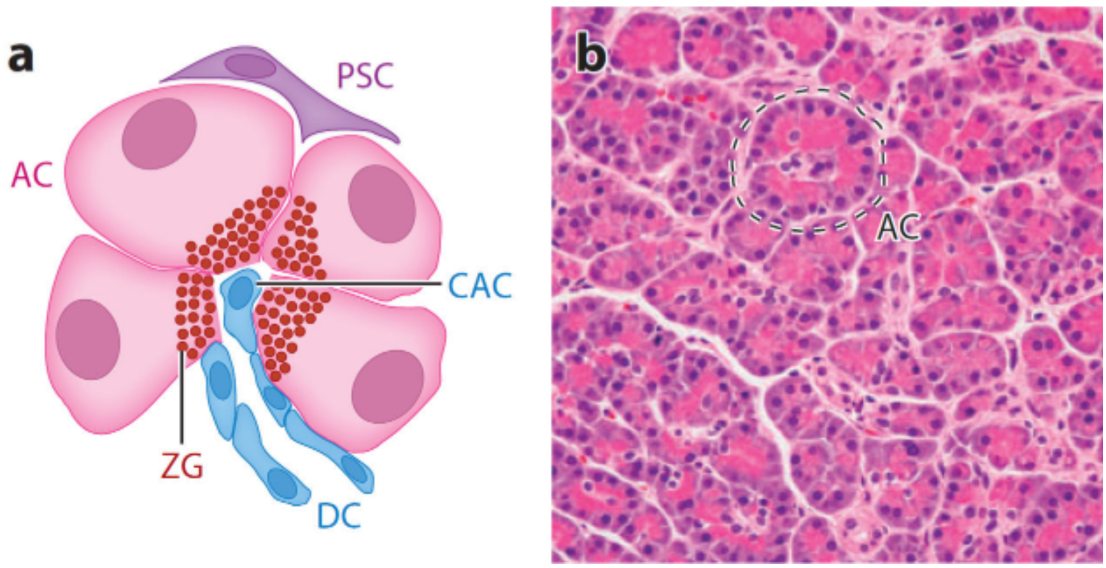

Figure 1: **Schematic (a) and histological representation (b) of normal acinar cells.** Acinar cells (AC) are organized in a grape-like bundle with zymogen granules (ZG) at their apical end. The apical end is directed towards the centroacinar cell (CAC) connecting the acinar cells and the ductal cells (DC). Pancreatic stellate cells (PSC) form the parenchym of the pancreas. Adapted with permission from [7].

1.2.2 Pancreatitis

Pancreatitis is an inflammatory disease of the pancreas which can be either acute or chronic. There are multiple causes for an acute pancreatitis (AP) ranging from external factors like alcohol and drugs over internals factors like bile salts and ductal obstructions to pathogens like viruses [13]. Despite these very heterogeneous inductions, the mechanism of the inflammation is quite conserved. The inflammation is caused by an autolysis of the pancreas caused by a premature activation of trypsin [14]. Digestive enzymes including trypsin are produced, stored and secreted as inactive zymogens (see section 1.1). These zymogens are proteolytically activated within the duodenum [15]. In addition, the pancreatic duct harbours inhibitors like serine peptidase inhibitor kazal type 1 (SPINK1) that inhibit the autolysis of trypsin. Additionally, proteases like mesotrypsin that cleave trypsin in the case of activation [16]. Under physiological conditions, these measures ensure that the pancreas stays protected from the proteases it produces. Pathophysiological conditions lead to a deregulated calcium homeostasis which in turn leads to a constant release of acinar granules or even an intracellular activation of trypsin [17] [18]. This hypersecretion exceeds the protective capacities within the pancreatic duct.
The damage to the acinar cells due to proteases leads to a secretion of several cytokines from the pancreas, such as interleukin (IL) 1β, IL6 and IL8 [19]. These proinflammatory cytokines recruit and activate macrophages which produce, for example, tumour necrosis factor α (TNFα). The recruitment of macrophages leads to a systemic manifestation of the inflammation [20]. Abdominal pain and elevated serum levels of amylase and lipase are the key parameters in the diagnosis and the monitoring of pancreatitis [21].
If the inflammation is not resolved after a single burst ,or if there are relapsing bursts of inflammation, a chronic pancreatitis (CP) can develop [16]. For the initiation of pancreatic cancer, CP is one of the risk factors. In mice, preneoplastic lesions start to develop already 4 weeks after the onset of a chronic pancreatitis [22]. In contrast, one to two decades usually pass between CP diagnosis and pancreatic cancer onset and only 5% of the CP patients develop pancreatic cancer within 20 years [23].
Risk factors for both, acute and chronical pancreatitis, are environmental factors like alcohol, drugs and cigarettes. However, genetic factors like overactive trypsin, impaired SPINK1 or defects in the cystic fibrosis transmembrane conductance regulator have been shown to increase the prevalence of pancreatitis [24].

1.2.3 Pancreatic Cancer

Pancreatic cancer is the 6th most common type of cancer in Germany but due to late detection and a bad prognosis it ranks at the 4th position with respect to cancer related deaths. It is predicted to rise to the 2nd position, by 2030 [25]. The high mortality is also reflected by the 5-year survival rate of 8%. The by far most common type of pancreatic cancer is the pancreatic ductal adenocarcinoma (PDAC). It is characterised by the expression of the ductal marker cytokeratin 19 (KRT19) [26]. In addition, there are also acinar cell carcinomas (ACC). These tumours have an acinar cell-like appearance and account for only 1% of all exocrine tumours [27]. Beside PDAC and ACC there are also tumours arising from the endocrine compartment of the pancreas. Depending on their origin, they are called insulinomas, glucagonomas or gastrinomas. The differentiation of these is done by staining for the different hormones produced by the subcompartments of the endocrine tissue such as insulin and glucagon [28].
It is assumed that despite their ductal phenotype, most PDACs arise from the acinar cell compartment. The acinar cells undergo a transdifferentiation into a ductal-like phenotype which is called acinar to ductal metaplasia (ADM) [29]. This metaplasia will be discussed further in section 1.3.1. After ADM, there are different sequences of precursor lesions leading to PDAC, namely pancreatic intraepithelial neoplasia (PanIN), intraductal mucinous neoplasm (IPMN) and the less frequent mucinous cystic neoplasms (MCNs) [30]. The PanINs are subdivided into PanIN1a, PanIN1b, PanIN2 and PanIN3 according to their grade of dysplascity. There is also a sequential gain of mutations which is associated with the different stages of PanIN progression. Similar to the PanINs progression, there is also a sequential progression of the IPMNs; namely, low-, intermediate- and high-grade [31]. Both, PanINs and IPMNs can result in PDAC. A schematic overview over the PanIN progression is depicted in Figure 2.

Genetically, mutant *KRAS* is the most common feature of PDAC. More than 90% of all PDAC patients carry an activating mutant of this protein. Therefore, *KRAS* is widely accepted as the major driver in PDAC [33]. Other common mutations are found in the TGFβ/SMAD4 pathway [34] or within the tumour suppressor genes *TP53* [35] and *CDKN4* [36]. All these will be discussed in more detail in section 1.3.2.
At the moment, treatment options are limited. Due to late diagnosis only 10-20% of the patients can be resected [37]. Chemotherapy is mainly based on gemcitabine and FOLFERINOX® [38]. In a more recent approach, gemcitabine was supplemented with the taxol derivate nab-paclitax [39]. This regiment is planned to be used on all subtypes of PDAC. In addition, there are experimental targeted therapies which are based on a better stratification

of the patients. Since KRAS is considered non-drugable, downstream targets and KRAS wild-type cancers are now being investigated. In KRAS wild-type tumours, there are often mutations in BRAF or EGF receptors which can be targeted. On the other hand, KRAS wild-type cancers account for only 5 - 10% of all patients [40].

There are several risk factors for the development of pancreatic cancer which can be divided into environmental and inherited factors. As part of the environmental factors, obesity is linked to many different forms of cancer. Also for PDAC, it is listed as a risk factor. Another common risk factor is smoking [31]. If it comes to pancreas-specific risk factors, a chronic pancreatitis is the most important one (section 1.2.2).

The inherited risk factors comprise mutations in the cell cycle regulation, DNA repair and the digestive enzymes [41]. A mutation in *CDKN4* causes a disruption of the cell cycle control. Bearing such a mutation increases the lifetime risk of developing pancreatic cancer to 17% [42]. Another risk gene is *BRCA2* which is important for the DNA damage response. A mutation in this gene leads to an impaired DNA repair and by this to an increased mutational load [43]. The most prominent pancreas specific-mutation is within the *PRSS1* gene. This mutation is leading to a more active trypsin and thereby to a higher susceptibility for pancreatitis. Since pancreatitis is a risk factor, a mutation in *PRSS1* leads to a life time risk for pancreatic cancer of around 40% [44]. In addition, there are also data about mutations in *CPA* and *CPB* as risk factors. In these cases, it seems to be less of a pancreatitis-driven carcinogenesis than the constant ER-stress which can also lead to carcinogenesis [45].

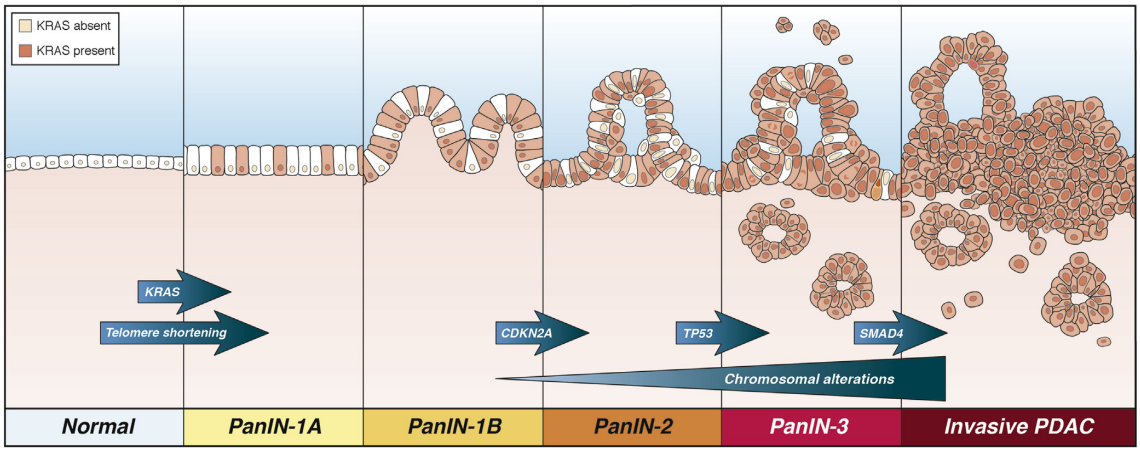

Figure 2: **Schematic progression from normal acinar cells via PanINs to PDAC.** In the course of carcinogenesis, normal acinar cells transform into pancreatic intraepithelial neoplasia (PanIN). These precursor lesions are divided by their grade of dyspasia. In addition, different stages are associated with frequent mutations; namely, gain of function of *KRAS* and loss of function of *CDKN2A*, *TP53* and *SMAD4*. Reprinted with permission from [32].

1.3 Pancreatic Cancer

1.3.1 Acinar to Ductal Metaplasia

ADM is considered to be the first step in carcinogenesis but it occurs also during the course of pancreatitis. In the context of pancreatitis, ADM is needed to replenish lost cell mass [46]. But this only holds true within a healthy setting. In the context of an oncogenic stimulus like $KRAS^{G12D}$, ADM is not reversible but can proceed into a PanIN lesion [47]. Therefore, ADM represents the link between the supposed cell of origin of most PDACs, an acinar cell, and the duct-like PanIN lesions [22].

So far, several different pathways have been identified to be involved in the regulation of ADM. Stimulation of the epithelial growth factor receptor (EGFR) has been shown to lead to ADM formation *in vitro* and *in vivo* [48]. *In vitro*, the EGFR can be stimulated using either the epithelial growth factor (EGF) or the transforming growth factor α (TGFα) [49]. Upon binding of TGFα, EGFR bind members of the erb-b2 receptor tyrosine kinase 2 (ERRB) family. The dimerization leads by to a phosphorylation of the intracellular part of EGFR and thereby to the start of the EGFR signalling cascade [50]. One part of this cascade is the small GTPase KRAS. Here, the signalling pathway branches into several ways. One leads via rapidly accelerated fibrosarcoma (RAF) and mitogen-activated protein kinase kinase (MEK) activation to the phophorylation of mitogen-activated protein kinase 1 (ERK). The second one fuels via the phosphoinositide 3-kinase (PI3K) and protein kinase B (AKT) the mammalian target of rapamycine (mTOR) and its downstream targets [51]. Activation of ERK and PI3K/AKT signalling leads to a strong survival and proliferative stimulus and increases protein synthesis [52].

Since ADM is also a response to inflammation, interleukins are another group of signal molecules that come into play. During pancreatitis, $CD4^+$ T-cells secret interleukin 17 a (IL17a) [53][54]. It was shown that just the presence of IL17a in the pancreas is sufficient to induce neutrophil mediated inflammation and acinar cell disruptions including ADM formation [55]. Also, there are reports that acinar cell at least in the presence of oncogenic KRAS express the IL17a receptor IL-17RA; however, wildtype acinar cells barely do. Still these low amounts of IL-17RA are sufficient to stimulate isolated wild-type acinar cells with IL17a in culture [56]. In sarcoma cell lines, IL17a was shown to induce the phosphorylation of ERK, mitogen-activated protein kinase 14 (p38-MAPK) and mitogen-activated protein kinase 8 (JNK) underlining its pro-proliferative and pro-survival effects [57]. Another pro-

inflammatory cytokine is IL6. IL6 has been shown to promote the progression of tumour development [58]. This makes IL6 also a potential factor influencing ADM formation. Further downstream of IL6, it has also been shown that the activation of signal transducer and activator of transcription 3 (STAT3) is the crucial factor in IL6 signalling [58]. STAT3 itself can be stimulated by a number of different cytokines [59]. Thus, it is a potential central regulator of cytokine-induced ADM.
Many different inflammatory pathways lead to the activation of nuclear factor κ B (NFκB). Activation of the NFκB signalling is initiated by the activation of the IκB kinase (IKK) which phosphorylates the inhibitor of NFκB α (IκBα). This in turn leads to the detachment of IκBα from NFκB and thereby to the activation of NFκB [60]. NFκB activation can be observed as soon as 15-30 min after pancreatitis is induced in rats [61].
Another important factor during ADM is the basic helix-loop-helix family member a15 (MIST1). This transcription factor consists of a basic domain for homodimerization and a helix-loop-helix domain which is important for DNA binding [62]. Beginning during the embryonic development, MIST1 is expressed in the exocrine tissue of the pancreas mediating the acinar identity [63]. Knocking out MIST1 does not prevent the maturation of acinar cells and the production of zymogen granules but inhibits the mature organization of the cytoskeleton. One-year-old mice harbouring a homozygous MIST1 knockout show signs of chronic pancreas damage and ADM [63]. When these mice are challenged with a pancreatitis, they show an increased severity of inflammation and a reduced regeneration [64]. In combination with oncogenic $Kras^{G12D}$, even a heterozygous depletion of MIST1 leads to massively increased ADM formation and development of preneoplastic lesions [65]. MIST1 itself is lost during the course of Kras-induced ADM formation [66]. Complementary to this finding, overexpression of MIST1 can counteract KRAS-induced ADM formation and leads to a stabilization of the acinar identity [31].

1.3.2 Signalling and Cancer

As mentioned before, KRAS is the most abundant mutation in human PDAC [33]. KRAS is a small GTPase which has GDP bound in its quiescent state [67]. Upon exchange of the GDP for GTP, it becomes active until the GTP is cleaved into GDP [68]. Oncogenic KRAS is unable to cleave GTP [69]. Thereby, it executes its signalling without exogenous stimulation of the cell. KRAS activation leads to a subsequent increase in MEK and AKT phosphorylation [70]. In addition, KRAS can sustain the stemness of embryonic stem cells which makes it

an interesting gene in the context of cancer stem cells [69]. It is thought that the mutation of KRAS is one of the first if not the first mutation during PDAC development in humans [71]. When KRAS is activated during embryonic development of the murine pancreas, it leads to the development of PDAC which is comparable to the human carcinogenesis [72]. But it has to be noted that KRAS alone is not sufficient to form a malignant tumour. Similar to the tumourigenesis in humans, further mutations are needed to acquire a malignancy in mice [73]. Some of these mutations will be mentioned later in the section.
A second prominent oncogene is the phosphoinositide 3-kinase (PI3K). The PI3K is activated in KRAS-driven tumours and is essential for tumour formation [74]. According to some publications, the PI3K is negligible in *Kras*-driven tumour onset [31]. On the other hand, activation of PI3K alone has been shown to initiate tumour formation in breast and lung [75] [76]. Furthermore, the PI3K seems to play an important role in tumour maintenance. If a tumour that was initiated by active KRAS is depleted of KRAS later on, the activation of the PI3K is sufficient to maintain tumour growth [77]. The targets of the PI3K signalling are the kinase AKT and the transcription factors c-MYC and NFχB [78].
Besides activation of oncogenes during tumourigenesis, there is also the inactivation of tumour suppressor genes. CDKN4A which is coding for the protein $p16^{INK4A}$ and $p19^{ARF}$ is frequently deleted and mutated in PDAC [36]. p16 binds and inhibits the cyclin-dependent kinase 4 (CDK4). By this mechanism p16 is able to block the cell cycle during G1 phase [79]. Mutations of p16 can be found already in the earliest lesions of carcinogenesis [80]. During the progression of PanIN lesions from PanIN1 to PanIN3 the mutation rate increases from 31% to 85% [81]. In fully established PDAC, at least on allele of p16 is mutated in 85% of all cases [82]. In addition to this, silencing of p16 takes place by promoter and gene methylation leading to an additive effect in the loss of p16 of 98% either by mutations or methylation [83]. The tumour supressive transcription factor p53 is mutated in more advanced lesions like PanIN3 with a frequency of around 50% [81]. This number rises to up to 70% of the cases in PDAC patients [84]. Active wild-type p53 reacts to cellular stress and DNA damage by inducing either DNA repair or senecence or apoptosis [85]. P53 is a target of $p19^{ARF}$ which is transcribed from an alternative open reading frame of the CDKN4A locus mentioned above [86]. In mouse models, the addition of a p53 mutation to *Kras*-driven tumourigenesis shortens the survival from 12 to 5 months. This effect is caused by introducing a heterozygous mutation of *p53* [87]. In this context, it has to be noted that mutant P53 has been reported to inactivate wild-type P53 thus leading to a functional loss of heterozygousity [88].
The transcription factor c-MYC (MYC) is a common oncogene. It is disregulated in numerous cancers such as leukaemia but also pancreatic cancer [89][90]. In addition, MYC plays an im-

portant role in the development of embryonic stem cells and can be found among the factors used to induce pluripotency in induced pluripotent stem cells [91]. MYC is important for proliferation and size regulation on cells [92]. To execute these global functions, MYC can bind to several ten thousands of sites in the chromatin covering at least 15,000 promoter regions [93]. In the pancreas, MYC plays an important role during organ development as well as during carcinogenesis [90]. Oncogenic KRAS or oncogenic PI3K leads to a post-transcriptional stabilization of MYC and thereby to an increase of its proliferative signalling. At the same time, the mRNA levels are not affected. This increase in MYC levels is specific to KRAS or PI3K and can not be achieved by activation of mTOR or Notch signalling [94]. On the other hand, activation of glycogen synthase kinase 3 β (GSK3β), part of the WNT signalling, can lead to a decrease in the MYC levels [95]. In the context of metabolic changes, MYC is thought to favour glycolysis over oxidative phosphorylation. In cancer stem cells which, are more quiescent MYC is downregulated leading to less proliferation and a metabolism which is more focused on oxidative phosphorylation [96]. The field of cancer metabolism will be further discussed in section 1.3.3.

The role of the transforming growth factor beta (TGFβ) and its target protein deleted in pancreatic cancer 4 (SMAD4/DPC4) are very heterogeneous. TGFβ is sensed via TGFβ receptors. Upon binding of TGFβ, the receptors dimerize and phosphorylate a receptor SMAD. SMAD4 binds to the phosphorylated receptor SMAD and the complex translocates into the nucleus [34]. Target genes of this complex regulate cell cycle, apoptosis, differentiation, migration and metastasis formation [34]. During PDAC development, SMAD4 acts as a tumour suppressor by inducing apoptosis. Accordingly, a knock-out of SMAD4 in KRAS-mice leads to an accelerated tumour formation [97]. The effect of TGFβ on tumour cells is depending on the availability of SMAD4. In the context of autophagy, SMAD4 signalling induces proliferation whereas the absence of SMAD4 leads to TGFβ -mediated migration and metastasis [98]. When isolated tumour cells in a 3D culture are treated with TGFβ they change their morphology from a spheric type to tubular complexes. Pre-existing tubular growth can be reverted to spheres by inhibiting TGFβ signalling [99]. For human acinar cells, it was reported that TGFβ can induce ADM *in vitro* [100]. Clinically, TGFβ and SMAD4 are discussed as either diagnostic or prognostic factors. Two TGFβ target proteins have been found to be upregulated in patients' serum with PDCA at various stages. Partially, this upregulation can also discriminate PDAC against chronic pancreatitis [101]. Additionally, detection of SMAD4 in tumour cells of patients' biopsies was linked to a shortened survival [102].

1.3.3 Metabolism and Cancer

In addition to aberrant cell signalling, cancer cell metabolism diverges heavily from normal cells. In the 1920s, Otto Warburg found that cancer tissue relies considerably more on glycolysis than oxidative phosphorylation (OxPhos) [103]. Non-transformed tissue uses glycolysis under anaerobic condition but switches to OxPhos when oxygen is available. In contrast to this, tumour tissue uses the vast majority of the glucose taken up for glycolysis even in the presence of oxygen; a phenomenon termed as aerobic glycolysis. In Warburg's experiments, the differences between normal and cancer tissue became more pronounced during the development from normal tissue to benign lesions to a malign tumour [103]. In a later work, Warburg and colleagues could also show that tumours take up substantially higher amounts of glucose from the blood stream than normal tissue. In return, high amounts of lactate, the product of the aerobic glycolysis, is secreted into the blood [104]. Today, the aerobic glycolysis of tumours is known as the "Warburg effect". In pancreatic cancer, a high expression of glycolytic enzymes is associated with a shortened survival of the patients [105]. Consequently, tumour cells are vulnerable towards glycolysis inhibition [105]. But especially pancreatic tumours consists not only of tumour cells but harbour also high amounts of stroma. These stroma cells have additional effects on the tumour cells. Cytokines released by cancer associated fibroblasts influence not only the degree of vascularization but increase the use of glucose for glycolysis and the pentose phosphate pathway in the tumour cells [106]. In addition, the tumour cells themselves are also heterogeneous. A subgroup of tumour cells, named cancer stem cells, have been shown to mainly rely on OxPhos instead of glycolysis [107]. These cells occur in low frequency and proliferate slower than "normal" cancer cells. Interestingly, they are even independent of mutant *Kras* [107]. Consistently with these finding, it was shown that forcing tumour cells to use OxPhos by supplying them with galactose instead of glucose enriches for cancer stem cells. These cells are not only using OxPhos but they are depending on it shown by their sensitivity towards OxPhos inhibition [108]. Two proteins which are brought into context with the different types of cancer cells are MYC and PGC-1α. In this context, PGC-1α is upregulated in cancer stem cells and promoting OxPhos within those. On the other hand, c-MYC is upregulated in differentiated cancer cells promoting glycolysis [96].

Glucose can not only be used to gain ATP. In addition, it can also be used for the glycosylation of proteins and lipids and can be metabolized via the pentose phosphate pathway (PPP). The PPP is the source for the redox equivalent NADPH and several sugars consisting of four to seven carbons. The most prominent example of what these sugars are used for are nucleosides. The ribose is built in the PPP but also the synthesis of the nuclear bases requires metabolites

from the PPP [109]. In PDAC cells, it was shown that especially mutant KRAS leads to an increased activity of the PPP and the upper part of the glycolysis which is connected to the PPP [110]. Especially the non-oxidative arm of the PPP supplying the cell rather with metabolites than with NAPDH is of importance to the anabolic metabolism. In addition, the biosynthesis of hexosamines was elevated. These sugars are important building blocks for glycosylation reactions. Both effects on the metabolism are mediated via KRAS-dependent activation of MEK and MYC [110]. Upon activation of the KRAS-MEK-MYC axis, key enzymes of the PPP (ribose 5-phosphate isomerase A, RPIA) and of the pyrimidines biosynthesis (mitochondrial dihydroorotate dehydrogenase , DHODH) are upregulated [111]. The increased amount of nucleosides following these upregulations is an important factor for the proliferation of cancer cells. Taken together, these findings underline the anabolic importance of glucose within the metabolism of cancer cells.

A second important source of energy and metabolites is glutamine. Glutamine is a proteogenic amino acid but can also serve as an amino donor and after deamination to α-ketoglutarate as a source for the tricarboxylic acid cycle (TCA cycle). For immune cells it was shown that the uptake of glucose and glutamine are connected [112]. Stimulation of the cells via cytokines and the simultaneous uptake of glucose lead to an increase of the transporter SLC6A19 importing glutamine among other neutral amino acids. This glutamine was mainly used as an amino donor in the biosynthesis of hexosamines [112]. Contrary to these findings, glioblastoma cells use glutamine mainly as a source of energy and not for amination [113]. In this case, glucose was mainly used for glycolysis and secreted as lactate while glutamine is used to fuel the TCA cycle. Both, the anaerobic use of glucose and the dependency on glutamine were mediated by high levels of MYC [113]. In addition to this, MYC was shown to indirectly promote the expression of glutaminase (*Gls*). This enzyme deaminates glutamine into glutamate, the first step towards α-ketoglutarate [114]. In pancreatic cancer, there is a third way of using glutamine: KRAS signalling leads to the formation of glutamine derived aspartate which is then converted within the cytosol into pyruvate. This metabolic pathway promotes the gain of NADPH independently of the PPP [115].

The mitochondrial ATP production fuelled by either glucose or glutamine is the major source of reactive oxygen species (ROS). ROS have been discussed to have various impacts on cancer development and maintenance. During the development of lung cancer, ROS are described to be not only beneficial but essential for KRAS-induced proliferation [116]. Also, within the pancreas it has been reported that mutant KRAS increases mitochondrial ROS which supports ADM formation and PanIN development [117]. In established tumours, high levels of ROS can cause DNA damage which can lead to cell death [118]. Therefore, ROS defence systems

are of great importance for cancer survival. One way of ROS defending adaptation can be the promotion of NAPDH production. NAPDH is an important cofactor for ROS defence enzymes. As mentioned before, in PDAC this can be facilitated via glutamine metabolism [115]. The more general way is the increase of the PPP, especially the oxidative arm. For pancreatic cancer it was shown that promotion of the PPP by tp53 induced glycolysis regulatory phosphatase (TIGAR) plays an important role for tumour maintenance and spreading [119]. Another approach to promote a ROS defence system is to increase the availability of cysteine. Cysteine is part of many anti-ROS-enzymes and of glutathione [120]. Depleting PDAC cell of cysteine leads to cell death *in vitro* and *in vivo* [120]. It has to be noted that these two strategies are just examples and do not represent a complete list of tumour cell related adaptations.

1.3.4 Mouse Models

In order to gain a better understanding of the development and the biology of pancreatic cancer, several mouse models have been developed. Many of these models are based on the investigations of mutations frequently found in human PDAC (see section 1.3.2). One of the first mouse models was based on the overexpression of TGFα in pancreatic cells [121]. These mice developed a heavily altered pancreas that was characterized by the formation of tubular complexes. At the same time, there were no additional mutations in the KRAS gene which is known for its prominent role in PDAC [121]. The TGFα-induced tubes were positive for KRT19 which is similar to ADM lesions. In addition, it was shown that P53 counteracted the TGFα effect [122]. If P53 or INK4/ARF, another well known tumour suppressor, are knocked out TGFα-overexpression can even lead to the formation of PDAC [73]. Besides the TGFα model, there is also the conditional knock-in of $KRAS^{G12D}$ [72]. Conditional alleles can be used to target a mutation to a specific tissue while leaving other tissues unharmed. In case of a pancreas specific activation of $KRAS^{G12D}$, a mouse model is generated that mainly recapitulates the progression of human PDAC development [72]. This model serves as a basis to study the interaction of additional genes with KRAS and their effect on the tumour development. One of these combinations is the simultaneous activation of KRAS and the inactivation of *p53* [87]. The inactivation leads not only to a more aggressive phenotype and a shortened survival but also to a higher mutational burden due to chromosomal instability. Both features are often seen in human PDAC, too [87]. Another mutation frequently seen in humans is the inactivation of SMAD4. This mutation was also transferred to the KRAS model

by using a conditional knock-out [123]. Interestingly, the effect of the SMAD4 knock-out is highly dependent on the zygosity of the allele. In contrast to the heterozygous knock-out, the homozygous deletion of SMAD4 results in a shortened overall survival. In addition, the type of the precursor lesions from PanIN to IPMN is independent of the zygosity [123]. Since most tumours acquire multiple mutations during their development, additional insight can be drawn from tumour models harbouring several mutations. One example for such a multi mutational tumour model is the knock-out of SMAD4 and INK4a/ARF in the presents of $KRAS^{G12D}$ [124]. The addition of the SMAD4 knock-out did not alter the survival or the disease progression but the subtype of the tumour. Tumours harbouring a *Ink4a/Arf* mutation are mostly undifferentiated and have a poor prognosis. Upon SMAD4 knock-out, the tumours became more differentiated [124]. These different models underline that it is possible to cover relevant parts of the heterogeneity seen in human PDAC in mouse models.
To study the induction, development and pathology of the acute pancreatitis several animal models have been described. In 1977, it was shown that excessive doses of caerulein can lead to an acute pancreatitis *in vivo* [125]. Caerulein, like other secretagogues, acts like cholecystakinin (CCK) by binding to the CCK receptor and leading to calcium mobilization and pancreatic enzyme release. In mice, there are two different receptors, a high and a low affinity one [126]. In humans, there is the cholecystokinin-1 receptor (CCK1R) mediating pancreatic exocrine secretion [127]. Despite the effect of physiological stimulation, a hyper-stimulation by repetitive injections of high caarulein doses leads to a decrease in the secretion of digestive enzymes. In turn, the zymogen granula get activated already within the acinar cells causing severe damage to the cells [128]. This damage is the onset for the development of a pancreatitis. In the beginning of the pancreatitis, there is ROS production activating NFχB. This activation leads to transcription of pro-inflammatory cytokines like IL6 [129]. As a clinical parameter, IL6 reaches its highest serum levels 36 – 48 hours after the onset of pancreatitis symptoms [130].

1.4 Aim of the Study

As described before, the late diagnosis of PDAC leaves only limited therapeutical options. To improve this situation, there is a clear need to investigate the early changes in PDAC development especially ADM. So far, a lot of studies have been conducted focusing on a single gene and its impact on different stages of PDAC development and the established tumour. But a systematic analysis of ADM as a phenomenon integrating different inducers of

ADM is missing. The advantage of this study is that it will be possible to distinguish specific features of the different inducers from a fundamental mechanism underlying ADM. The combination of inflammatory and carcinogenic stimuli is important to cover the full spectrum of ADM-inducing conditions.
In this study, different inducers of ADM shall be investigated for their common dependency on basic signalling pathways during transdifferentiation. In addition, the metabolic changes which often go along with differentiation processes should be elucidated.

2 Methods

2.1 Cell Culture Methods

2.1.1 Isolation of Murine Acinar Cells

For the isolation of murine acinar cells, young mice (3-5 weeks of age) were deeply anaesthetised with isoflurane (cp-pharma) and sacrificed by punctuation of the diaphragma. Afterwards, the pancreas was quickly resected and transferred into a small cell culture dish (Ø 60 mm, Sarstedt) filled with 5 ml of sterile, cold PBS (Gibco®). All further steps took place under sterile conditions using a Herasafe class II Hera Safe biological safety cabinet (ThermoFisher).
The pancreas was washed twice in new PBS-filled dishes and was transferred into a new small dish containing 4.5 ml of solution II (Table 1). Solution II was injected into the pancreas twice with a 20 G needle before the pancreas was chopped into small pieces with a sterile pair of scissors, pipetted up and down and transferred into a Heracell® 240 incubator (ThermoFisher) at 37°C and 5% CO_2 for 10 min with gentle shaking every 2.5 min. After the incubation, the suspension was transferred into a 50 ml Falcon tube, pipetted gently up and down three times and 10 ml of solution I (Table 1) were first used to rinse the dish and then added to the suspension. After 5 min of centrifugation at 14 g and 18°C, the supernatant was removed. The pellet was aspirated with 4.5 ml of solution II, transferred to a new small dish and after one time of pipetting up and down put into the incubator for another 10 min with gentle shaking every 2.5 min. To separate the acini clusters from each other, the suspension was passed through a 100 µm cell strainer (Falcon), pre-wetted with 1 ml of solution I. The cell suspension was pushed through the mesh using the plunger of a 10 ml syringe and the mesh was flushed twice with 4.5 ml solution I. Afterwards, the suspension was centrifuged for 5 min at 14 g and 18°C and the supernatant was carefully removed. The cell pellet was aspirated in 19 ml solution I, transferred to a new 50 ml Falcon tube and centrifuged again for 5 min at 14 g and 18°C. After removal of the supernatant, the cell pellet was resuspended in 2 ml of culture medium (Table 2) supplemented with 30% FCS (Gibco®). The acini suspension was incubated for 30-60 min at 37°C and 5% CO_2. Afterwards, the cells were collected and the plate was flushed with 1 ml of culture medium or PBS. The cell suspension was spun down for 5 min at 14 g and 18°C. The supernatant was removed and the cells resuspended in 500 - 1500 µl of culture medium according to the size of the pellet. These acinar cells were then ready to either be embedded into collagen (section 2.1.2), used for suspension culture or to extract protein (section 2.2.4) or RNA (section 2.2.2).

Table 1: Solution I and II for acinar cell isolation (amounts for one mouse).

Solution I		
Component	**brand**	**amount**
Soybean trypsin inhibitor	Sigma	1 ml
10% BSA	Sigma	500 µl
McCoy's 5A Medium	Sigma	48.5 ml
Solution II		
Component	**brand**	**amount**
Collagenase form *clostridium histolyticum*	Sigma	12 mg
Solution I		10 ml

Table 2: Culture medium for acinar cell (amounts for one mouse).

Component	**brand**	stock	final concentration	**amount**
Soybean trypsin inhibitor	Sigma	100%	1%	100 µl
BSA	Sigma	10%	0.1%	100 µl
Insulin-Selenium-Transferrin	Gibco®	100x	1x	100 µl
HEPES	Gibco®	1 M	10 mM	100 µl
FCS	Gibco®	100%	0.1%	10 µl
BPE	Gibco®	LOT dependent	50 µg/ml	x µl
$NaHCO_3$	Merck		2.6 g/l	26 mg
Waymouth medium	Gibco®			ad 10 ml

2.1.2 Cultivation and Harvesting of Acinar Cells in Collagen Gels

For cultivation for longer than 24 h, acinar cells were embedded into a collagen gel system consisting of 3 layers. A summary of the different volumes of the collagen layers and the culture medium for the different culture formates can be found in Table 3. The first layer consisted of 2.5 mg/ml collagen I from rat tail (Corning®), 1/10 of the total volume of 10x PBS (Biochrome), 0.023 times the collagen volume of 1 M NaOH and H_2O to dilute the collagen. The collagen mixture was equally spread within the well and left in the incubator (37°C, 5% CO_2) for 30 min to solidify. For the second layer 1/2 of the volume of collagen, 0.023 times the collagen volume of 1 M NaOH and 1/2 of the total volume of acinar cell suspension (section 2.1.1) were mixed. The cell containing collagen mixture was spread evenly on top of the first collagen layer without disrupting the bottom layer and allowed to solidify for 30 min in the incubator (37°C, 5% CO_2). The third layer was prepared like the first one and distributed evenly over the second layer. After 30 min of solidification in the incubator (37°C, 5% CO_2), the culture medium (section 2.1.1) was gently added. To assess the influence of different

pathways, various inhibitors were added to the medium. A list of all stimuli and inhibitors can be found in the Tables 4 and 5. The cells were seeded in duplicates for each condition. If inhibitors were added to the medium a part of the cell suspension was used as a positive control for the LDH assay (section 2.3.1). The day of isolation was considered as day 0. At day 1, the medium was exchanged for fresh medium containing fresh inhibitors. All supernatants were collected and pooled per well for the LDH assay. The transdifferentiation rate for wild-type (WT) and Kras$^{G12D/+}$ acinar cells was determinated at day 3, for Pi3k$^{CAH1047R/+}$ and Mek1dd$^{CA/+}$ acini at day 2. To determine the transdifferentiation rate, 4 fields of view per well were counted using the 10x objective of Axiovert 200M (Zeiss). The transdifferentiation rate was calculated as the ratio of the ADM structures and all acini structures (including the ADM structures). ADM structures were defined as hollow, sphere-like structures (Figure 3). The supernatant after day 3 or 2, respectively, was also collected and added to the day 1 supernatant of the matching well for the LDH assay.

To harvest the acinar cells from the 8 well chamber slides (Sarstedt), the medium was removed and both collagen gels from one condition were pooled into 700 µl solution II (see section 2.1.1) and incubated for 10 min at 37°C being inverted every 2.5 min. After digestion, 500 µl of cold PBS were added and the suspension was centrifuged for 5 min at 300 g and 4°C. After removal of the supernatant, 1 ml of PBS was added and the suspension was centrifuged again. The supernatant was discarded and the cells resuspended in 200 µl homogenisation buffer for RNA isolation (section 2.2.2).

If the acinar cells were cultured in a 12 well plate (Falcon) the pooled collagen gels from one condition were digested with 10 ml of solution II for 10 min at 37°C during constant rotation. Then the 50 ml Falcon tube was filled up to 40 ml with cold PBS and spun down at 300 g at 4°C. After removal of the supernatant 1 ml of PBS was added and the cells were pelleted again at 300 g at 4°C. The pellet was either resuspended in 200 µl RIPA buffer (section 2.2.4) or stored at -80°C for the metabolome analysis (section 2.3.2).

Table 3: Collagen gel and culture medium volumes for different culture formates

Plate formate	**collagen mixture per layer [µl]**	**medium amount [µl]**
96 well Seahorse plate	7	80
8 well chamber slide (Sarstedt)	70	200
12 well plate (Falcon)	240	750

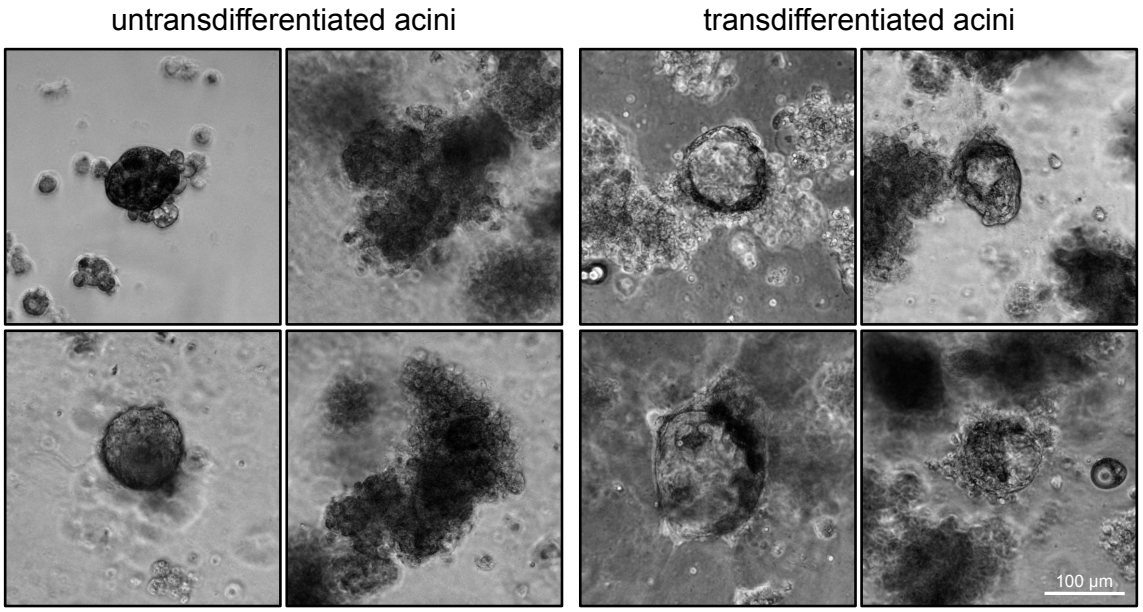

Figure 3: **Examples for untransdifferentiated and transdifferentiated acini.** Grape-like or solid structures were counted as untransdifferentiated acini (left panel). Hollow, spheric structures were counted as ADM structures (right panel).

2.1.3 Seahorse Analysis

To analyse the metabolic status of acinar cells, the Seahorse XFe96 Analyzer (Agilent) system was used.

One day before the measurement, acinar cells were isolated (section 2.1.1) and seeded into the Seahorse XF96e cell culture plate with collagen layer volumes of 7 µl. The concentration of acinar cells within the cell suspension used for seeding was three time higher than in the suspension for the transdifferentiation assay. 80 µl of medium were added to each well and 6 wells per condition were seeded. 100 µµl of the cell suspension were collected to determine the amount of protein in the suspension. Later on, the values from the Seahorse measurement were normalised by the protein amounts. In addition, 2 wells per condition were seeded at normal density in 8-well chamber slides, treated like acinar cells in the inhibitor experiments (section 2.1.2) and their transdifferentiation was evaluated at day 2 after isolation. In the evening, the Seahorse XFe96 extracellular flux assay kit cartige (Agilent) was hydrated by adding 200 µl of water into the utility plate and incubated at 37°C overnight.

On the day of analysis, the water from the utility plate of the cartige was replaced by 200 µl of calibrant (Agilent). The catrige was kept at 37°C. The medium of the cells in the cell culture plate was exchanged for 180 µL XF base medium (pH 7.5) (Agilent) supplemented with 5 g/l of glucose and the indicated treatment. For equilibration, the cell plate was incubated at 37°C

without CO_2 control for 1 h. In the meantime, the inhibitors were prepared and the cartige was loaded with those.

Table 4: Stimuli and inhibitors of signalling pathways for acinar culture

Trivial name	**compound name**	**solvent**	**stock concentration**	**working concentration**
TGFα		10 mM acetic acid	100 µg/ml	10 - 100 ng/ml
IL17a		0.1% BSA in H_2O	5 µg/ml	5 - 20 ng/ml
IL6		0.1% BSA in H_2O	200 µg/ml	50 - 500 ng/ml
IL22		0.1% BSA in H_2O	5 µg/ml	20 ng/ml
TGFβ		4 mM HCl	50 µg/ml	5 ng/ml
HIF1α stabilisator	Deferoxamine	DMSO	100 mM	100 µM
HIF1α stabilisator	$CoCl_2$	H_2O	15 mM	150 µM
PI3K inhibitor	GDC0941	DMSO	1 mM	1 µM
MEK inhibitor	PD035901	DMSO	5 mM	1 µM
CDK4/6 inhibitor	PD0332991	DMSO	1 mM	1 µM
IKK2 inhibitor	BMS-345541	DMSO	5 mM	5 µM
mTOR inhibitor	Rapamycin	DMSO	0.2 ng/ml	200 µM
EGFR inhibitor	Erlotinib	DMSO	20 mM	1 µM
STAT3 inhibitor	S3L-201	DMSO	100 mM	200 µM
c-MYC inhibitor	10058-F4	DMSO	50 mM	25 - 100 µM
FOXO1 inhibitor	AS1842856	DMSO	56 mM	50 - 200 nM
AMPK inhibitor	Compound C	DMSO	100 mM	100 µM
GSK3β inhibitor	LY2090314	DMSO	800 µM	20 - 40 nM
DNA synthesis inhibitor	Aphidicolin	DMSO	10 mM	1 µM
Protein synthesis inhibitor	Cycloheximide	DMSO	100 mg/ml	100 µg/ml

To perform the Seahorse analysis, the following running protocol was used: Every assay cycle started with 1 min mixing, followed by 2 min waiting and 4 min measuring. Firstly, the basal state was measured (5 assay cycles), then Oligomycin was added to a final concentration of 2 µg/mL to inhibit mitochondrial ATP production (4 assay cycles). Afterwards, carbonyl cyanide m-chlorophenylhydrazone (CCCP) (1 µM) and pyruvate (5 mM) were added to determine the maximal rate of the respiratory chain (4 assay cycles). Rotenone (2.5 µM) and Antimycin A (2.5 µM) were added to inhibit complexes I and III of the respiratory chain leading to a total inhibition of the respiratory chain (3 assay cycles). In addition, 2-desoxyglucose (2-DG) (100 mM) was added to inhibit glycolysis (6 assay cycles). The ATP production of

Table 5: Metabolic inhibitors for acinar culture

Trivial name	**compound name**	**solvent**	**stock concentration**	**working concentration**
Complex I inhibitor	Rotenone	DMSO	100 mM	10 µM
Complex III inhibitor	Antimycin A	DMSO	5 mM	100 nM
Complex V inhibitor	Oligomycin	DMSO	5 mM	10 nM
Uncoupling	CCCP	DMSO	2.5 mM	35 nM
GLUT1 inhibitor	WZB117	DMSO	30 mM	30 - 240 µM
LDH inhibitor	Galloflavin	H_2O + 10% DMSO	20 mM	100 - 200 µM
Hexokinase inhibitor	2-Desoxyglucose	H_2O	2 M	2 - 8 mM
PDH inhibitor	CPI-613	DMSO	400 mM	200 - 400 µM
Serine		H_2O	40 mM	0.4 mM
NAD supplementation	Nicotinamide	H_2O	100 mM	1 mM
PHGDH inhibitor	NCT-502	DMSO	10 mM	10 µM
PHGDH inhibitor	NCT-503	DMSO	10 mM	10 µM
PHGDH inhibitor	CBR-5884	DMSO	30 mM	30 µM
Glutaminase inhibitor	BPTES	DMSO	1 mM	500 nM

the cells was calculated according to Mookerjee *et al.* [131].

2.2 Molecular Methods

2.2.1 Genotyping

For genotyping of mice, biopsies either from the ear or from the tail were lysed over night with 200 µl DirectPCR buffer (Viagen) and 10 µl protease K (Roche) at 55°C. To inactivate the proteinase K, the samples were heated to 85°C for 45 min. Afterwards, the samples were spun down for 1 min at maximum speed and the supernatant was transferred to a new Eppendorf tube. The supernatant was used as DNA input for the genotyping PCR.
For the genotyping PCR, 6 µl of GoTaq® master mix green (Promega) were mixed with 5 µl water, 0.5 µl 10 µM primer mix (Table 6) and 0.5 µl isolated DNA. For all genotyping PCR, the following program was used: 95°C for 1 min, 95°C for 30 sec, 58°C for 30 sec, 72°C for 1 min, 72°C for 10 min; steps 2-4 were repeated 35 times. The genotypings for Pi3k and Pi3k_homo were the only ones differing from this program. For those, the annealing temperature was increased from 58°C to 64°C.
To evaluate the genotyping, 10 µl of the PCR product were loaded into a pocket of a 2% (w/v) agarose gel. The gel was prepared by mixing LE agarose (Biozyme) with 100 - 300 ml TEA buffer (depending on the size of the gel) and heated in a microwave oven until the agarose was compleatly dissolved. Afterwards, 5 µl ROTI® GelStain (Roth) per 100 ml gel were added. The gel was run in an electrophoresis chamber (ThermoFisher) at 90 - 150 V (depending of the size of the gel chamber) until the bands were clearly separated. For size estimation, pegGold Ladder Mix (VWR) was used.

2.2.2 RNA Isolation

For RNA isolation, the Maxwell® 16 LEV simplyRNA Purification Kit Tissue (Promega) was used. Tissue samples were disintegrated in 600 µl homogenisation buffer containing 12 µl 1-thioglycerol using the Silent crusher M (Heidolph) and stored at -80°C.
Cells were pelleted at 300 g and resuspended in 200 µl homogenisation buffer containing 4 µl 1-thioglycerol, vortexed shortly and stored at -80°C. To isolate the RNA, 200 µl of the homogenisate were centrifuged for 3 min at maximum speed. The supernatant was mixed with 200 µl lysis buffer and vortexed for 15 s. Afterwards, all 400 µl were transferred to well 1 of the isolation cartige. A plunger was put into well 8 of the cartige, 10 µl of DNAse I solution were added to well 5 of the cartige and 40 µl of nuclease-free water to the elution

tube. The prepared rack was put into the Maxwell® machine and the RNA was isolated using the program "simplyRNA". The RNA concentration was measured using the nanodrop (ThermoFisher).

2.2.3 RNA-Seqencing

The RNA sequencing was done by the group of Roland Rad at the university clinic MRI Munich as they describe in reference [132].
The RNA was transcribed into cDNA using oligo-dT primer harbouring a unique molecular identifier as a barcode (Integrated DNA Technologies). Un-incorporated primers were di-

Table 6: Genotyping Primers

Gene	Primer Sequence 5‘->3‘	product size allele	product size WT
Cre	ACCAGCCAGCTATCAACTCG	199 bp	324 bp
	TTACATTGGTCCAGCCACC		
	CTAGGCCACAGAATTGAAAGATCT		
	GTAGGTGGAAATTCTAGCATCATCC		
Ptf1a-Cre	GTCCAATTTACTGACCGTACACCAA	1155 bp	600 bp
	CCTCGAAGGCGTCGTTGATGGACTGCA		
Kras	CCATGGCTTGAGTAAGTCTGC	180 bp	280 bp
	CACCAGCTTCGGCTTCCTATT		
	AGCTAATGGCTCTCAAAGGAATGTA		
Pi3k	TGAATAGTTAATTGGAGCGGCCGCAATA	630 bp	
	AAATAGCCGCAGGTCACAAAGTCTCCG		
Pi3k_homo	AAAGTCGCTCTGAGTTGTTAT	410 bp	600 bp
	GCGAAGAGTTTGTCCTCAACC		
	GGAGCGGGAGAAATGGATATG		
Mek	TTGTTCGGATCCATAACTTCG	347 bp	297 bp
	AAGGGAGCTGCAGTGGAGTA		
	CCGAAAATCTGTGGGAAGTC		
Stat3	CCTGAAGACCAAGTTCATCTGTGTGAC	350 bp	250 bp
	CACACAAGCCATCAAACTCTGGTCTCC		
Stat3 recombinded	TTTGGAAAGTACTGTAGGCCCGAGAGC	135 bp	
	CACACAAGCCATCAAACTCTGGTCTCC		
Egfr	AAGGTCGGAACCTCTGAGACG	320 bp	180 bp
	CAGAGAGATCTCCACACTTCC		
cMyc	GCCCCTGAATTGCTAGGAAGACTG	500 bp	350 bp
	CCGACCGGGTCCGAGTCCCTATT		

gested by Exonuclease I (New England Biolabs) and the pooled cDNA was aplified using the KAPA HiFi ReadyMix (KAPA Biosystems). Afterwards, the cDNA was tagged, fragmented and amplified with the Nextera XT Kit (Illumina) to generate the sequencing library. For sequencing on the HiSeq1500 (Illumina) 16 cycles were used to read the barcode and 51 to read the cDNA.

2.2.4 Protein Isolation and Concentration Determination

For protein isolation, the cells were resuspended and lysed in 200 µl of RIPA buffer (Table 7) supplemented with inhibitors by vortexing and stored in liquid nitrogen. As inhibitor PhosSTOP EasyPack and cOmplete Tablets mini, EasyPack (both Roche) were used according to the manufacturer‘s protocol.
For concentration determination, the Pierce^{TM} BCA Protein Assay Kit (Thermo Fisher) was used. As a standard curve, the provided BSA stock was diluted within a range of 0 - 2000 µg/ml with water. In a 96 well plate, 20 µl of the standard and 5 µl of RIPA buffer were mixed. For the samples, 20 µl of water and 5 µl of the sample were mixed. The standards were prepared in duplicates, the samples in triplicates. The reaction mix was prepared of solution A and 1/50 of the volume of solution A of solution B. Then, 200 µl of reaction mix were added to each well and the plate was incubated at 37°C for 30 min. Afterwards, the absorbance at 570 nm was measured and the protein concentrations were calculated from the standard curve. Since the protein samples were diluted 1 in 5, the concentration had to be corrected for this.

2.2.5 Western Blot

For a Western Blot, the isolated proteins (section 2.2.4) were adjusted with RIPA buffer to equal concentrations and supplemented with 1/5 of the total volume 6x sample buffer (Table 7) and mixed well. For all western blots except for glucose transporter 1 (GLUT1), the samples were heated to 95°C for 5 min. The samples were loaded onto a 8% SDS polyacrylamide gel (Table 9). For size estimation the Precision Plus Protein^{TM} All Blue Prestained Protein Standards (Bio-Rad) was used. To run the gel electrophoresis and the transfer later on the mini-PROTEAN Tetra Cell system and the Mini Trans-Blot Cell (Bio-Rad) were used. The gel tank was filled with SDS-Polyacrylamide gel running buffer (Table 8) and the electrophoreses was started to run at 80 V. When the marker and the loading dye crossed the border from the stacking to the separation gel the voltage was raised to 200 V except

Table 7: RIPA and sample buffer for protein isolation.

RIPA buffer		
Component	**brand**	**amount**
1 M Tris-HCl, pH 7.5	CarlRoth	ml
5 M NaCl	Sigma	3 ml
Nonidet® P-40 substitute	CarlRoth	1 ml
Sodium Deoxycholat	Sigma	0.5 g
20% SDS	AppliChem	500 µl
H_2O		ad 100 ml
Sample buffer (6x)		
Component	**brand**	**amount**
Stacking gel buffer		7 ml
Glycerine	CarlRoth	3 ml
SDS	AppliChem	1 g
Bromophenole blue	CarlRoth	1.2 mg
Dithiothreitol	Sigma	0.93 g
H_2O		ad 10 ml

for gels were c-myc was probed for. These gels were left at 80 V. When the marker and the loading dye reached the end of the gel the electrophoresis was stopped and the gels were set up for transfer. All proteins were transferred to a 0.2 µm nitrocellulose blotting membrane (GE Healthcare). Prior to usage, the membrane was immersed in transfer buffer (Table 10). The transfer was performed at 100 V for 2 h. To confirm the transfer, the membranes were shortly immersed in Ponceau S solution (Fluka) and in water afterwards. To reverse the red staining, the membranes were quickly washed with TBS-T (TBS (Table 10) + 0.1% Tween20® (Sigma)). Then the membranes were treated with blocking solution for 1 h at room temperature before the primary antibody was incubated overnight at 4°C shaking. The blocking solutions and dilutions for all antibodies are listed in Table 11. The next day, the membrane was washed once for 15 min and 4 times for 5 min with TBS-T before being incubated with the secondary HRP-conjugated antibody (Table 11, bottom) for 1 h at room temperature. The secondary antibody was not needed for β-actin since this antibody was already conjugated to HRP. After washing the membrane again with TBS-T, Amersham ECL Western Blotting Detection Reagent (GE Healthcare) was applied for 1 min before the HRP signal was detected by the CHEMIDOC XRS+ (Bio-Rad).

If membranes were used for multiple antibodies they were washed after imaging for 5 min with TBS-T and then stripped using Restrore^{TM} PLUS Western Blot Stripping Buffer (Ther-

moFisher) for 10 min at room temperature. After being washed trice for 5 min with TBS-T, the membranes were blocked again and treated with antibodies as described above.

Table 8: Gel buffers for Western Blot.

Stacking gel buffer		
Component	**brand**	**amount**
Tris base	CarlRoth	6.05 g
H_2O		40 ml
adjust pH with HCl	CarlRoth	6.8
H_2O		ad 100 ml
SDS	AppliChem	0.4 g
Seperation gel buffer		
Component	**brand**	**amount**
Tris base	CarlRoth	91 g
H_2O		300 ml
adjust pH with HCl	CarlRoth	8.8
H_2O		ad 500 ml
SDS	AppliChem	2 g
SDS-Polyacrylamide gel running buffer (10x)		
Component	**brand**	**amount**
Tris base	CarlRoth	30.2 g
Glycin	CarlRoth	144 g
20% SDS	AppliChem	50 ml
H_2O		ad 1000 ml

2.2.6 Immunofluorescence

The immunofluorescence staining of acinar cells was performed in collagen gels in 8 well chamber slides (section 2.1.2). The medium was removed and the gels were washed with PBS, then 200 µl methanol:DMSO (4:1, CarlRoth and Sigma) were added to fix the cells over night at 4°C. After fixation, the gels were stored in 100% methanol at -20°C. Before staining, the gels were washed with 200 µl PBS + 0.05% Triton®X-100 (PBS-T, Sigma) and blocked with 200 µl 5% BSA in PBS for 1 h. The first primary antibody was directed against either AMY2A (rabbit anti-mouse, A8273, Sigma) or GLUT1 (rabbit anti-mouse, ab115730, Abcam). The antibody was diluted 1:300 in 5% BSA in PBS and incubated over night at 4°C. On the next day, the gels were washed twice with PBS-T for 5 min at room temperature

Table 9: Gel composition for a 8% Polyacrylamid gels.

Separation gel		
Component	**brand**	**amount**
Rotiphorese	CarlRoth	3.111 ml
separation gel buffer		2.917 ml
H_2O		5.639 ml
APS	Sigma	70 µl
TEMED	Sigma	14 µl
Stacking gel		
Component	**brand**	**amount**
Rotiphorese	CarlRoth	0.607 ml
stacking gel buffer		1.167 ml
H_2O		2.847 ml
APS	Sigma	46.67 µl
TEMED	Sigma	9.33 µl

Table 10: Blotting buffers for Western Blot.

Transfer buffer (10x)		
Component	**brand**	**amount**
Tris base	CarlRoth	30 g
Glycin	CarlRoth	144 g
H_2O		ad 1000 ml
Transfer buffer (1x)		
Component	**brand**	**amount**
Transfer buffer (10x)		100 ml
methanol	CarlRoth	200 ml
H_2O		ad 1000 ml
TBS buffer (10x)		
Component	**brand**	**amount**
Tris-HCl	CarlRoth	31.5 g
NaCl	Sigma	80 g
adjust pH with HCl	CarlRoth	7.6
H_2O		ad 1000 ml

before the second primary antibody was added. The antibody staining KRT19 (rat anti-mouse, Troma-III, Hybridoma Bank) was diluted 1:500 in 5% BSA in PBS and incubated overnight at 4°C. Afterwards, the gels were washed once with PBS-T before the secondary antibodies

were applied. The secondary antibodies Alexa568 (goat anti-rabbit) and Alexa488 (goat anti-rat, both ThermoFisher) were diluted 1:500 in 5% BSA in PBS and incubated over night at 4°C. In the last step, the gels were washed once with PBS, transferred to a glas slide, mounted with HardSet ^{TM} Antifade Mounting Medium with DAPI (VectaShield®) and covered with a coverslide. For imaging, the Leica SP8 confocal microscope was used. The nuclei were stained in blue, AMY2A or GLUT1 in red and KRT19 in green.

2.3 Biochemical Methods

2.3.1 Cytotoxicity Assay (LDH activity)

To estimate the amount of cell death during acinar culture the Cytotoxicity Detection Kit (LDH) (Roche) was performed. As a positive control, 60 µl of acinar cell suspension were mixed with 360 µl of culture medium (section 2.1.1) and lysed with 8 µl Triton®X-100

Table 11: Antibodies used for Western Blots and Immunofluorescence. TBS + 0.1 % Tween20 (Western Blots) or PBS (Immunofluorescence) were used as solvent for skimmed milk powder and BSA.

Target	order no	brand	size	blocking	dilution	host
AMPK	2535	Cell Signalling	70	5% milk	1/1000 in 5% BSA	rabbit
p-AMPK	2532	Cell Signalling	70	5% BSA	1/1000 in 5% BSA	rabbit
AMY2A	A8273	Sigma	52	5% milk	1/1000 in 5% milk	rabbit
β-ACTIN	A3854	Sigma	42	5% milk	1/1000 in 5% milk	mouse
c-MYC	ab32072	Abcam	57-70	5% milk	1/1000 in 5% milk	rabbit
KRT19	Tromma-III	Hybridoma Bank	49	5% milk	1/1000 in 5% BSA	rat
ERK1/2	4695	Cell Signalling	42/44	5% milk	1/1000 in 5% milk	rabbit
GLUT1	ab115730	Abcam	40-60	5% milk	1/10000 in 5% milk	rabbit
HIF1α	10790	Santa Cruz	120	5% milk	1/1000 in 5% milk	rabbit
HSP90	4875	Cell Signalling	90	5% milk	1/1000 in 5% BSA	rabbit
LDHA	NBP1-48336	Novus bio	36	5% milk	1/1000 in 5% BSA	rabbit
PDH	MA5-32545	Invitrogen	44	5% milk	1/1000 in 5% BSA	rabbit
p-PDH	AP1062	Calbiochem	44	5% BSA	1/5000 in 5% BSA	rabbit
rabbit IgG	NA934V	GE Healthcare			1/5000 in 5% milk	donkey
rat IgG	NA935V	GE Healthcare			1/5000 in 5% milk	goat
rabbit IgG Alexa Flour®568	A11036	ThermoFisher			1/500 in 5% BSA	goat
rat IgG Alexa Flour®488	A11006	ThermoFisher			1/500 in 5% BSA	goat

(Sigma) for 30 min at 37°C.
All supernatants from the acinar culture collected during the medium change at day 1 and after culturing (day 2 or 3) were combined for each well. In a 96 well plate, 10 µl of the supernatant or the positive control were diluted in 90 µl of Waymouth medium, the positive control was prepared as duplicate. Two different kinds of blanks were prepared; one only containing 10 µl of medium and one with 10 µl of medium containing 2% Triton®X-100. 100 µl of the reaction mix from the kit were added to each well and the plate was incubated for 30 min at room temperature in the dark. Afterwards, the absorption was measured at a wavelength of 405 nm.
The amount of dead cells was calculated according to equation (1) where Abs_{max} is the mean absorption of the positive control and Abs_{min} the absorption of the medium control for the treatment induced cell death or the absorption of the blank for absolute cell death.

$$\%CellDeath_{sample} = \frac{Abs_{sample} - Abs_{min}}{Abs_{max} - Abs_{min}} * 100 \quad (1)$$

2.3.2 Metabolome Analysis by Nuclear Magnetic Resonance (NMR)

This analysis was performed by the group of Tobias Madl at the University of Graz, AT (Gottfried Schatz Research Center for Cell Signaling, Metabolism and Aging, Molecular Biology and Biochemistry, Medical University of Graz).
Cultivated acinar cells, the corresponding supernatants and tissue samples from 10-week-old mice were used for the analysis. Solid samples were homogenised in 66% methanol in H_2O using a Precellys24 tissue homogenizer (Bertin Technologies). In case of the culture media, 200 µl of medium were mixed with 400 µl methanol. Homogenates and media were incubated for 1 h at -20°C and spun down at 18000 g for 30 min at 4°C. Supernatants were lyophilised at <1 Torr, 213 g and 25°C for 10 h using a vacuum-drying chamber (Savant Speedvac SPD210). Prior to NMR measurements, the extracts were dissolved in 500 µl of NMR buffer. NMR buffer consisted of 0.08 M Na_2HPO_4, 5 mM TSP (3-(trimethylsilyl) propionic acid-2,2,3,3-d_4 sodium salt), 0.04% (w/v) NaN_3 in D_2O, pH adjusted to 7.4 with 8 M HCl and 5 M NaOH. Afterwards, samples were transferred to 5 mm NMR tubes and analysed using the following setup: A 600 MHz Bruker Avance Neo NMR spectrometer with a TXI600S3 head was used at 310 K. To acquire ^{1}H-D-NMR spectra, the Carr-Purcell-Meiboom-Gill (CPMG) pulse se-

quence was used with a presaturation for water (512 scans, 73728 points in F1, 12019.230 Hz spectral width, 1024 transients, recycle delay 4 s) [133]. Data analysis was performed as described in [134].

2.3.3 Isotopic Tracing

To investigate the usage of glucose by the acinar cells, fully labelled ^{13}C-glucose (Sigma) was used as a tracer. Acinar cells were isolated as described in section 2.1.1. After the resting step, the cells were pelleted at 14 g for 5 min and afterwards resuspended in glucose-free culture medium (glucose-free Waymouth + all supplements (Table 2)). The cells were distributed into 6 well plates, one well per condition, containing 2 ml culture medium without glucose. Then either normal or ^{13}C-labeled glucose was added to a final concentration of 27.7 mM (glucose concentration of standard Waymouth medium). In addition, stimuli (100 ng/ml TGFα or 20 ng/ml IL17a) or inhibitors (10 nM Oligomycin, 35 nM CCCP, 50 µM 10058-F4) were added. The labelling took place for 2 h, either from 0 h to 2 h of incubation or from 22 h to 24 h. For later labelling (22-24 h), the cells were pelleted at 14 g for 5 min after 22 h of incubation and the medium was exchanged for ^{13}C-labelled glucose containing medium. For harvest, the cells were pelleted at 300 g for 5 min. The supernatants were collected to investigate the secreted metabolites and stored at -80°C. The cells were washed once with cold PBS and also stored as pellet at -80°C. The pellet weight was determined by taking the weight of the empty and the cell containing tube.
The analysis of the supernatants and the cell pellets were done by Werner Schmitz from the Biocenter of the University of Würzburg. To extract the water-soluble metabolites, the cells were homogenised in 0.5 ml of ice cold 80% methanol in water + 0.1 µM Lamivudine and 0.1 µM sucrose. The homogenate was cleared by centrifugation and loaded on a RP18 SPE column which was activated before with 0.5 ml CH_3CN and conditioned with 0.5 ml 80% methanol in water. The elutates were dried and dissolved in 50 µl 5 mM NH_4OAc in 50% CH_3CN in water.

Metabolites were analyzed by LC-MS using the following settings:
For LC-MS analysis 3 µl of each sample were applied to a ZIC-cHILIC column (SeQuant ZIC-cHILIC, 3 µm, 100 x 2.1 mm). Metabolites were separated at 30°C by LC using a DIONEX Ultimate 3000 UPLC system (ThermoScientific) and with the following solvents: Solvent A consisting of 5 mM NH_4OAc in CH_3CN/H_2O (5/95, v/v) and solvent B consisting of 5 mM NH_4OAc in CH_3CN/H_2O (95/5, v/v). At a flow rate of 200 µl/min, a linear gradient starting

at 100% solvent B decreasing to 40% solvent B over 23 min was applied followed by 17 min constant elution with 40% solvent B, followed by a linear increase to 100% solvent B over 1 min. Recalibration of the column was achieved by 7 min prerun with 100% solvent B.

All MS-analyses were performed on a high-resolution QExactive mass spectrometer (ThermoScientific) in alternating positive- and negative full MS mode applying the following scan and HESI source parameters: Scan Range: 69.0 - 1000 m/z. Resolution: 70,000, AGC-Target: 3E6, Maximum Injection Time: 200 ms. Sheath gas: 30, auxiliary gas: 10, sweep gas: 3, Aux Gas Heater temperature: 120°C. Spray voltage: 2.5 kV in positive ion mode and 3.6 kV in negative ion mode, capillary temperature: 320°C, S-lens RF level: 55.0. Signal determination and quantitation was performed using TraceFinder^{TM} Software Version 3.3 (ThermoFisher).

2.4 Mouse Experiments

2.4.1 Mouse Models

If not stated differently mice were bred with a C57BL/6J background. The genetic mutations were based on the Cre/Lox system utilising the cre endonuclease of the bacteriophage P1, which specifically recognises and excerts lox sequences [135]. To achieve pancreas specific mutations the Ptf1a-Cre was used. In this allele, the acinar specific Ptf1a gene is replaced by the cre recombinase. Mice were bred heterozygously for the cre allele leading to the genotype Ptf1a$^{+/cre(ex1)}$ [136]. The allele's name is Ptf1a$^{tm1(cre)Hnak}$. All other alleles were generated harbouring lox sites and therefore being cre-dependent in their effect.
As tumour models, three different oncogenic gain of function mutations were used. The first one is the *Kras* mutation *Kras*^{G12D}. The mutation of this small GTPase leads to a GTP independent activation. The inserted lox-stop-lox cassette ensures a cre-dependent activation of the mutation. Without recombination, the allele is silenced. The mutant allele is located in the endogeneous locus [72]. Animals harbouring this allele heterozygously will be referred to as Kras$^{G12D/+}$. The allele's name is Kras^{tm4Tyj}. The second oncogene is the *Pi3k* mutation *p110α*^{H1047R} which is located in the Rosa26 locus [74]. This constitutive active form of the catalytic subunit of the PI3K is silenced by a lox-stop-lox cassette leading to a cre-dependent expression. Animals harbouring this allele heterozygously will be refered to as Pi3k$^{CAH1047R/+}$. The allele's name is LSL-PI3K^{CAH1047R}. The third oncogene is the *Mek* mutation Mek1DD which is located in the Rosa26 locus [137]. This constitutive active form of MEK1 is silenced by a lox-stop-lox cassette leading to a cre-dependent expression. Animals harbouring this allele heterozygously will be referred to as Mek1dd$^{CA/+}$. The allele's name is

Gt(ROSA)26Sor$^{tm8(Map2k1*,EGFP)Rsky}$.
In addition to the tumour models, three different knockouts were used. The first one is a knockout of the epithelial growth factor receptor (EGFR) [138]. In the allele, the exon 1 is flanked by loxP sites and can be cut out by the cre recombinase. This leads to a knockout of the *Egfr* gene. Animals were bred homozygously for this allele. The combination of this allele with Ptf1a$^{+/cre(ex1)}$ will be referred to as Egfr$^{\Delta panc}$. The allele's name is Egfr^{tm1Msi}. The second knockout is a signal transducer and activator of transcription 3 (STAT3) knockout. This allele is harbouring two loxP sites flanking exon 2 of the gene [139]. After recombination, a truncated version of the gene is expressed missing the phosphorylation site Y705 [58]. The missing phosphorylation site leads to a functional inactivation of the protein. Animals were bred homozygously for this allele. The combination of this allele with Ptf1a$^{+/cre(ex1)}$ will be referred to as Stat3$^{\Delta panc}$. The allele's name is Stat3^{tmAkin}. The third knockout is targeting c-MYC. In this allele, the exons 2 and 3 are flanked by two loxP sites. Among cre recombination, the exons are cut out leading to a complete inactivation of the gene [140]. Animals bred heterozygously for this allele in combination with Ptf1a$^{+/cre(ex1)}$ will be referred to as myc$^{+/-}$. The allele's name is Myc^{tm2Fwa}.
Breeding of all lines was approved by the Regierung von Oberbayern.

2.4.2 Induction of Acute Pancreatitis

To generate an *in vivo* model for ADM, the caerulein-induced acute pancreatitis (AP) was used following a protocol published by Jensen *et al.* [141]. Caerulein (Bachem) was dissolved in water (1 mg/ml) and diluted 1/50 with 0.9% NaCl (Fresenius). 8-12 week old mice were starved during the night before the pancreatitis for 14 h. In the morning, the first injection was considered as timepoint 0 (t0). The mice received 8 hourly injections of 100 µl caerulein (2 µg) on two consecutive days (t0 - t7 and t24 - t31). To monitor the course of the AP, blood samples were taken at t0, t8 and t32. Therefore, the *vena faciales* was punctuated with a blood lancets supra (Megro) and 5 - 10 drops of blood were collected in a Microvette® (Sarstedt). The blood was spun down at 10640 g, 4°C for 10 min and the supernatant was collected and stored at -80°C. Mouse preparation and tissue sampling was done at t72 as described in section 2.4.3.
If inhibitors were used, they were given at timepoints -24 h, 0 h, 24 h and 48 h. The injected volume was 10 µl/g body weight. For the injections at -24 h and 48 h, 93% (v/v) of NaCl were mixed with 7% DMSO (v/v) containing the respective inhibitor. For the injections at 0 h and 24 h, the 93% (v/v) of NaCl contained 100 µl caerulein. The used inhibitors were Rotenone

(15 µmol/kg) and WZB117 (7 mg/kg).
All experiments were approved by the Regierung von Oberbayern.

2.4.3 Tissue Harvesting and Generation of Formalin-Fixed, Paraffin-Embedded (FFPE) Tissue Blocks

Mice were sacrificed either at the end of a pancreatitis experiment or as control animals with an age between 8 and 12 weeks. Before sacrificing, mice were injected with 50 mg/kg (10 µl/g) body weight 5-Bromo-2-deoxyuridine (BrdU, Sigma) for later proliferation analysis. 2 hours after injection, mice were anaesthetised with isoflurane (cp-pharma) and sacrificed by debleeding from the heart. The withdrawn blood was centrifuged in a Microvette® (Sarstedt) at 10640 g, 4°C for 10 min and the serum was stored at -80°C.
Pancreas, spleen, duodenum, liver and lung were quickly resected. From all organs small pieces were embedded into O.C.T ^{TM} Compound (Tissue-Tek®) and snap frozen in liquid nitrogen. A small piece of the pancreas was disintegrated in homogenisation buffer for RNA isolation (see 2.2.2) and snap frozen and another piece was snap frozen in liquid nitrogen for protein isolation. The remaining tissue parts were locked in an embedding cassette and fixed in 4% paraformaldehyde (16% PFA stock, EMS, diluted with PBS) over night at 4°C, dehydrated using the S300 tissue processing unit (Leica) and embedded into paraffin.
For further histological analysis, 1 - 2,5 µm thick sections were cut of the pre-cool tissue block using a Microm HM335S (ThermoFisher).

2.4.4 Hemalaun-Eosin (H&E) Staining

For Hemalaun-Eosin (H&E) staining, tissue sections were rehydrated using an descending alcohol series: Roti®-Histol (xylene replacement, Roth), 100%, 96%, 70% ethanol (all Otto Fischar GmbH & Co), water. The slides were incubated at each concentration for 2 times 5 min. Afterwards, staining with Mayer's hemalum solution (Merck) took place for 3 min followed by 10 min of rinsing with tap water. Eosin staining was performed by incubating the slides in ethanolic eosin solution (0.33%) for 3.5 min, in 96% ethanol for 25 s and isopropanol for 25 s. Final dehydration was done by Roti-Histol, 2 times 1.5 min. Finished stainings were mounted with Pertex® (Medite) and covered with a coverslide.

2.4.5 Histological Analysis of Acute Pancreatitis

To determine the effect of pancreatitis on the pancreas two different histological features were investigated: ADM and edema formation. In order to quantify both parameters, H&E stained FFPE slides (section 2.4.4) were scanned and the images were cropped down to the pancreas area using Fiji [142]. All vessels, ducts, cysts and fat tissue were also cropped from the image leaving only acinar tissue, ADM structures and edema. The remaining tissue area was quantified, using the tool "Versatile Wand Tool", to serve as a reference area. Then, the edema was labelled in cyan. After quantifying the cyan area by applying the "color pixel counter" tool, the cyan channel of the picture was eliminated. The picture was binarised and the number and area of the ADM lesion measured by the "analyse particles" tool of ImageJ. The setting of the tool were the following: size = 60 - 150000; circularity = 0.25 - 1.00. The measured values for the edema area were used as ratios to the total pancreas area; the values for ADM area and number were uses as ratios to the edema-free pancreas area.

2.4.6 Immunohistochemistry

Immunohistochemistry was performed and evaluated by the Institute of Pathology, TU Munich.
2 µm thick sections were cut either from murine FFPE tissue blocks (see 2.4.3) or from human tissue micro arrays generated by the Institute of Pathology. The staining was performed on a Bond Rxm system (Leica). After deparaffinisation, the slides were incubated with antigen retrieval solution 1 (ER1, Leica) for 30 - 40 min. Afterwards, the slides were treated with the primary antibody (see Table 12) which was visualised using the Polymere Refine Detection Kit (Leica). After scanning of the slides by an AT2 scanning system (Leica) slides were evaluated by trained pathologists. For murine slides, evaluation was done by Nils Wirges using a semiquantitative scoring system from 0 (no staining) to 5 (strong staining). For human slides, evaluation was done by Katja Steiger using a semiquantitative scoring system from 0 (no staining) to 3 (strong staining).

2.5 Statistical Analysis

The graphical arrangement of data and statistically testing for significance was done using GraphPad Prism 8 (GraphPad Software). For parametric data a Student's t-test or an ANOVA was performed. For non-parametric data (histological scores) a Kruskal-Wallis test was used.

Table 12: Antibodies used for immunohistochemistry

Target	**order no**	**brand**	**dilution**
GLUT1	ab115730	Abcam	1/750
HK1	2024	Cell Signalling	1/500
LDHA	NBP1-48336	Novus bio	1/10,000
ATP5D	2865	Sigma	1/100

The analysis of RNA sequencing data was performed in R Studio (RStudio, PBC) [143] with help of the DESeq2 package [144].

3 Results

3.1 Basal Characterization

It has been shown in the literature that there are several factors that can induce acinar to ductal metaplasia (ADM) both *in vitro* and *in vivo*. Among these factors, there are the transforming growth factor alpha (TGFα) and the activating mutations of KRAS, namely KRAS^{G12D}, and of PI3K, namely PI3K^{CAH1047R}. To study ADM *in vitro*, the acinar cells of 4 - 6-week-old mice were isolated as acinar clusters. This isolation maintained the original architecture of an acinus *in vivo*. The acinar clusters were embedded into a collagen gel and cultured as a 3D culture. On top of the gels, culture medium was added along with additional stimuli or inhibitors. To investigate a broad spectrum of ADM inducing conditions, five different ways to induce ADM *in vitro* were chosen: wild-type acinar cells were stimulated using TGFα or interleukin 17a (IL17a) to reflect an inflammatory induction of ADM formation; and oncogenic initiation was addressed by constitutively active forms of the known oncogenes *Kras*, *Pi3k* and *Mek*. All oncogenes, Kras^{G12D}, Pi3k^{CAH1047R}, Mek1dd^{CA}, were used as heterozygous alleles.
All five inducers showed transformation of acinar cells into spheres which represent ADM structures *in vitro* (Figure 4A, upper panel). These spherical structures stained positive for the ductal marker cytokeratin 19 (KRT19) and negative for the acinar marker amylase 2a (AMY2A). The nuclear staining DAPI was used as counterstaining (Figure 4A, lower panel). The quantification of the transdifferentiation rates revealed that all five inducers led to a higher transdifferentiation rate than wild-type acinar cells treated with medium only (Figure 4B). It became obvious that PI3K$^{CAH1047R/+}$ and MEK1DD$^{CA/+}$ acinar cells had a notably higher transdifferentiation rate than the other three inducers, even though they were incubated one day shorter than the other inducers. The shorter incubation time was performed for technical reasons. The ADM formation was verified on the protein and RNA levels of *Amy2a* and *Krt19* as acinar and ductal markers, respectively. Compared to freshly isolated acinar cell ("0 days"), the cultivated acinar cells ("2 days"or "3 days") had an increased expression of KRT19 expression while the AMY2a expression was decreased during the culture (Figure 4C). The same pattern was seen for the RNA expression of *Amy2a* (Figure 4D) and *Krt19* (Figure 4E) when comparing basal and transdifferentiated conditions.

Since both ligands TGFα and IL17a can induce ADM formation in wild-type acinar cells, it could be hypothesized that other cytokines can induce ADM as well. To answer this question,

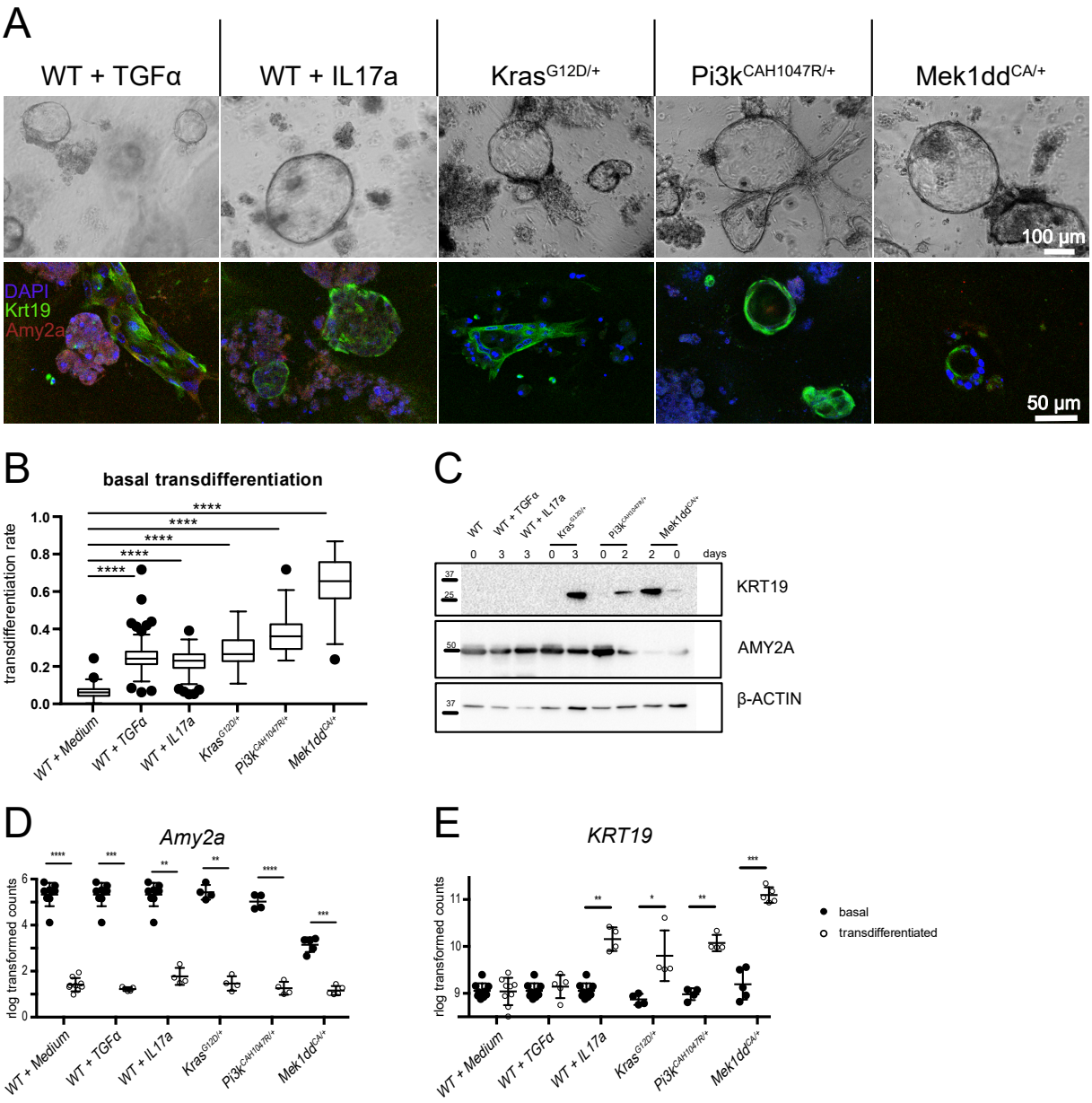

Figure 4: **ADM formation via five different inducers. A.** Light microscopic images of transdifferentiated acinar cells (top) and immunofluorescent images stained against amylase (AMY2A, red), cytokeratin 19 (KRT19, green) and DAPI as counterstaining (blue). **B.** Ratio of transdifferentiated acinar cells and all acinar structures. **C.** Western blot of freshly isolated and cultivated acinar cells. Blots were performed against AMY2A, KRT19 and β-ACTIN as loading control. **D, E.** RNA expression of *Amy2a* (**D**) or *Krt19* (**E**) in freshly isolated and cultivated acinar cells. All values are displayed as mean ± SD. * = $p < 0.05$, ** = $p < 0.01$, *** = $p < 0.001$, **** = $p < 0.0001$.

wild-type acinar cells were treated with either interleukin 22 (IL22) or interleukin 6 (IL6). Both these interleukins are known from the literature to promote PDAC development. As

it can be seen in Figure 5A, IL22 did not alter the transdifferentiation rate of wild-type acinar cells in comparison to acinar cells treated only with medium. Similar to IL22, the IL6-treatment of wild-type acinar cells did not increase the ADM rate (Figure 5B). To confirm a successful isolation of the acinar cells and their ability to undergo ADM, TGFα was used as a positive control.

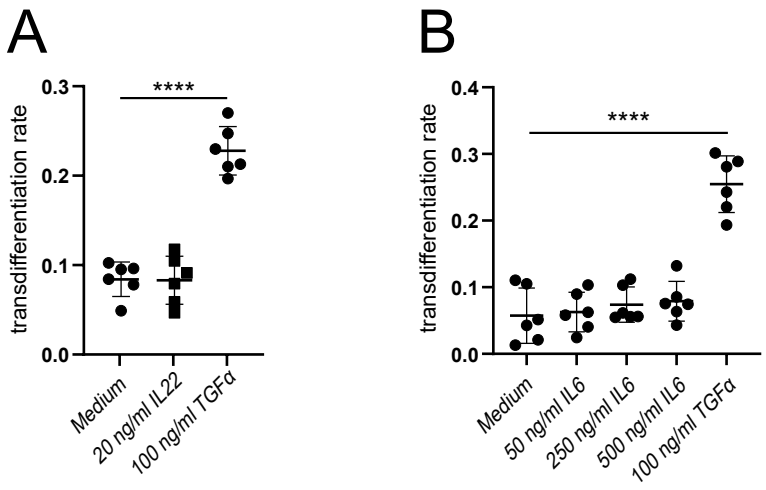

Figure 5: **No ADM formation via IL6 or IL22. A.** Transdifferentiation rates of wild-type acinar cells after treatment with IL22. **B.** Transdifferentiation rates of wild-type acinar cells after treatment with different concentrations of IL6. TGFα was used as positive control. All values are displayed as mean ± SD. **** = $p < 0.0001$.

In the literature, oncogenic ADM structures in tissue are often stained positive for markers of proliferation. To test whether proliferation is not only a characteristic of ADM *in vivo* but also a requirement *in vitro*, two different means of inhibition of proliferation were chosen. Firstly, the cyclin dependent kinase 4/6 (CDK4/6) was inhibited. This inhibition leads to a cell cycle arrest and thereby an inhibition of proliferation. The inhibition of the CDK4/6 had mild to no effects on the transdifferentiation (Figure 6A). IL17a- and MEK1DD$^{CA/+}$-induced ADM were not sensitive towards the CKD4/6-inhibition at all. KRAS$^{G12D/+}$ showed a mild but not significant elevation of the transdifferentiation rate. The effect on TGFα was very heterogeneous, while the transdifferentiation of PI3K$^{CAH1047R/+}$ was mildly but significantly reduced.

The second approach towards proliferation inhibition was to inhibit the DNA synthesis. By using a specific inhibitor for the DNA synthesis spearing the RNA synthesis, proliferation was inhibited in the S-phase, but transcription was still possible. The inhibition of DNA synthesis showed no effect on any of the five inducers (Figure 6B).

An additional aspect of basal cellular functions is protein synthesis. Cycloheximide is known

to inhibit the lateral movement of the ribosome along the mRNA and thereby the synthesis of new proteins. The inhibition of the protein synthesis led to a drastic inhibition of transdifferentiation with all five inducers (Figure 6C). For all inducers apart from PI3K$^{CAH1047R/+}$, this reduction was also significant. Although the transdifferentiation in PI3K$^{CAH1047R/+}$ was reduced to nearly 0 this change was unable to reach significance.

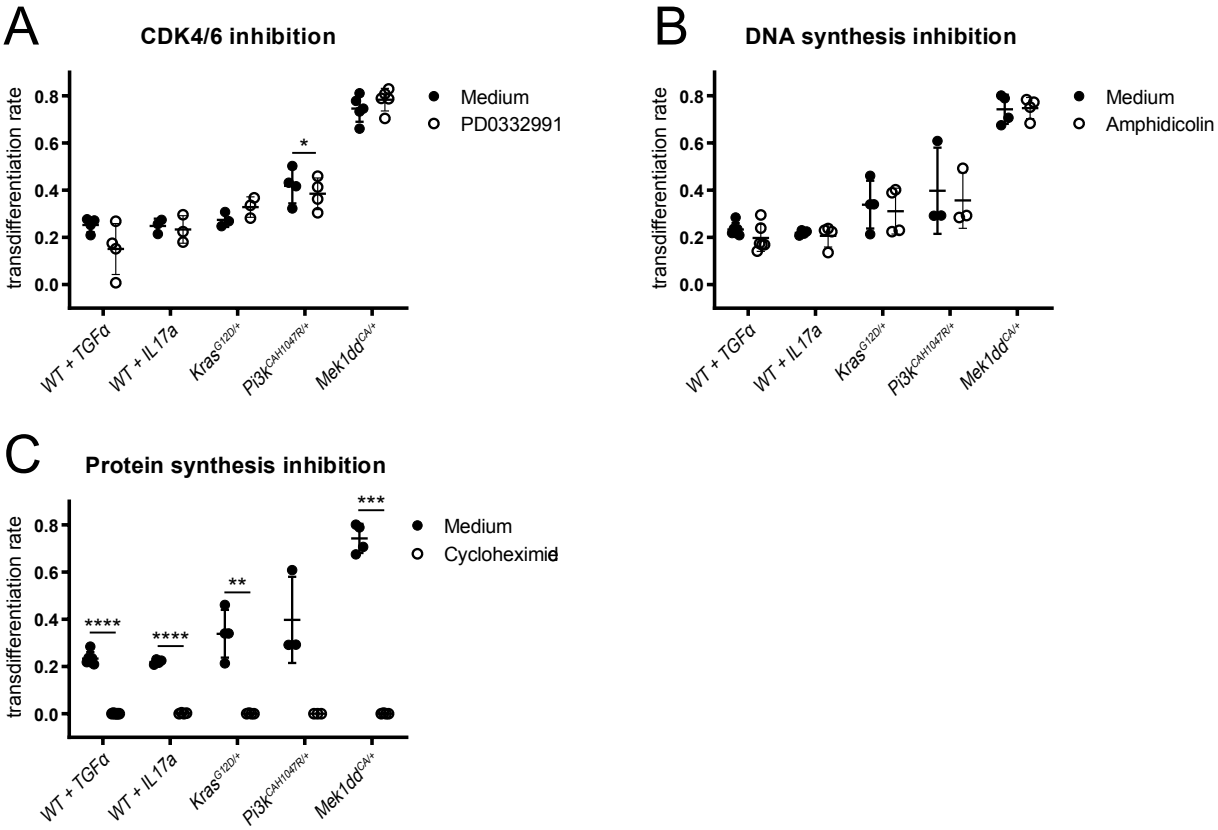

Figure 6: **Proliferation but not protein synthesis is dispensable for ADM induction. A.** Transdifferentiation rates after treatment with the CDK4/6 inhibitor PD0332991. **B.** Transdifferentiation rates after treatment with the DNA synthesis inhibitor Amphidicolin. **C.** Transdifferentiation rates after treatment with the protein synthesis inhibitor Cycloheximide. All values are displayed as mean ± SD. * = $p < 0.05$, ** = $p < 0.01$, *** = $p < 0.001$, **** = $p < 0.0001$.

Since TGFα and IL17a can both induce transdifferentiation in wild-type acinar cells, it was tested if they can also act synergistically. Therefore, wild-type acinar cell were treated with increasing concentrations of TGFα with or without the addition of IL17a. The ADM rates after TGFα-treatment increase in a dose-dependent manner (Figure 7A). Adding IL17a elevated the transdifferentiation rate of low TGFα concentrations. This combination of TGFα and IL17a led to ADM rates comparable to treatment with high concentrations of TGFα. It must be noted that there are only two biological replicates for this experiment.

In addition, it was tested if the used ligands have an effect not only on wild-type but also on mutant acinar cells. For this experiment, acinar cells harbouring an active oncogene were treated either with TGFα or with IL17a (Figure 7B). No significant changes in the transdifferentiation rates upon treatment could be observed.

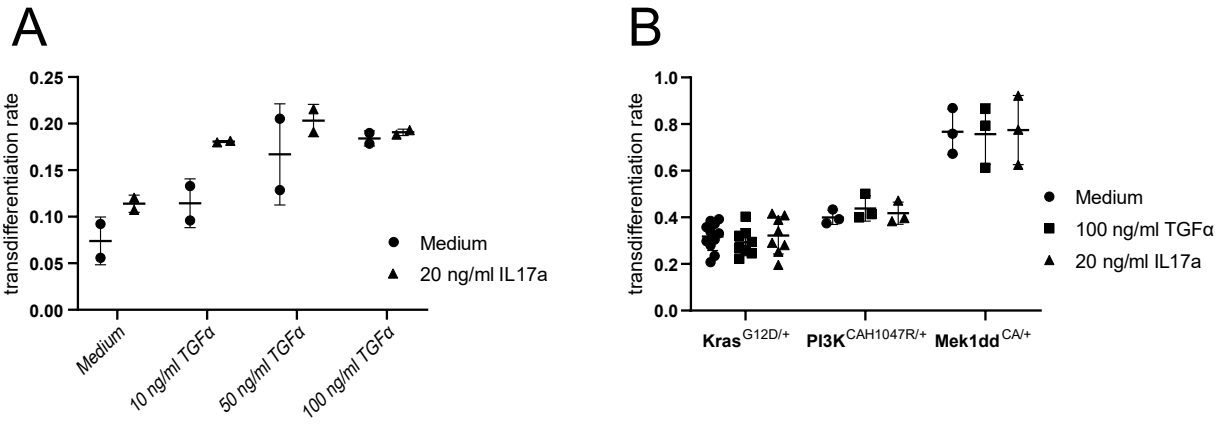

Figure 7: **Interaction between chemical and genetical inducers. A.** Transdifferentiation rates after treatment with increasing concentrations of TGFα with and without addition of IL17a. **B.** Transdifferentiation rates of oncogene harbouring acinar cells after treatment with either TGFα or IL17a. All values are displayed as mean ± SD.

3.2 Investigation of Different Signalling Pathways during the Induction of ADM

In the previous section it was shown that five inducers covering inflammatory and oncogenic stimuli are able to induce ADM *in vitro*. Since the inducers potentially have different ways of action, it is of interest to evaluate which signals are common among the different ways of induction and which are unique. In the following section, the sensitivities of the inducers towards the inhibition of central signalling pathways will be systematically investigated.
The first step was to directly target the signalling pathways of TGFα and IL17a. For TGFα, the epidermal growth factor receptor (EGFR) was either inhibited pharmacologically or genetically by a pancreas specific knock-out. For IL17a, the signal transducer and activator of transcription 3 (STAT3) was inhibited pharmacologically or genetically inactivated by alteration of a phosphorylation site.
As expected, the inhibition of EGFR both pharmacologically and genetically led to a drastic reduction of TGFα-induced ADM (Figure 8A). The inhibition of STAT3 during TGFα-induced ADM formation showed a more heterogeneous pattern. The genetic inactivation of STAT3 had only a small, non-significant impact on the ADM formation. In contrast, the pharmacological inhibition blocked ADM in two out of four biological replicates. It must be noted that the STAT3 inhibitor had an additional mild effect on STAT1 and STAT5, too. The combination of EGFR and STAT3 inhibition completely prevented ADM induction by TGFα. This effect was comparable to the effect of EGFR inhibition alone.
When wild-type acinar cells were treated with IL17a, they were sensitive towards the inhibition of STAT3, which is a downstream effector of IL17a signalling (Figure 8B). This sensitivity could be found with both the pharmacological and the genetic inhibition, with the pharmacological inhibition having a more pronounced effect. The inhibition of the EGFR showed only a minor but still significant effect on ADM formation. Combining both inhibitors led to a complete prohibition of IL17a-induced ADM formation, reflecting the STAT3-only inhibition.
Both genetic inhibitions (EGFR and STAT3) had only minor but significant effects on $KRAS^{G12D/+}$-mediated ADM induction (Figure 8C). However, the pharmacological inhibition of EGFR had even less impact on the transdifferentiation rate, also missing significance. Whereas, the pharmacological inhibition of STAT3 led to a complete blockage of the transdifferentiation. Therefore, the combined inhibition of EGFR and STAT3 was quite different in comparing the pharmacological and genetic inhibition. The combination of both inhibitors led to nearly no transdifferentiation, like it had been seen before with the STAT3 inhibitor alone.

The double knock-out of EGFR and STAT3 had only a mild effect on KRAS$^{G12D/+}$-induced ADM.

For PI3K$^{CAH1047R/+}$ and MEK1DD$^{CA/+}$ there is only data for the pharmacological inhibition available (Figure 8D). For both inducers, STAT3 inhibition led to a strong decrease of the transdifferentiation rate, and in the case of PI3K$^{CAH1047R/+}$ it reached significance. In contrast, the inhibition of EGFR had nearly no effect on the transdifferentiation rates of both inducers. Combining EGFR and STAT3 inhibition resulted in a low rate of ADM formation for PI3K$^{CAH1047R/+}$ and MEK1DD$^{CA/+}$. This low rate is comparable to the inhibition of STAT3 only.

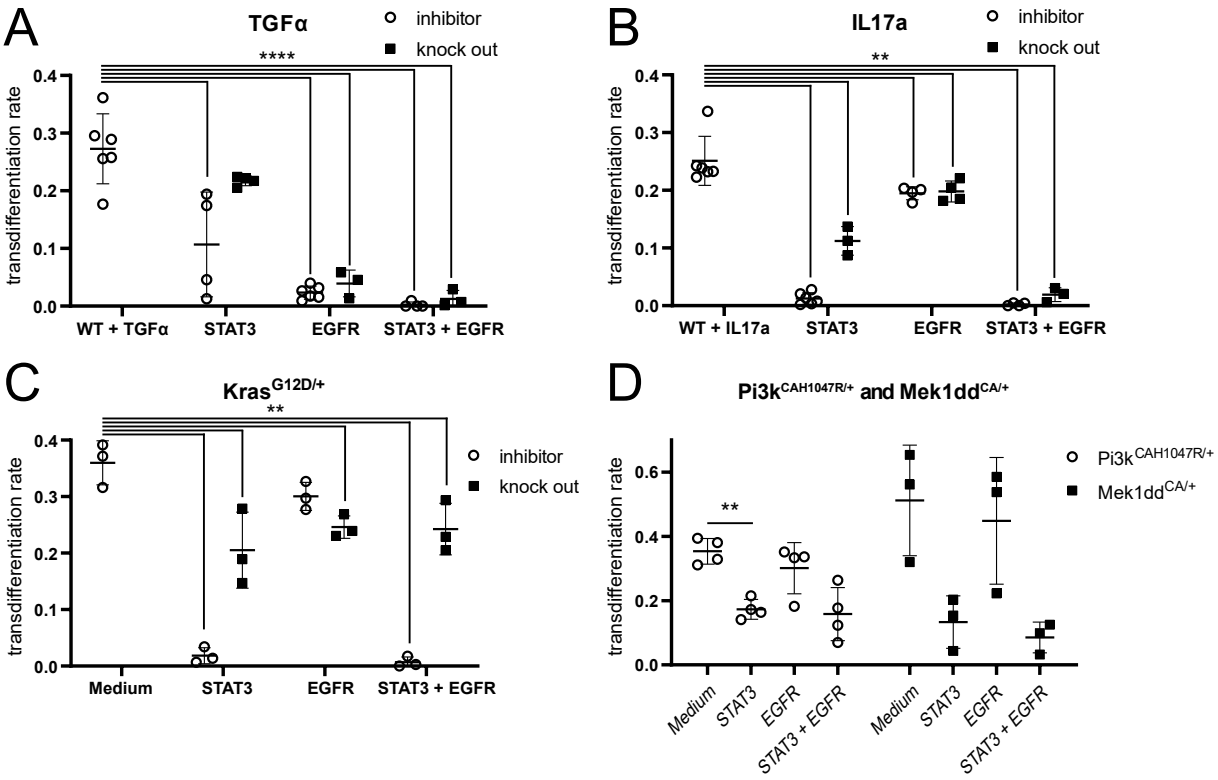

Figure 8: **Sensitivity to genetical and pharmacological inhibition of STAT3 and EGFR. A.** Transdifferentiation rates of wild-type acinar treated with TGFα after genetical or pharmacological inhibition of STAT3 or EGFR. **B.** Transdifferentiation rates of wild-type acinar treated with IL17a after genetical or pharmacological inhibition of STAT3 or EGFR. **C.** Transdifferentiation rates of KRAS$^{G12D/+}$ acinar cells after genetical or pharmacological inhibition of STAT3 or EGFR. **D.** Transdifferentiation rates of PI3K$^{CAH1047R/+}$ and MEK1DD$^{CA/+}$ acinar cells after pharmacological inhibition of STAT3 or EGFR. S3L-201 was used as a STAT3 inhibitor; Erlotinib as a EGFR inhibitor. All values are displayed as mean ± SD. ** = $p < 0.01$, **** = $p < 0.0001$.

The second step was to target the signalling of the oncogenes. PI3K was inhibited using

GDC0941, MEK by PD035901. Both the stimuli of wild-type acinar cells, TGFα and IL17a, showed a high sensitivity towards PI3K and MEK inhibition (Figure 9). Except for one outlier, all transdifferentiation rates were close to zero. Also, KRAS$^{G12D/+}$ was highly sensitive towards PI3K or MEK inhibition. Similar to TGFα- and IL17a-induced ADM, the transdifferentiation rate of KRAS$^{G12D/+}$ acinar cells were close to zero when either PI3K or MEK were inhibited. PI3K$^{CAH1047R/+}$ acinar cells were only treated with the MEK inhibitor. Inhibition of MEK led to a strong reduction of PI3K$^{CAH1047R/+}$-induced ADM formation. This reduction went down to an average of 5%. Along the same line, PI3K inhibition in MEK1DD$^{CA/+}$ acinar cells was followed by a transdifferentiation rate as low as 3.5% on average.

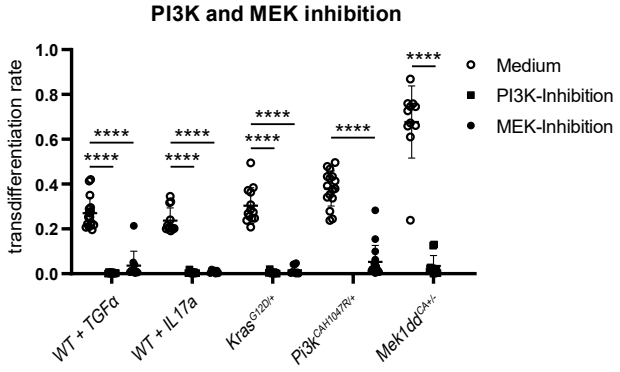

Figure 9: **Sensitivity to PI3K and MEK inhibition.** Transdifferentiation rates after treatment with the PI3K inhibitor GDC0941 or the MEK inhibitor PD035901. PI3K$^{CAH1047R/+}$ and MEK1DD$^{CA/+}$ cells were only treated with the complementary inhibitor. All values are displayed as mean ± SD. **** = $p < 0.0001$.

Following the analysis of the signalling pathways directly linked to the inducers, the sensitivity of the ADM formation by the five different inducers towards central signalling pathways was investigated.

An important factor in PDAC development is the Smad family member 4 (SMAD4). SMAD4 is activated by the TGFβ-receptor. Therefore, acinar cells with the different inducers were treated with TGFβ to investigate the role of SMAD 4 activity (Figure 10A). The transdifferentiation rate of all inducers, TGFα, IL17a, KRAS$^{G12D/+}$, PI3K$^{CAH1047R/+}$ and MEK1DD$^{CA/+}$, was reduced to around 5%. The transdifferentiation rate ranged from 2% with TGFα- to 6% with PI3K$^{CAH1047R/+}$- and MEK1DD$^{CA/+}$-induced ADM formation. Next, Rapamycin was used to inhibit mTOR, a central protein integrating signals from many different pathways (Figure 10B). Inhibition of mTOR led to drastic reduction of ADM induction with transdifferentiation rates below 10% for all inducers apart from MEK1DD$^{CA/+}$. The effect on

MEK1DD$^{CA/+}$ acinar cells was a bit more heterogeneous leading to a transdifferentiation rate of around 20% on average.
For the inhibition of the known oncogene c-MYC a pharmacological and a genetic inhibition was used. The MYC-inhibitor 10058-F4 was used in 3 different concentrations (Figure 10C). The DMSO control reflected the amount of DMSO in the highest inhibitor concentration of 100 µM. For TGFα, IL17a and KRAS$^{G12D/+}$ acinar cells, even the lowest concentration of the inhibitor led to a complete block in ADM formation. At the same time, DMSO had either no or only a very small effect. The effect of the lowest inhibitor concentration on PI3K$^{CAH1047R/+}$ and MEK1DD$^{CA/+}$ was not as big as it was for the other inducers. However, with rising concentrations of the MYC-inhibitor, the transdifferentiation rate of PI3K$^{CAH1047R/+}$ and MEK1DD$^{CA/+}$ decreased in a dose-dependent manner. For the DMSO control, there were no or only minor changes in the transdifferentiation rates. In the genetic model, acinar cells with a heterozygous knock-out of *Myc* were isolated and treated with either TGFα or IL17a (Figure 10D). The induction by TGFα- or IL17a-treatment was quite heterogeneous on the *Myc*$^{+/-}$-acinar cells. Out of the seven animals tested, ADM-induction failed in four animals completely, while the other three animals showed transdifferentiation rates which were comparable to those of wild-type animals or slightly below.

In addition, the WNT and the NFχB pathway were investigated. The central signalling protein of the WNT pathway is β-catenin. When the WNT pathway is inactive, the Glycogen Synthase Kinase 3 Beta (GSK3β) phosphorylates β-catenin which leads to its degradation. Upon activation of the WNT pathway the GSK3β is inactivated and β-catenin is stabilized. To analyse the effect of WNT activity, two different concentrations of the GSK3β inhibitor LY2090314 were used. The TGFα- and IL17a-induced ADM was reduced to 10% upon GSK3β-inhibition, regardless of the concentration (Figure 11A). In the oncogene-induced ADM, there was a dose-dependent decrease of the transdifferentiation rate that was never lower than 13%.
The central protein of the NFχB pathway is NFχB. If the pathway is inactive, NFχB is bound to the inhibitor of NFχB α (IχBα). During the activation of the pathway, IχBα gets phosphorylated by the inhibitor of Nuclear Factor Kappa B Kinase Subunit Beta (IKK2). This phosphorylation leads to the dissociation of IχBα from NFχB, so NFχB can translocate into the nucleus. To study the impact of NFχB on ADM, the IKK2 inhibitor BMS-345541 was use to block the activation of the NFχB pathway. The inhibition of IKK2 in TGFα- and IL17a-treated wild-type acinar cells led to a strong reduction of the transdifferentiation rate (Figure 11B). The same was observed when KRAS$^{G12D/+}$ acinar cells were treated with the

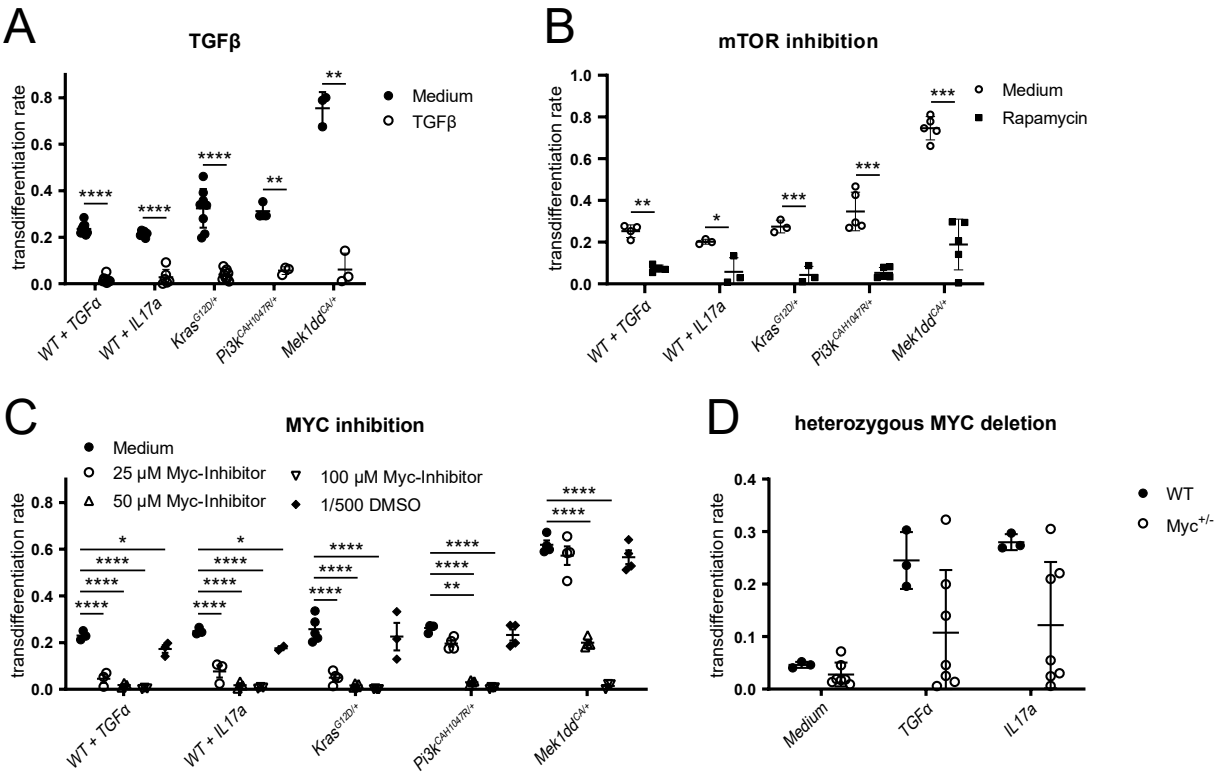

Figure 10: **Common sensitivities in all five inducers. A.** Transdifferentiation rates after treatment with TGFβ. **B.** Transdifferentiation rates after treatment with the mTOR inhibitor Rapamycin. **C.** Transdifferentiation rates after treatment with increasing concentrations of the MYC inhibitor 10058-F4. The amount of DMSO in the DMSO control corresponds to the amount of DMSO in the highest inhibitor concentration. **D.** Transdifferentiation rates of wild-type and $Myc^{+/-}$ acinar cells after treatment with either TGFα or IL17a. All values are displayed as mean ± SD. * = p < 0.05, ** = p < 0.01, *** = p < 0.001, **** = p < 0.0001.

inhibitor. In contrast, IKK2 inhibition had no effect on PI3K$^{CAH1047R/+}$-induced ADM. As for MEK1DD$^{CA/+}$ acinar cells, the treatment with the IKK2 inhibitor led to an average effect of a 50% reduction in the ADM formation. However, it has to be noted that the effect on MEK1DD$^{CA/+}$ acinar cells was very heterogeneous and not significant.

The results of the inhibition experiment can be seen summarized in a heatmap (Figure 12A). By using this representation, it becomes visible that there are three different groups of inhibitions. The first group contains inhibitors that had no effect on the transdifferentiation, namely, the inhibitors of proliferation. The second group consists of the inhibitors that had a partial effect on the ADM formation meaning that the effect of the inhibitor only reduced ADM but did not completely block it or there was a complete block of the transdifferentiation but not with all inducers. For example, the GSK3β inhibitor reduced the transdifferentiation of all

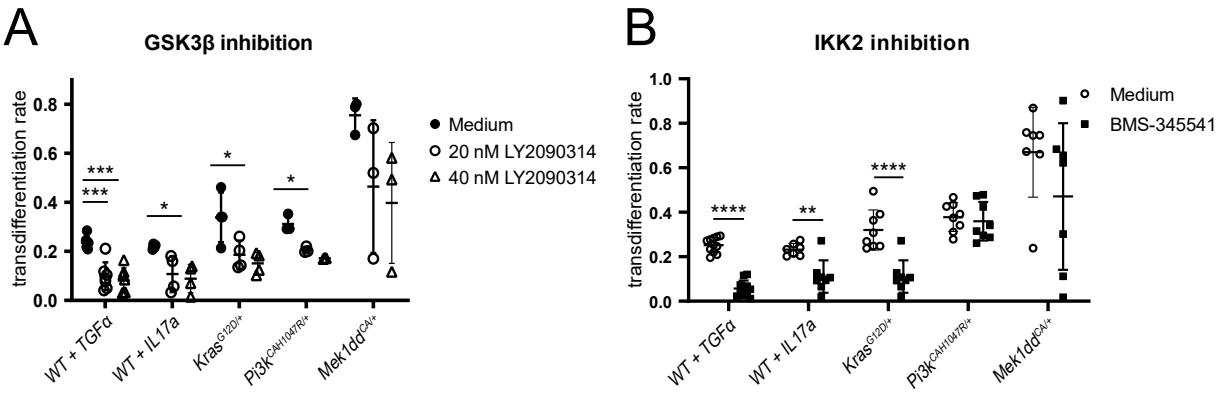

Figure 11: **Individual sensitivities in all five inducers. A.** Transdifferentiation rates after treatment with increasing concentrations of the GSK3β inhibitor LY2090314. **B.** Transdifferentiation rates after treatment with the IKK2 inhibitor BMS-345541. All values are displayed as mean ± SD. * = $p < 0.05$, ** = $p < 0.01$, *** = $p < 0.001$, **** = $p < 0.0001$.

A

	TGFα	IL17a	$Kras^{G12D/+}$	$Pi3k^{CAH1047R/+}$	$Mek1dd^{CA/+}$	
Medium	1.00	1.00	1.00	1.00	1.00	
CDK4/6 inhibitor	0.58	1.00	1.11	1.08	1.17	No inhibition
Amphidicolin	0.77	0.89	1.05	0.82	1.12	
Erlotinib	0.09	0.84	1.02	0.84	0.67	
Δstat3	0.84	0.48	0.69			
Δegfr	0.15	0.85	0.83			
IKK2 inhibitor	0.22	0.05	0.37	1.01	0.71	Partial inhibition
GSK3β inhibitor	0.31	0.38	0.51	0.49	0.60	
Δstat3; Δegfr	0.05	0.08	0.82			
S3I-201	0.41	0.05	0.06	0.48	0.20	
Rapamycin	0.28	0.25	0.14	0.15	0.28	
Erlotinib + S3I-201	0.01	0.01	0.02	0.44	0.13	
TGFβ	0.07	0.12	0.13	0.19	0.09	
MEK1/2 inhibitor	0.14	0.04	0.05	0.15		Total inhibition
MYC inhibitor	0.01	0.03	0.00	0.03	0.14	
PI3K inhibitor	0.01	0.02	0.02		0.05	
Cycloheximid	0.00	0.01	0.00	0.00	0.00	

B

	TGFα	IL17a	$Kras^{G12D/+}$	$Pi3k^{CAH1047R/+}$	$Mek1dd^{CA/+}$
Medium	0.00	0.00	0.00	0.00	0.00
CDK4/6 inhibitor	0.04	0.04	-0.16	-0.04	-0.04
Amphidicolin	-0.20	-0.09	-0.03	-0.03	-0.04
Erlotinib	0.09	0.12	-0.08	0.04	-0.21
Δstat3					
Δegfr					
IKK2 inhibitor	-0.03	-0.01	0.05	-0.06	0.00
GSK3β inhibitor	-0.16	-0.12	-0.09	-0.04	-0.15
Δsta3; Δegfr					
S3I-201	0.00	-0.05	-0.05	0.07	-0.23
Rapamycin	-0.03	-0.06	-0.02	-0.06	-0.08
Erlotinib + S3I-201	-0.06	0.01	0.01	0.17	-0.22
TGFb	-0.08	-0.14	-0.12	0.13	0.12
MEK1/2 inhibitor	0.03	-0.01	0.08	0.00	
MYC inhibtor	-0.15	0.06	-0.01	0.02	-0.04
PI3K inhibitor	0.07	0.00	-0.07		0.10
Cycloheximid	-0.11	0.04	0.09	0.02	0.06
TritonX-100	1.00	1.00	1.00	1.00	1.00

Figure 12: **Summarised results of inhibiting central signalling pathways during ADM formation. A.** All transdifferentiation rates are normalised to the transdifferentiation rate of the respective inducer. If multiple concentrations were used, values are given for the highest concentration. **B.** Treatment-induced LDHA release during ADM formation. All values were normalized to just medium treatment (defined as zero) and the TritonX-100 positive control (defined as one). No values are given for genetic models since they don't reflect a treatment. If multiple concentrations were used values are given for the highest concentration.

inducers to 30-60% of the original rates, whereas Erlotinib was only highly effective against TGFα-induced ADM. The third group comprises inhibitors that had a strong effect which was consistent within all inducers, such as the inhibitors of MEK and PI3K.

To monitor the cytotoxic effect of the inhibitor treatments, an LDH activity assay was performed using the supernatants of the acinar cell cultures. For most treatments, there was no extensive cytotoxicity (Figure 12B). Only the $PI3K^{CAH1047R/+}$ acinar cells were vulnerable towards treatment with TGFβ or the combination of EGFR and STAT3 inhibition. Negative

values can be understood as a protective function of the treatment against culture-induced cytotoxicity.

3.3 Metabolic Changes during the Induction of ADM

Many (trans-)differentiation processes are accompanied by changes in the metabolism. To gain insight into the metabolic state of transdifferentiating acinar cells, the Seahorse assay was employed. This assay allows a real-time estimation of the oxygen consumption and extracellular acidification. Additionally, ATP productions rates can be calculated from these values. Acinar cells of all different genotypes and wild-type acinar cells treated with TGFα or IL17a were isolated and kept in culture for 24 h before being assayed. In addition, cells were seeded for transdifferentiation and the transdifferentiation rate was determined after 48 h. In the Seahorse assay, it could be seen that most of the genotypes had a comparable oxygen consumption rate (OCR) (Figure 13A). Only MEK1DD$^{CA/+}$ acinar cells showed both an increased basal respiration rate as well as an elevated maximal respiration (as seen after the treatment with CCCP and pyruvate). At the level of the extracellular acidification rate (ECAR), MEK1DD$^{CA/+}$ acinar cells had the highest values at the basal state and after the inhibition with Oligomycin (Figure 13B). In contrast to KRAS$^{G12D/+}$ and (stimulated) wild-type acinar cells, PI3K$^{CAH1047R/+}$ acinar cells showed an increased acidification rate ranging between wild-type and MEK1DD$^{CA/+}$ acinar cells. This effect was even more pronounced after the treatment with Oligomycin.
From the OCR and ECAR data, it is possible to calculate the ATP production rates from both glycolysis and oxidative phosphorylation (OxPhos) separately (Figure 13C). When looking at the ATP from OxPhos, there are no big changes among the genotypes apart from the higher ATP production of Mek1dd$^{CA/+}$ acinar cells. In contrast to this, there was more variation in the ATP derived from glycolysis. The ATP production rose slightly from stimulated wild-type to KRAS$^{G12D/+}$ acinar cells. This difference was even bigger with PI3K$^{CAH1047R/+}$ and was maximal with MEK1DD$^{CA/+}$ acinar cells. The transdifferentiation rates of the acinar cells 24 h after these measurements followed the same pattern (Figure 13D). This hints towards a potential role of the glycolysis during ADM formation.

To further investigate this hypothesis, the expression of the glucose transporter 1 (GLUT1) and the lactate dehydrogenase A (LDHA) were analysed on RNA and protein level (Figure 14A, B, C). The mRNA levels for *Glut1* of wild-type acinar cells increased slightly after being cultured in medium (d0 vs Med). Upon stimulation with TGFα the expression level increased significantly, whereas the stimulation with IL17a only led to a graduate increase. A significant increase in the *Glut1* expression could also be observed for KRAS$^{G12D/+}$ and PI3K$^{CAH1047R/+}$ acinar cells after transdifferentiation (d0 vs d3 or d2, respectively). In

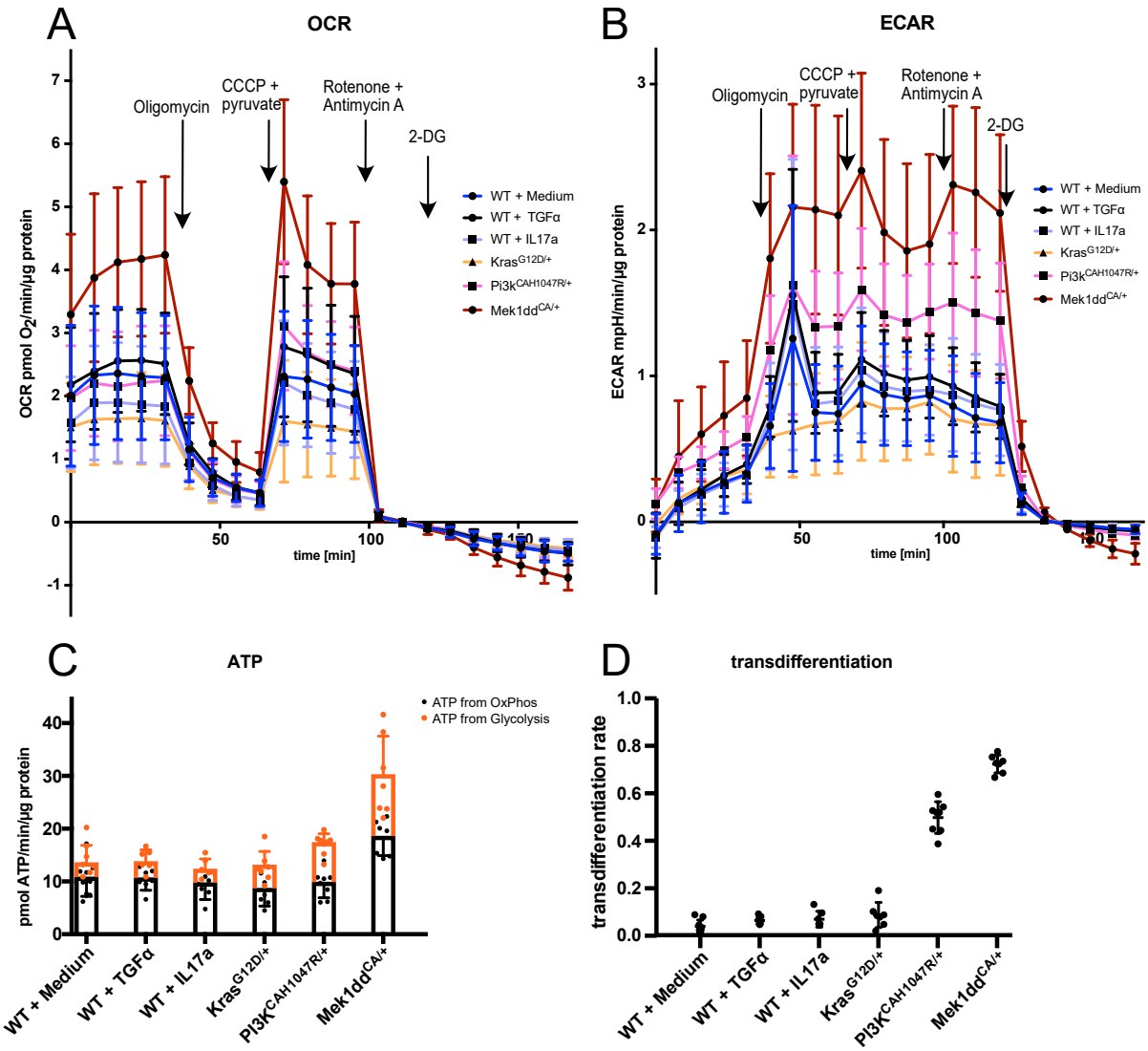

Figure 13: **ATP production during ADM development. A.** Oxygen consumption rate of acinar cells 24 h after isolation. Values were normalised to the protein amounts per sample. **B.** Extracellular acidification rate of acinar cells 24 h after isolation. Values were normalised to the protein amounts per sample. **C.** Calculated ATP production rates from oxidative phosphorylation and glycolysis. **D.** Transdifferentiation rate at day two after isolation for the animals and conditions in A and B. All values are displayed as mean ± SD.

MEK1DD$^{CA/+}$ acinar cells, there were no changes on the mRNA level. The expression of *Ldha* displays a homogeneous pattern: Within all cultured acinar cells the mRNA levels for *Ldha* were significantly increased.

In addition, these expression patterns of GLUT1 and LDHA were confirmed at the protein level (Figure 14C). The protein levels of GLUT1 increase dramatically with transdifferentiation for all five inducers. The LDHA levels were stable during transdifferentiation within

KRAS$^{G12D/+}$ and MEK1DD$^{CA/+}$ acinar cells. In stimulated wild-type and PI3K$^{CAH1047R/+}$ acinar cells, the levels rose during transdifferentiation to the levels of the other inducers. When acinar cells were stained for GLUT1 the staining co-localized with the transdifferentiation marker KRT19 (Figure 14D). Taken together these findings, there is a conserved upregulation of the key proteins of the anaerobe glycolysis during the course of ADM.

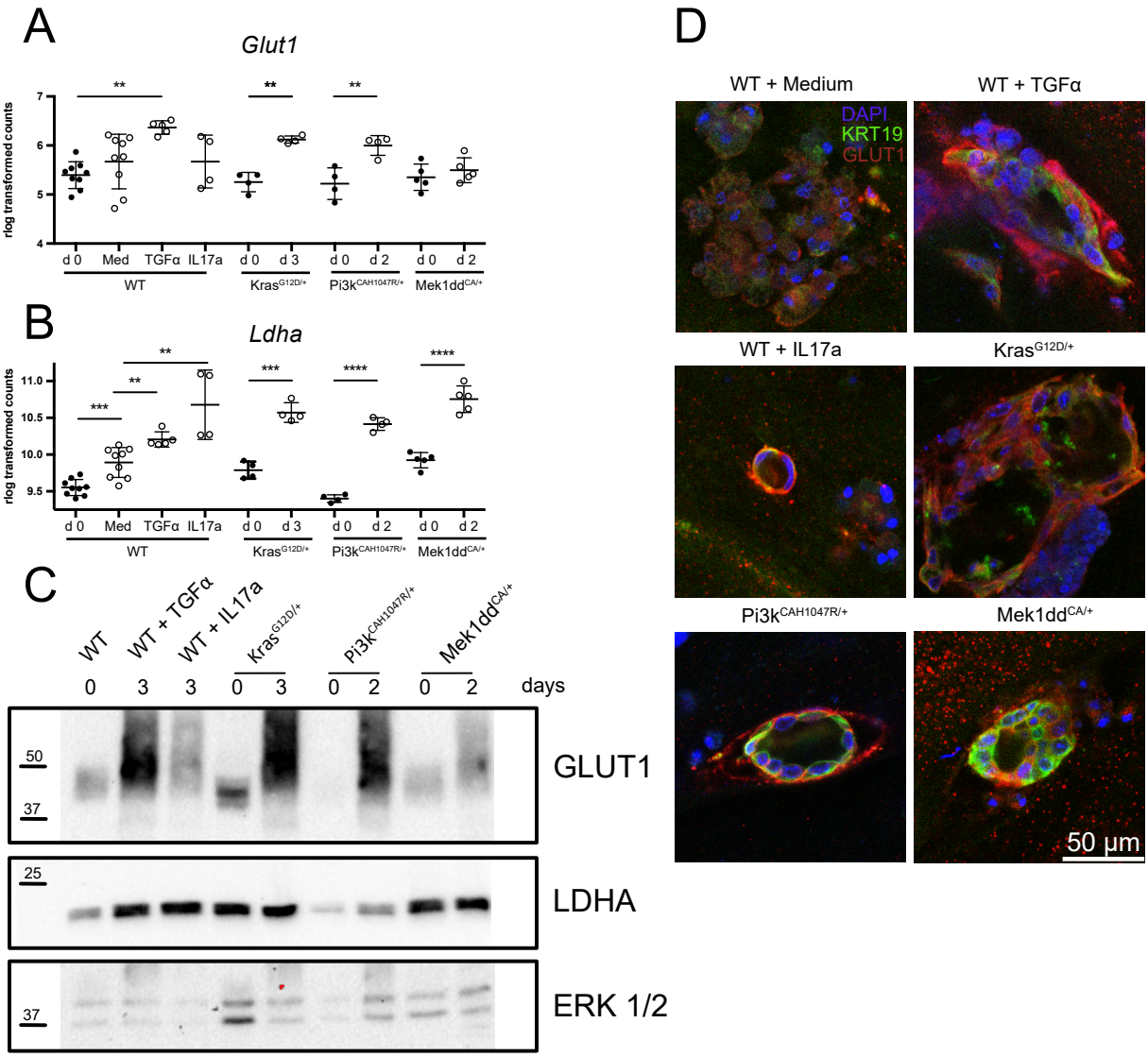

Figure 14: **GLUT1 and LDHA are upregulated during ADM. A, B.** mRNA expression of *Glut1* (**A**) and *Ldha* (**B**) in acinar cell before ("d0") and after transdifferentiation ("d2" and "d3"). **C.** Western blot for GLUT1 and LDHA. ERK1/2 served as loading control. Proteins from acinar cells before and after transdifferentiation were loaded. **D.** Stained acinar cells after transdifferentiation. Cells were stained for GLUT1 (red), KRT19 (green) and DAPI (blue). All values are displayed as mean ± SD. ** = $p < 0.01$, *** = $p < 0.001$, **** = $p < 0.0001$.

To get a more detailed picture of the metabolite distribution before and after transdifferentiation, an NMR-based metabolomic analysis was performed with freshly isolated and cultured acinar cells. At the same time the transdifferentiation rates of the cultured acinar cells were determined to correlate these rates with the measured metabolite levels. Both the intracellular and extracellular amounts of glucose decreased in comparison to freshly isolated acinar cells (Figure 15 A, B). This decrease became more pronounced with higher transdifferentiation rates. At the same time, the intracellular and extracellular levels of lactate were increased with a more prominent increase in the extracellular levels (Figure 15C, D). This increase was higher with higher transdifferentiation rates. The combination of the glucose and lactate levels hints towards a high rate of glucose uptake and conversion into secreted lactate in transdifferentiating acinar cells.

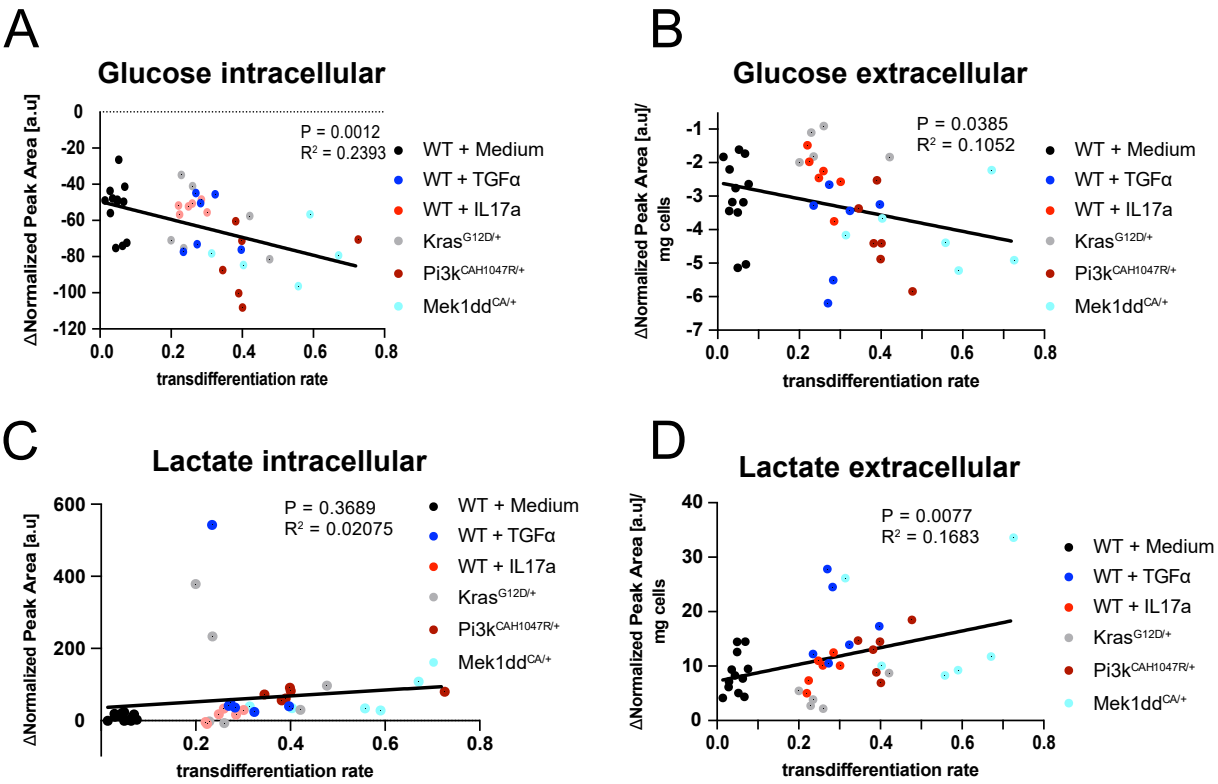

Figure 15: **Glucose uptake and lactate production during ADM. A, C.** Amounts of intracellular glucose (**A**) and lactate (**C**) in transdifferentiated acinar cell. Values for intracellular glucose/lactate of each animal before transdifferentiation were subtracted from the transdifferentiated ones. **B, D.** Amounts of extracellular glucose (**B**) and lactate (**D**) in supernatants of transdifferentiated acinar cells. Values for unused medium were subtracted and the differences were normalised by the cell pellet weight of the respective acinar cells.

To have an additional look at the mitochondrial metabolism, intermediates of the TCA were

analysed. The total levels of citrate were only slightly altered with the weak inducers (stimulated wild-type and KRAS$^{G12D/+}$) (Figure 16A). In contrast, there was a strong decrease in citrate levels with the strong inducers (PI3K$^{CAH1047R/+}$ and MEK1DD$^{CA/+}$). Intracellular levels of both succinate and fumarate were also decreased compared to basal levels (Figure 16B, C). The decrease of both metabolites was independent of the transdifferentiation rate.

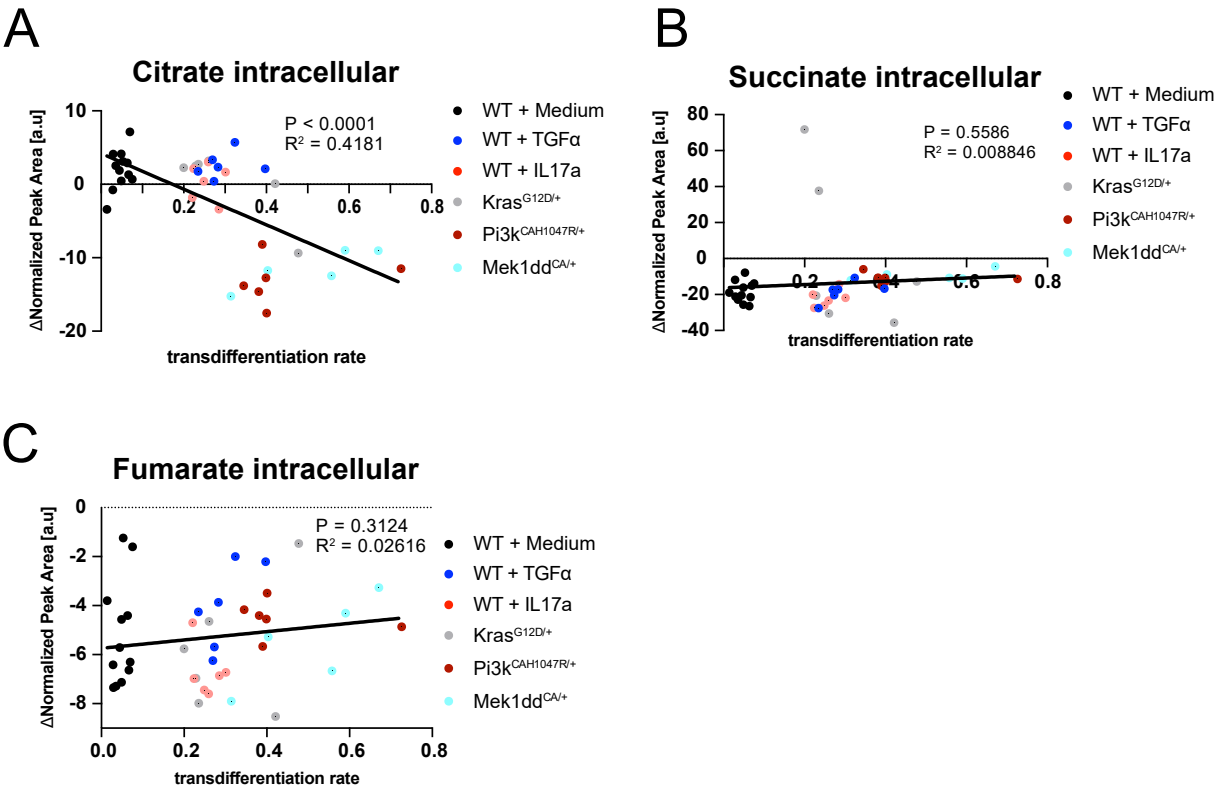

Figure 16: **Changes in TCA metabolites during ADM. A-C.** Amounts of intracellular citrate (**A**), succinate (**B**) and fumarate (**C**) in transdifferentiated acinar cells. Values for intracellular citrate/succinate/fumarate of each animal before transdifferentiation were subtracted from the transdifferentiated ones.

In addition to the central energy metabolism, intra- and extracellular amounts of amino acids were investigated. Essential amino acids like leucine, isoleucine and valine were enriched in cultured acinar cells independently of the transdifferentiation rate (Figure 17A, B, C). At the same time, the extracellular amounts of these amino acids were decreased hinting towards an uptake and consumption of essential amino acids (Figure 17D, E, F). This effect was slightly stronger with higher transdifferentiation rates. In contrast to the essential amino acids, non-essential amino acids like glutamine and glutamate decreased in their intracellular levels during culturing (Figure 17G, H). In case of glutamine, the decrease was independent of

the transdifferentiation rate while the decrease of glutamate was lower with higher ADM formation. On the extracellular side, the glutamine levels decreased as well, again, independently of the transdifferentiation (Figure 17I). In contrast to this, extracellular levels of glutamate were increased (Figure 17J). This increase was less pronounced at high transdifferentiation rates.

To not only investigate the abundances of metabolites but also study the changes in the metabolic fluxes during transdifferentiation, acinar cells were treated with ^{13}C-labelled glucose (Figure 18). The first intracellular metabolite of glucose is hexose-P. The total amount of hexose-P was decreased with time in all conditions (Figure 18A). This decrease was in line with the decrease of glucose seen in the NMR analysis of freshly isolated and transdifferentiated acini (Figure 15A). The preserved relative labelling pattern between 2 h and 24 h after isolation indicated an increased throughput of hexose-P rather than a consumption without new synthesis. While the isotopologue NP+6 was derived immediately from fully labelled glucose, the isotopologue NP+3 hinted towards glucose that entered glycolysis via the pentose phosphate pathway (PPP). When glucose is metabolised via the PPP, it can re-enter glycolysis as fructose-P. Due to the different steps of the PPP this fructose-P was labelled as NP+3. Consistently, the proportion of pentose-5-P, the central metabolite of the PPP, labelled as NP+3, increased during incubation in all conditions (Figure 18B). This increase went along with an increase of the total amount of pentose-5-P in all conditions apart from wild-type acini treated with either medium or IL17a.
For pyruvate, the final product of the glycolysis, there was no clear pattern in the changes over time among the conditions (Figure 18C). While there was a decrease of both abundance and labelling with KRAS$^{G12D/+}$ acini, IL17a-treated wild-type and PI3K$^{CAH1047R/+}$ acinar cells displayed a strong increase of abundance and labelling. In the other conditions, there were no pronounced changes. The strong labelling of 30-40% of the pyruvate underlined the high throughput of pyruvate. To end glycolysis in an anaerobic way, pyruvate can be reduced to lactate regenerating the NADH produced during glycolysis. As well as for pyruvate, there was no clear pattern for the changes in the abundance and labelling of lactate (Figure 18D). The most distinct change was the increase in the labelled lactate with TGFα-treated wild-type acinar cells. The high percentage of labelled lactose in all conditions indicated that most of the lactate was produced within the 2 hours of labelling.
If pyruvate is used for OxPhos, it is transferred into the mitochondria and feeds into the TCA cycle. The first metabolites of the TCA cycle are citrate and isocitrate. Since they could not be separated by the applied method, they are displayed together (Figure 18E).

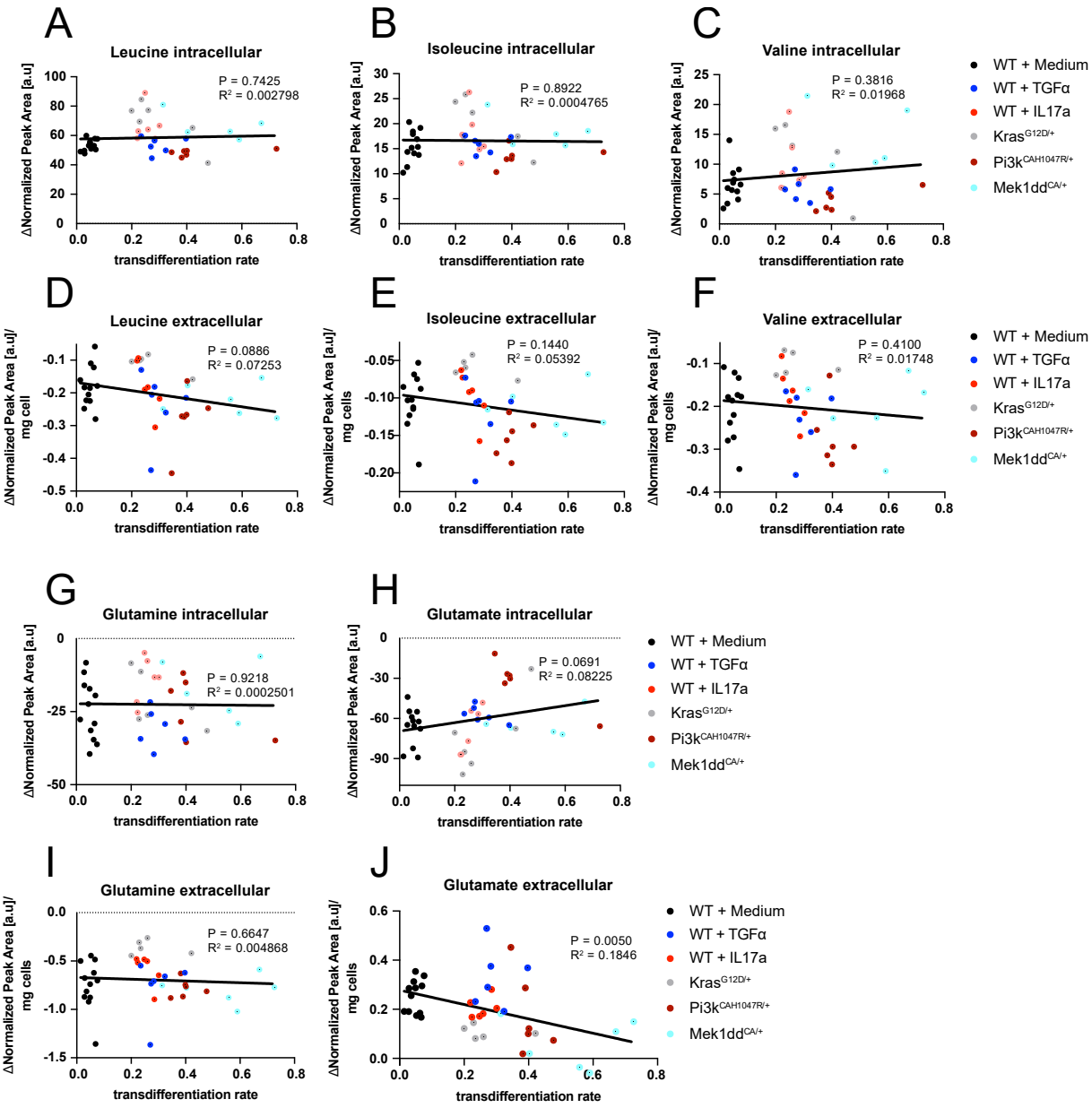

Figure 17: **Changes in amino acids during ADM. A-C, G, H.** Amount of intracellular leucine (**A**), isoleucine (**B**), valine (**C**), glutamine (**G**) and glutamate (**H**) in transdifferentiated acinar cells. Values for intracellular metabolite amounts of each animal before transdifferentiation were subtracted from the transdifferentiated ones. **D-F, I, J.** Amount of extracellular leucin (**D**), isoleucine (**E**), valine (**F**), glutamine (**I**) and glutamate (**J**) in supernatants of transdifferentiated acinar cells. Values for unused medium were subtracted and the differences were normalised by the cell pellet weight of the respective acinar cells.

Among all conditions, the amount of citrate/isocitrate is either stabilised (wild-type treated with medium or TGFα) or decreased (all others) during the incubation time. The decrease was most pronounced with MEK1DD$^{CA/+}$ acinar cells. In addition to this, the labelling

of the citrate/isocitrate was strongly diminished, too. This indicates that there was only a small turnover of these metabolites. The decrease of citrate/isocitrate especially in the strong inducers was in line with the results of the NMR analysis of freshly isolated and transdifferentiated acini (Figure 16A). Not only citrate/isocitrate was lower in its abundance but also α-ketoglutarate, another metabolite of the the TCA cycle. In all conditions there was a drastic decrease in both abundance and labelling after incubation (Figure 18F).
The combination of the NMR and the isotopic tracing analysis suggested an important role of glycolysis during ADM formation while OxPhos was decreasing in relevance.

To investigate if the metabolic changes towards more glycolysis are also functionally relevant, acinar cells of all genotypes were treated with inhibitors targeting glycolysis. Therefore, the glucose import via the glucose transporter 1 (GLUT1), the first enzyme of glycolysis, namely hexokinase 1 (HK1) and the final enzyme of the anaerobic glycolysis, lactate dehydrogenase (LDHA), were targeted (Figure 19). After treatment with the GLUT1 inhibitor WZB117, a drastic reduction in the transdifferentiation was observed (Figure 19A). For strong ADM inducers like PI3K$^{CAH1047R/+}$ and MEK1DD$^{CA/+}$, there was only a mild effect on ADM formation at low concentrations of WZB117. At higher concentrations, there were no big differences among the inducers. Inhibition of HK1 by 2-DG resulted in a dose-dependent attenuation of transdifferentiation (Figure 19B). This reduction was independent of the stimulus. To test the dependence on the anaerobic branch of glycolysis, LDHA was inhibited using galloflavin (Figure 19C). The inhibition led to a dose-dependent decrease of transdifferentiation. In case of stimulated wild-type or KRAS$^{G12D/+}$ acinar cells, the transdifferentiation rate nearly dropped to zero.
Taken together, these findings show that the increase in the importance of glycolysis is not only a bystander effect but fundamental to ADM formation.

Besides glycolysis, glutaminolysis can also provide substrates for the mitochondrial metabolism. During transdifferentiation the expression of the mitochondrial glutamine transporter *Slc25a12* was significantly down regulated in stimulated wild-type acinar cells (Figure 20A). Acinar cells harbouring oncogenes had lower expression levels already after isolation. The enzyme glutaminase (GLS) produces glutamate from glutamine which than can feed into the TCA cycle. The expression levels of *Gls* mainly remained unaltered during transdifferentiation (Figure 20B). Only in PI3K$^{CAH1047R/+}$ acinar cells, there was a small increase in the RNA levels.

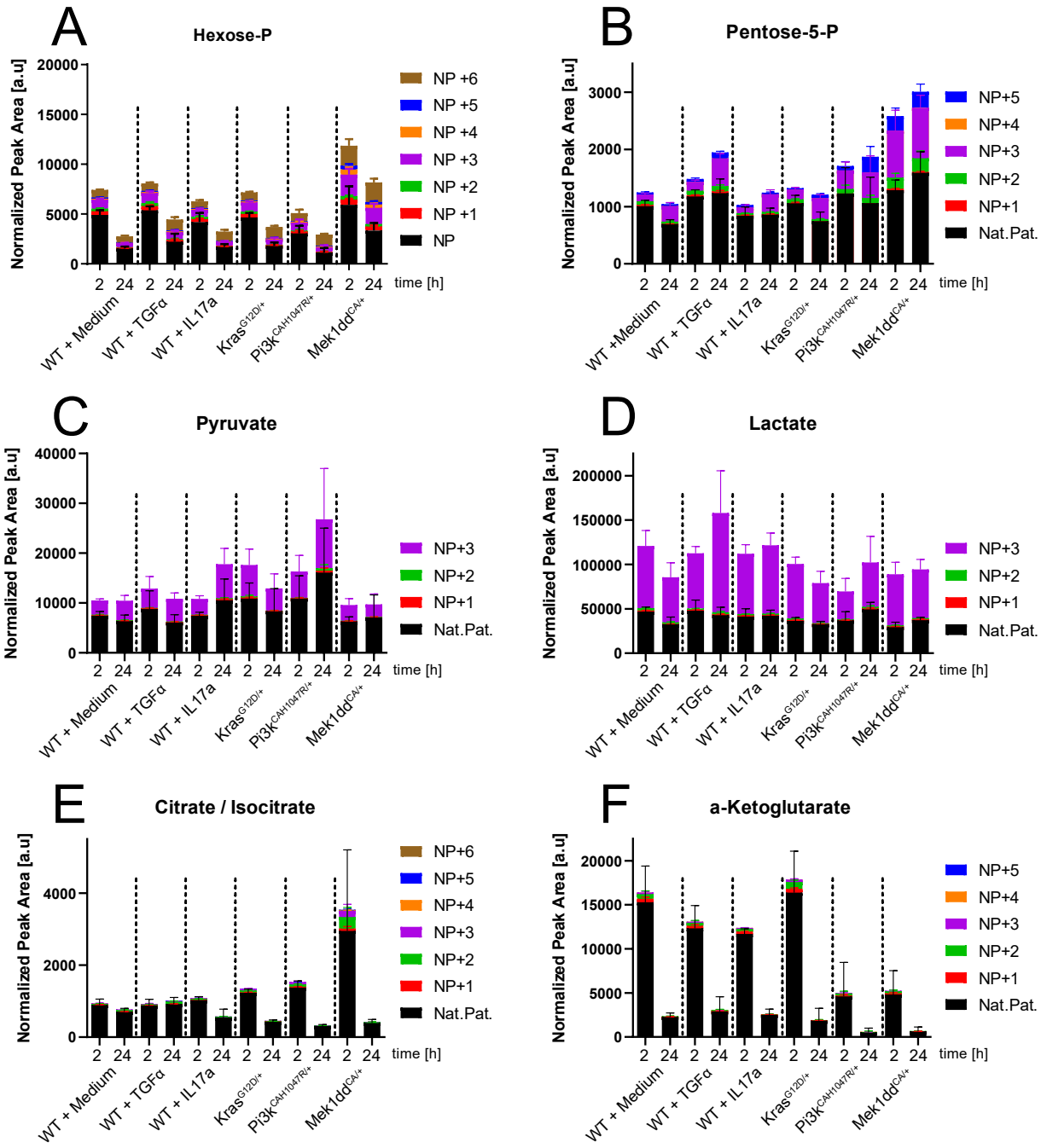

Figure 18: **Isotopologue distribution of central metabolites during transdifferentiation after ^{13}C-labelling.** Isotopologue distribution of hexose-P (**A**), pentose-5-P (**B**), pyruvate (**C**), lactate (**D**), citrate/isocitrate (**E**) and α-ketoglutarate (**F**) after 2 h of treatment with ^{13}C-glucose. Acinar cells have been treated immediately after isolation or after 22 h. All values are displayed as mean ± SD.

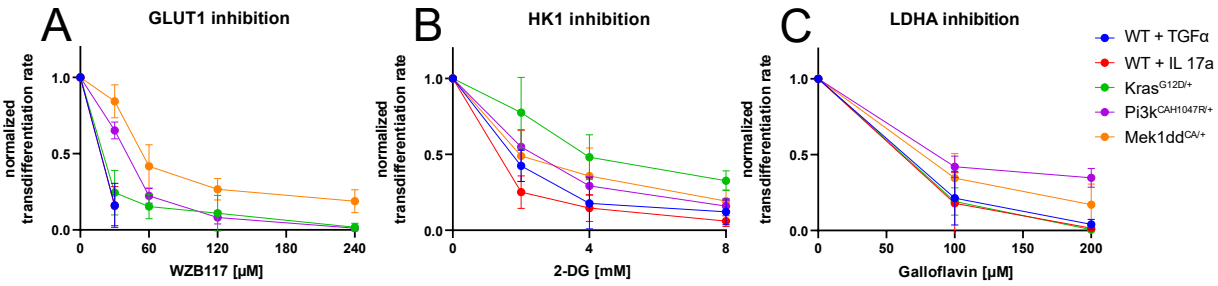

Figure 19: **Influence of glycolysis inhibition on transdifferentiation rates. A.** Transdifferentiation rates after treatment with different concentrations of the GLUT1 inhibitor WZB117. **B.** Transdifferentiation rates after treatment with different concentrations of the HK1 inhibitor 2-DG. **C.** Transdifferentiation rates after treatment with different concentrations of the LDHA inhibitor galloflavin. All values are displayed as mean ± SD.

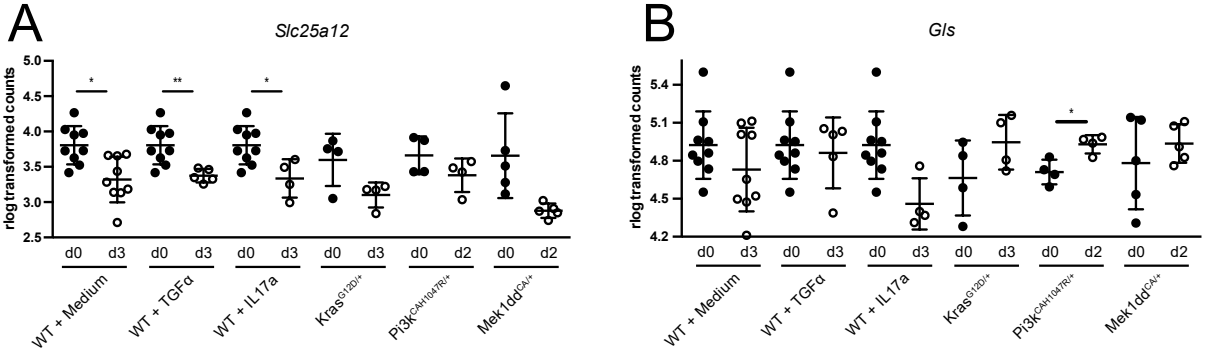

Figure 20: **Expression of glutaminolysis-associated transcripts.** mRNA expression of *Slc25a12* (**A**) and *Gls* (**B**) in acinar cells before ("d0") and after transdifferentiation ("d2" and "d3"). All values are displayed as mean ± SD. * = $p < 0.05$, ** = $p < 0.01$.

In addition to the expression data, the functional importance of glutaminolysis was tested. To inhibit the function of GLS and thereby the usage of glutamine for ATP production, the inhibitor BPTES was used (Figure 21). GLS inhibition had no effect on the transdifferentiation rate. Only with TGFα-stimulated wild-type acinar cells, there was a minor impairment in ADM formation.
In summary, the mitochondrial capacity for glutaminolysis is downregulated and glutaminolysis itself is dispensable for transdifferentiation.

All results presented so far, led to the conclusion that glycolysis is the main source of energy during the process of ADM. Still, the oxygen consumption of transdifferentiating acinar cells was comparable or even higher than in medium-treated wild-type acini (Figure 13). The enzyme linking glycolysis and OxPhos is the pyruvate dehydrogenase (PDH). PDH uses pyruvate from the glycolysis to produce acetyl-CoA. To investigate the role of the mitochon-

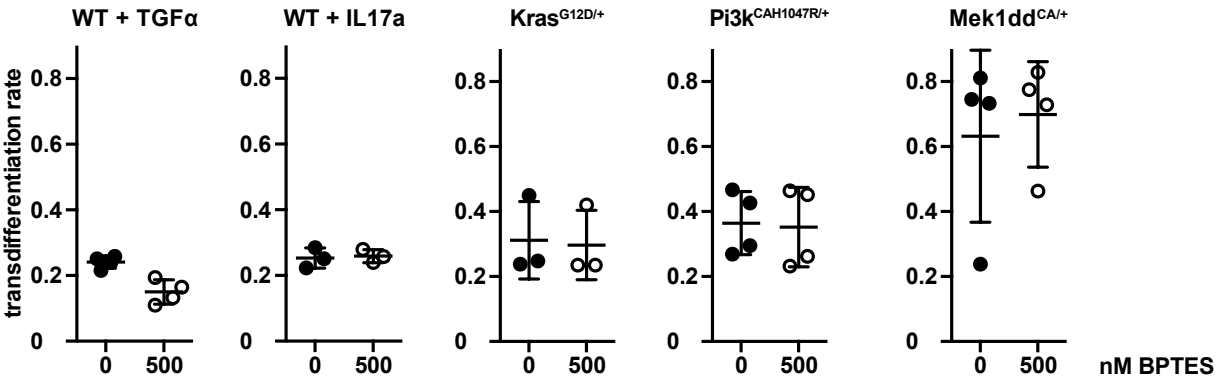

Figure 21: **Influence of glutaminolysis inhibition on transdifferentiation rates.** Transdifferentiation rates after treatment with the glutaminase inhibitor BPTES. All values are displayed as mean ± SD

drial metabolism, the phosphorylation status of pyruvate dehydrogenase (PDH) was assessed (Figure 22A). During transdifferentiation, the phosphorylated, thus, inactive form of PDH decreased. At the same time, the total amount of PDH decreased, too, but to a lesser extent. In line with this finding, the inhibition of PDH using CPI-613 resulted in a dose-dependent decrease in transdifferentiation (Figure 22B). Among all different inducers, it led to a decrease of 50% in ADM formation.

To further investigate the role of the mitochondrial metabolism, several complexes of the electron transport chain (ETC) were inhibited by Rotenone, Antimycin and Oligomycin for complexes I, III or V, respectively (Figure 22C). The inhibition of the ETC resulted in a drastic decrease in ADM formation in all inducers. Especially blockage of complex I by Rotenone led to transdifferentiation rates around zero. An additional way of inhibiting the ETC is via uncoupling. Uncoupling means that the proton gradient of the mitochondrial membrane is reduced without producing ATP. Therefore, the proton gradient can not be used for ATP production any more while, at the same time, the complexes of the ETC remain functional. Surprisingly, uncoupling of the ETC using CCCP had either no or only minor effects on the transdifferentiation (Figure 22C). This result was opposing the other inhibitors of the ETC. To combine these two findings, acinar cells were treated with either Oligomycin or CCCP or the combination of both (Figure 22D). Treatment with CCCP clearly led to a rescue of the Oligomycin-mediated inhibition of transdifferentiation. In TGFα-induced wild-type or $KRAS^{G12D/+}$-harbouring acinar cells, this rescue was only partial. For the other inducers, there was a complete rescue.

The combination of Oligomycin and CCCP led to a situation where there is no ATP production via the mitochondria because of the inhibition of complex V. At the same time, the ETC is still operating because CCCP degrades the proton gradient of the inner mitochondrial membrane.

Since ADM is still taking place under these conditions, a functional mitochondrion but not the ATP from it is needed for transdifferentiation.

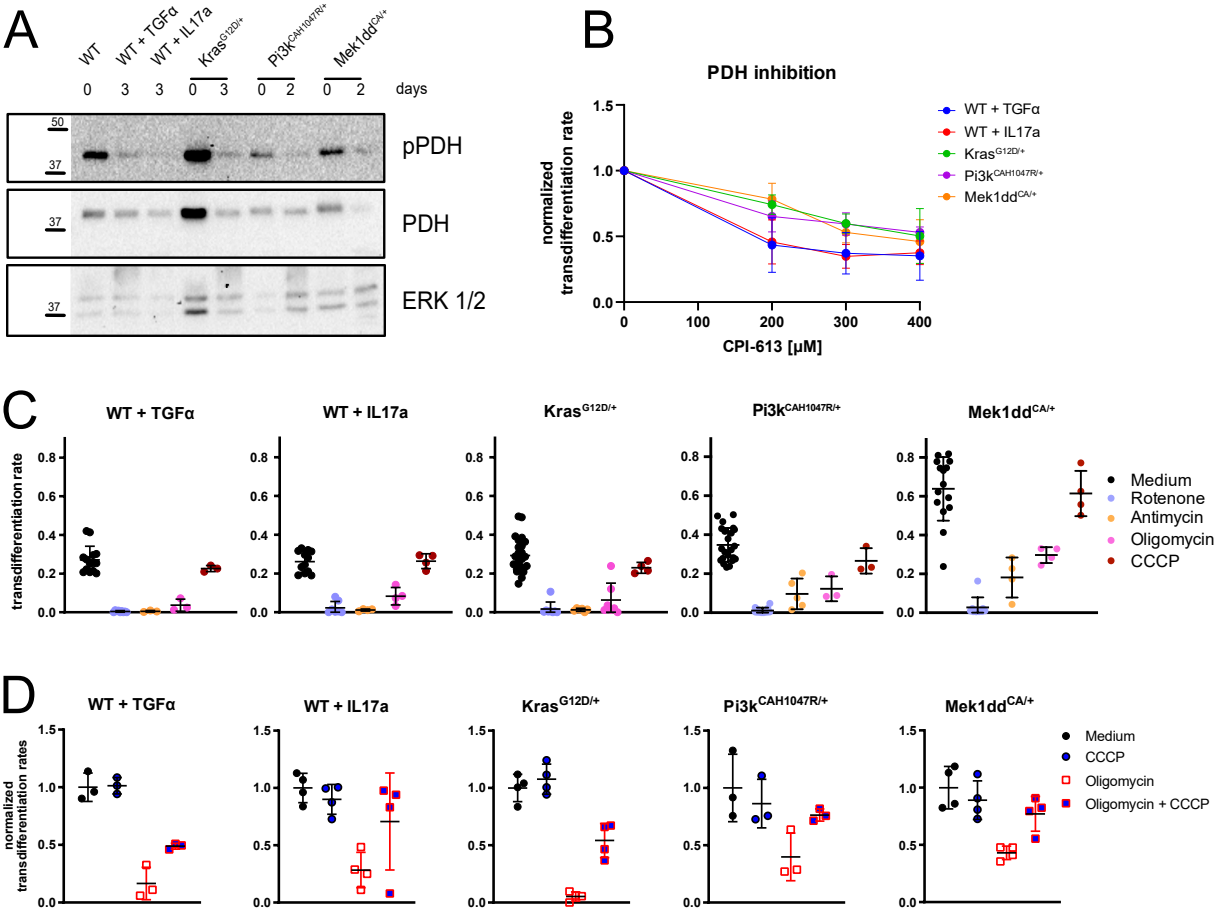

Figure 22: **Influence of inhibition of the electron transport chain (ETC) on transdifferentiation rates. A.** Western blot for pPDH and PDH. ERK1/2 served as loading control. Proteins from acinar cells before ("d0") and after transdifferentiation ("d2" and "d3") were loaded. **B.** Transdifferentiation rates after treatment with different concentrations of the PDH inhibitor CPI-613. **C.** Transdifferentiation rates after treatment with the respiratory chain inhibitors Rotenone (complex I), Antimycin (complex III), Oligomycin (complex V) and CCCP (uncoupling). **D.** Transdifferentiation rates after treatment with Oligomycin, CCCP and the combination. All values are displayed as mean ± SD.

In order to understand the role of mitochondria metabolism during transdifferentiation, the metabolome of acinar cells was analysed. To this end, isotopic tracing using fully labelled ^{13}C-glucose was employed. Acinar cells were harvested either 2 or 24 h after incubation in suspension. In addition, cells were treated with Oligomycin or CCCP or both in parallel to the conditions in Figure 22D. The total abundance of serine mainly followed the effect of the inhibitors seen on the transdifferentiation (Figure 23A). Serine amounts rose in all

different inducers comparing the 2 h and 24 h timepoint. This increase was diminished by the addition of Oligomycin. By adding CCCP to Oligomycin-treated acinar cells, the serine levels rose again compared to the Oligomycin-treated acinar cells. There was only a partial rescue with TGFα-induced wild-type or KRAS$^{G12D/+}$-harbouring acinar cells, but a complete restoration for all other inducers. To functionally validate this finding, acinar cells were again treated with Oligomycin but this time serine was supplemented instead of the CCCP treatment (Figure 23B). The addition of serine led to a rescue of the Oligomycin effect. This rescue was less pronounced with TGFα-induced wild-type or KRAS$^{G12D/+}$-harbouring acinar cells as seen before with CCCP or on the serine levels. For IL17a-induced wild-type or MEK1DD$^{CA/+}$-harbouring acinar cells, the rescue was close to 100%.

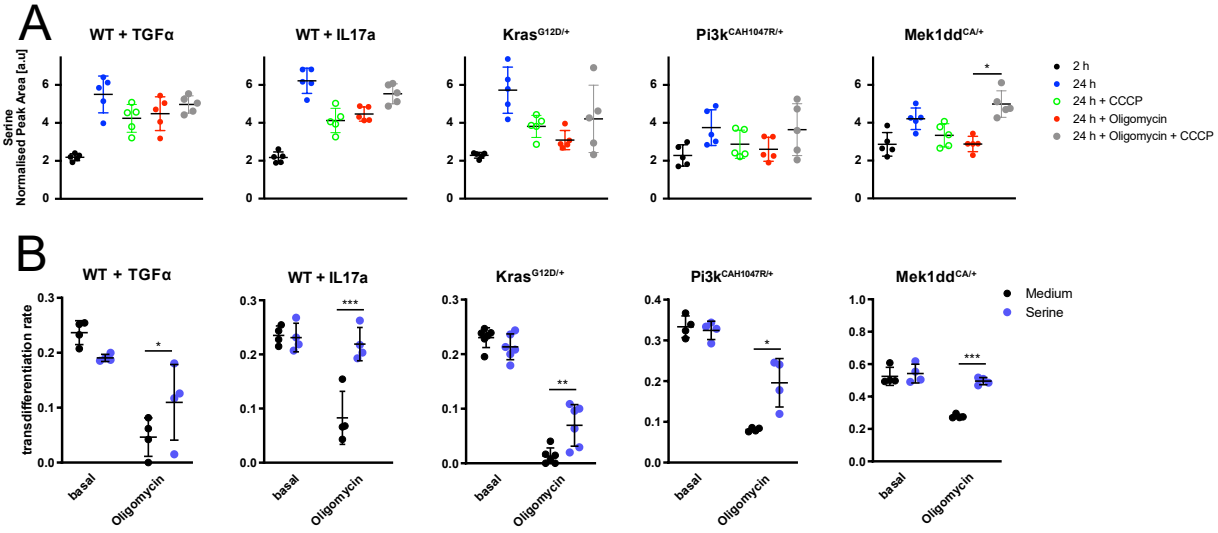

Figure 23: **Role of serine on ADM formation. A.** Total abundance of serine in acinar cells 2 h or 24 h after isolation in suspension culture. Cell were treated with either Oligomycin or CCCP or both. **B.** Transdifferentiation rates after treatment with Oligomycin, serine or the combination. All values are displayed as mean ± SD. * = $p < 0.05$, ** = $p < 0.01$, *** = $p < 0.001$.

De novo synthesis of serine originates from glycolysis via 3-phosphoglycerate (Figure 25). The first step of synthesis requires NAD^+. The produced NADH is restored by the ETC which links serine synthesis to a functional ETC. To show that NAD^+ is important within the rescue experiments of the Oligomycin phenotype, nicotinamide (NAM) was used. NAM is a membrane permeable precursor of NAD^+. In order to compare the effects of CCCP, serine and NAM, acinar cells were treated with all three substances in the absence or presents of Oligomycin in parallel (Figure 24A). For all inducers, there were no changes in the basal transdifferentiation rate caused by any of the rescuing compounds (CCCP, serine, NAM). Treatment with Oligomycin led to a decrease in ADM formation as seen before. Addition

of CCCP and serine but also of NAM to Oligomycin-treated acini was followed by a rescue of the phenotype. In case of IL17a-treated wild-type or PI3K$^{CAH1047R/+}$- or MEK1DD$^{CA/+}$-harbouring acinar cells, there was a complete rescue with transdifferentiation rates in the range of the Oligomycin-free conditions. For TGFα-treated wild-type acini the transdifferentiation rates of the rescued conditions were slightly lower than in the Oligomycin-free conditions. The ADM formation of KRAS$^{G12D/+}$ harbouring acinar cells was only partially rescued. But still the effects of the different rescues were comparable.
To underline the importance of serine synthesis during ADM directly, acinar cells were treated with three different inhibitors against the first enzyme of serine synthesis, phosphoglycerate dehydrogenase (PHGDH): NTC-502, NTC-503, CBR-5884. Treatment with Oligomycin was used as a reference (Figure 24B). In most conditions, inhibition of PHGDH was followed by a strong decrease in transdifferentiation. The resulting ADM rates were comparable to those of Oligomycin-treated acini. For KRAS^{G12D} harbouring acini the effect of PHGDH inhibition was less pronounced. This finding was in line with the smaller rescue by CCCP, serine or NAM seen before (Figure 24A).
To combine these findings, the effect of the PHGDH inhibitor NTC-502 on the CCCP rescue was investigated (Figure 24C). As seen before, the addition of CCCP was able to re-establish transdifferentiation of Oligomycin-treated acini. The decreased ADM formation after treatment with NTC-502 remained unchanged by the addition of CCCP. On the other hand, adding NTC-502 to Oligomycin- and CCCP-treated acinar cells resulted in an annihilation of the CCCP effect. Thereby, the transdifferentiation rate remained at the Oligomycin level.

Taken together the findings about the metabolism during ADM formation, the following model was established (Figure 25): The demand for glucose is increased due to an upregulation of glycolysis. Metabolites of the glycolysis feed into several pathways. Glucose-6-P and fructose-6-P are connecting glycolysis to the PPP which supplies the cells with different pentoses and NADPH (Figure 18). Pyruvate, the end product of glycolysis, is mainly converted into lactate. This step is important to restore NAD^+ which is needed for glycolysis. This anaerobe version of glycolysis is important for fast ATP production and it is increase with increasing ADM rates (Figure 13, 15). A fraction of pyruvate is also used to feed into the ETC which is still essential (Figure 22). The important role of ETC is to provide additional NAD^+ which is not needed for glycolysis but for the first step of serine synthesis. The synthesis of serine is crucial for ADM formation (Figure 24).

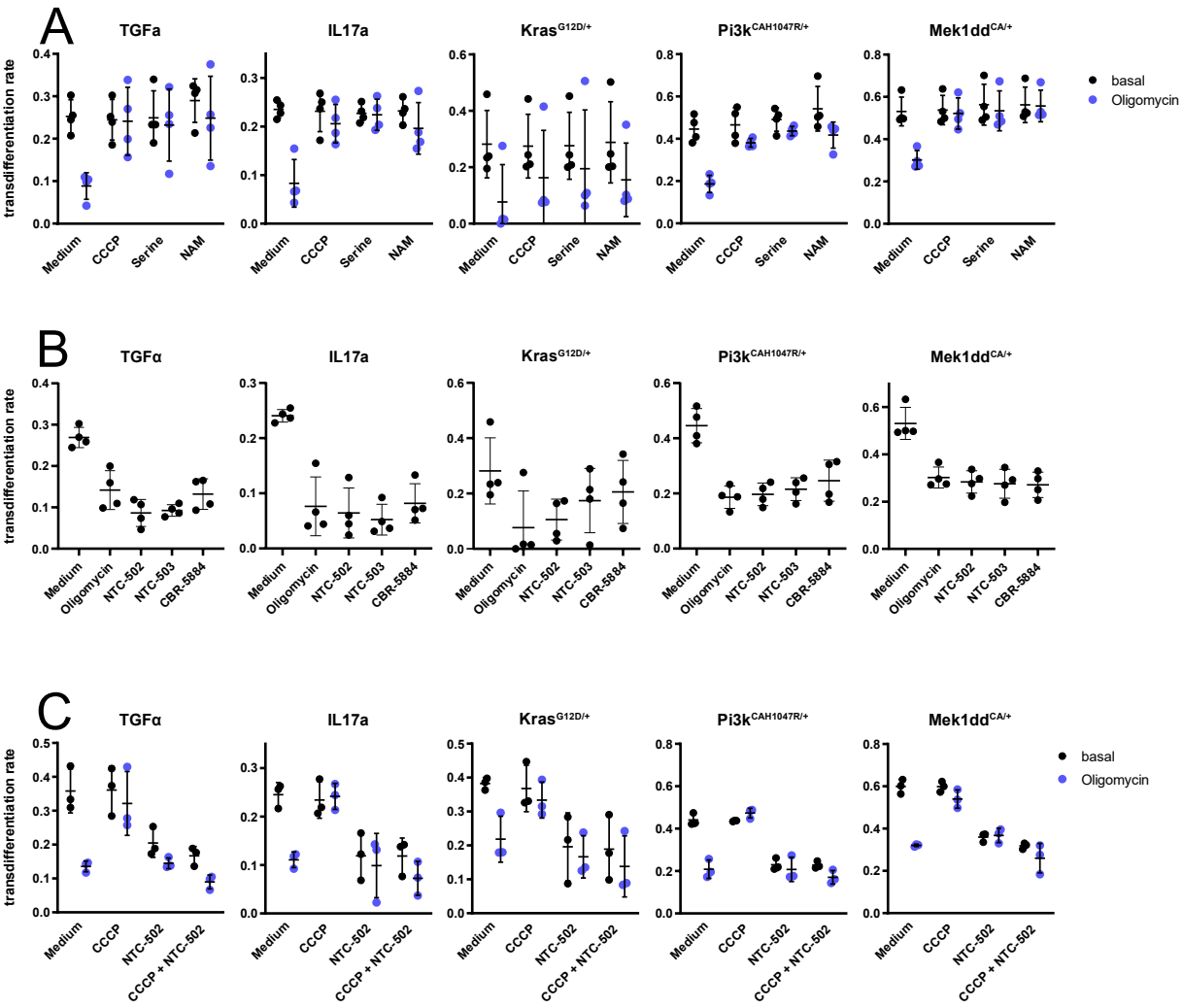

Figure 24: **Role of serine synthesis during ADM formation. A.** Transdifferentiation rates after treatment with Oligomycin, CCCP, serine, nicotinamide (NAM) or a combination. **B.** Transdifferentiation rates after treatment with Oligomycin or PHGDH inhibitors NTC-502, NTC-503 and CBR-5884. **C.** Transdifferentiation rates after treatement with Oligomycin, CCCP, NTC-502 or combinations of these. All values are displayed as mean ± SD.

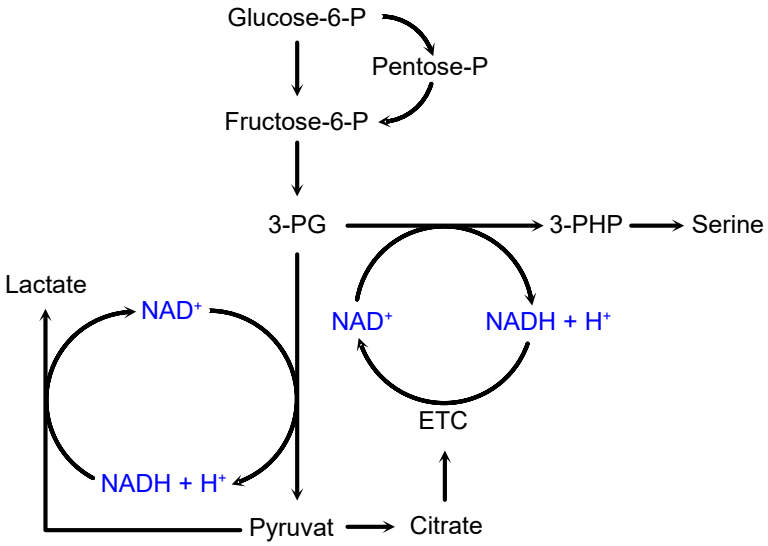

Figure 25: **Schematic overview of the connection between glycolysis, lactate production, electron transport chain (ETC) and serine synthesis from 3-phosphoglycerate (3-PG). (3-PHP = 3-phosphohydroxypyruvate)**

3.4 Crosstalk between Signalling and Metabolism

Signalling and metabolism are tightly connected. Two master regulators integrating metabolic and cellular signals are the AMP-activated protein kinase (AMPK) and the hypoxia induced factor 1α (HIF1α). While AMPK is activated via phosphorylation, HIF1α is stabilised to become active. To investigate the activation status of both AMPK and HIF1α during transdifferentiation, Western Blots for AMPK, pAMPK and HIF1α were performed (Figure 26A). The HIF1α stabilisation showed no clear pattern among the different inducers. In TGFα-induced wild-type, $KRAS^{G12D/+}$ and $MEK1DD^{CA/+}$, the amount of HIF1α was reduced. In contrast, IL17a treatment and oncogenic PI3K led to an unchanged or increased amount of HIF1α, respectively. The phosphorylation of AMPK showed an inverse pattern to HIF1α. In cytokine-induced wild-type acinar cells and $MEK1DD^{CA/+}$ acinar cells, the phosphorylation of AMPK was increased. At the same time, the phosphorylation in the other conditions decreased.
To test the functional importance of the AMPK, acinar cells were treated with the AMPK inhibitor compound C (Figure 26B). Despite the heterogeneous pattern of the AMPK phosphorylation, the treatment with compound C led to a homogenous attenuation of ADM formation. This inhibition was most pronounced with TGFα-treated wild-type and $KRAS^{G12D/+}$ harbouring acinar cells. The weakest effect was observed on IL17a-treated wild-type acinar cells. To investigate the role of HIF1α, two different compounds were used: $CoCl_2$ and deferoxamine (Figure 26C). Both compounds are known to stabilise HIF1α and thereby, activate its signalling function. Apart from IL17a-treated wild-type acinar cells, there was no effect of $CoCl_2$ treatment on the transdifferentiation. The ADM induction by IL17a was blocked by $CoCl_2$. This inhibition was in line with the effect of deferoxamine. Apart from IL17a-treated wild-type acinar cells, $KRAS^{G12D/+}$- and $PI3K^{CAH1047R/+}$-harbouring acinar cells were also susceptible to deferoxamine. Due to the heterogeneous results from $CoCl_2$ and deferoxamine there was no conclusive answer towards the impact of HIF1α-stabilisation on ADM formation. Whereas for AMPK, it appeared that AMPK activity was indispensable during transdifferentiation.

Another master regulator of metabolism is c-MYC. As seen before (section 3.2), MYC is important for transdifferentiation. To also investigate the metabolic influence of MYC, isotopic tracing using fully labelled ^{13}C-glucose was performed. The decrease of intracellular hexose-P after incubation of acinar cells was already seen before (section 3.3). Addition of the MYC-inhibitor 10058-F4 resulted in an even stronger decrease (Figure 27A). Since the

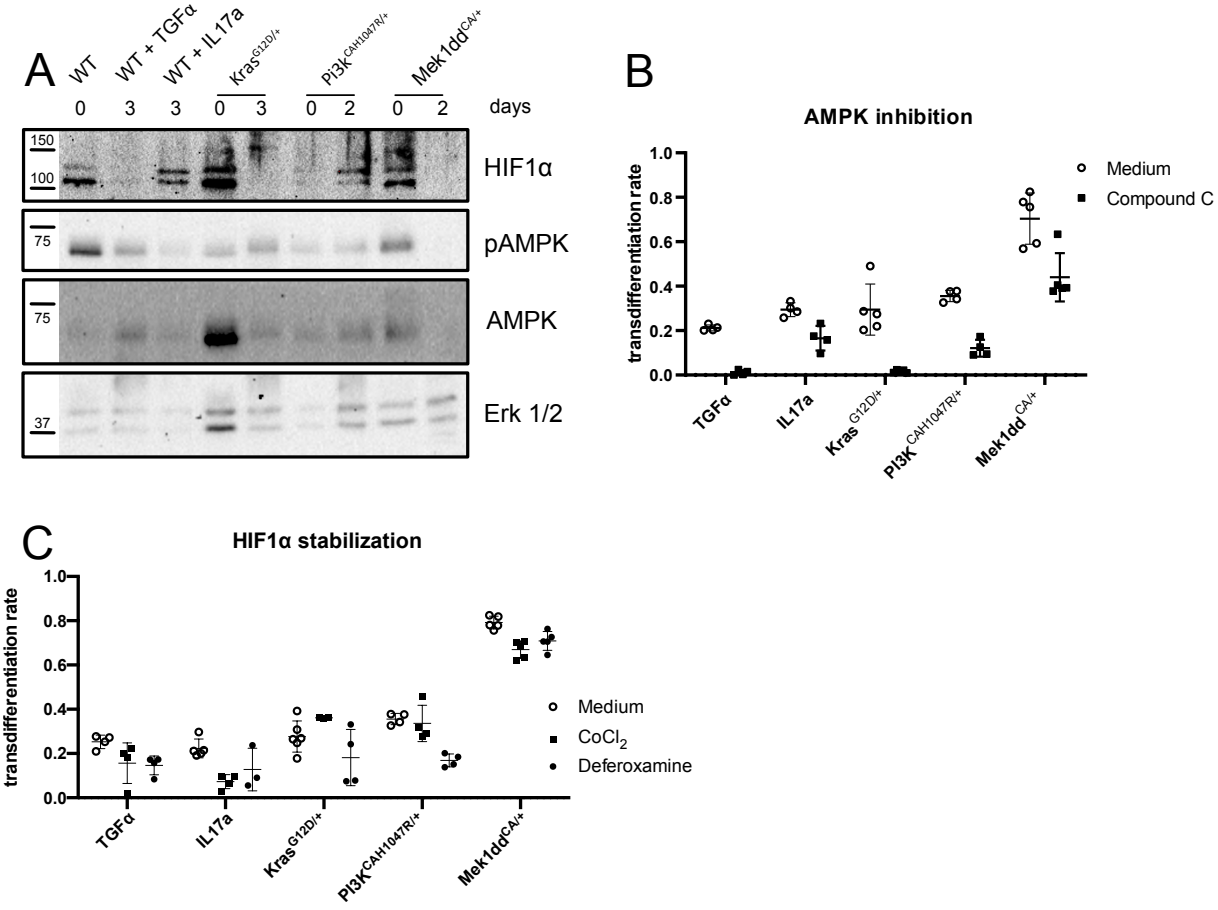

Figure 26: **Role of HIF1α and AMPK during transdifferentiation. A.** Western blot for HIF1α, p-AMPK and AMPK. ERK1/2 served as loading control. Proteins from acinar cells before and after transdifferentiation were loaded. **B.** Transdifferentiation rates after treatment with the AMPK inhibitor compound C. **C.** Transdifferentiation rates after treatment with the HIF1α stabilising compounds $CoCl_2$ or deferoxamine. All values are displayed as mean ± SD.

labelling pattern was comparable between the different conditions, there was rather a higher usage of hexose-P than an impaired glucose uptake. For pentose-5-P, MYC-inhibition had a more heterogeneous effect (Figure 27B). After 24 h of incubation, MYC-inhibition led to a decrease in the total abundance of pentose-5-P in medium- and TGFα-stimulated wild-type and in PI3K$^{CAH1047R/+}$-harbouring acinar cells. For IL17a-treated wild-type and KRAS$^{G12D/+}$-harbouring acini, the abundance was increasing while it was stable in MEK1DD$^{CA/+}$ acinar cells. The analysis of the labelling of pentose-5-P revealed a more homogeneous pattern. In most conditions, MYC-inhibition was followed by an increase of unlabelled pentose-5-P, indicating a reduced turnover. Consistently, the amount of labelled pentose-5-P was diminished in all conditions apart from IL17a-treated and KRAS$^{G12D/+}$-harbouring acini where it remained unchanged. The reduction was most pronounced with the isotopologue NP+3. This

indicates a decreased use of the non-oxidative part of the pentose-phosphate-pathway.
The two amino acids aspartate and glutamate can be synthesised from TCA cycle intermediates: Aspartate from oxaloacetate and glutamate from α-ketoglutarate. In addition, aspartate can be generated from pyruvate. In an isotopic tracing experiment using fully labelled glucose, the labelling of glucose-derived glutamate reflects the labelling of α-ketoglutarate. Therefore, all isotopologues from NP+2 to NP+5 are possible. Glucose-derived aspartate can be labelled from NP+2 to NP+4. If aspartate is labelled as NP+3, it can also be derived from pyruvate directly, without entering the TCA cycle. The amount of glucose-derived aspartate decreased after 24 h of incubation (Figure 27C). In contrast, inhibition of MYC not only restored the original amount but increased it clearly above the amount of the early timepoint. This effect was also visible if the isotopologue NP+3 which could also be derived from pyruvate is excluded. Strikingly, the increase was most pronounced with the isotopologue NP+2 which can only be derived from the TCA. The influence of MYC-inhibition on the aspartate levels was conserved among the different inducers. For glutamate, there was a similar pattern after MYC-inhibition (Figure 27D). In all inducers apart from oncogenic PI3K, glutamate levels dropped after incubation for 24 h but were stabilised at their original level by MYC-inhibition. In acinar cells with active MEK, this pattern was the least pronounced. For PI3K$^{CAH1047R/+}$-harbouring acini, the glutamate levels slightly rose after 24 h and remained unchanged by MYC-inhibition.
Since serine plays an important role during transdifferentiation, the serine levels following MYC-inhibition were investigated as well (Figure 27E). In all conditions, MYC-inhibition led to a drastic decrease of serine. Taken together, these findings suggest that MYC was important to direct glucose away from TCA cycle and towards side branches of glycolysis like PPP and serine synthesis. Inhibition of MYC reversed this phenotype.
Since MYC-inhibition led to decreased hexose-P levels, a combination with GLUT1-inhibition was used to investigate the functional impact of the increased glucose demand (Figure 27F). As seen before (Figures 10 and 19), low doses of either the GLUT1 or the MYC inhibitor only had minor influence on the transdifferentiation of PI3K$^{CAH1047R/+}$- or MEK1DD$^{CA/+}$-harbouring acinar cells. The combination of both inhibitors resulted in a strong inhibition of ADM formation. This inhibition was stronger than only mathematically adding up of the single effects. Therefore, MYC-inhibition acts synergistically with GLUT1-inhibition.

During earlier analysis of RNA sequencing data, it was found that promoter sequences bound by FOXO1 are enriched in genes regulated during ADM. FOXO1 is a know transcription

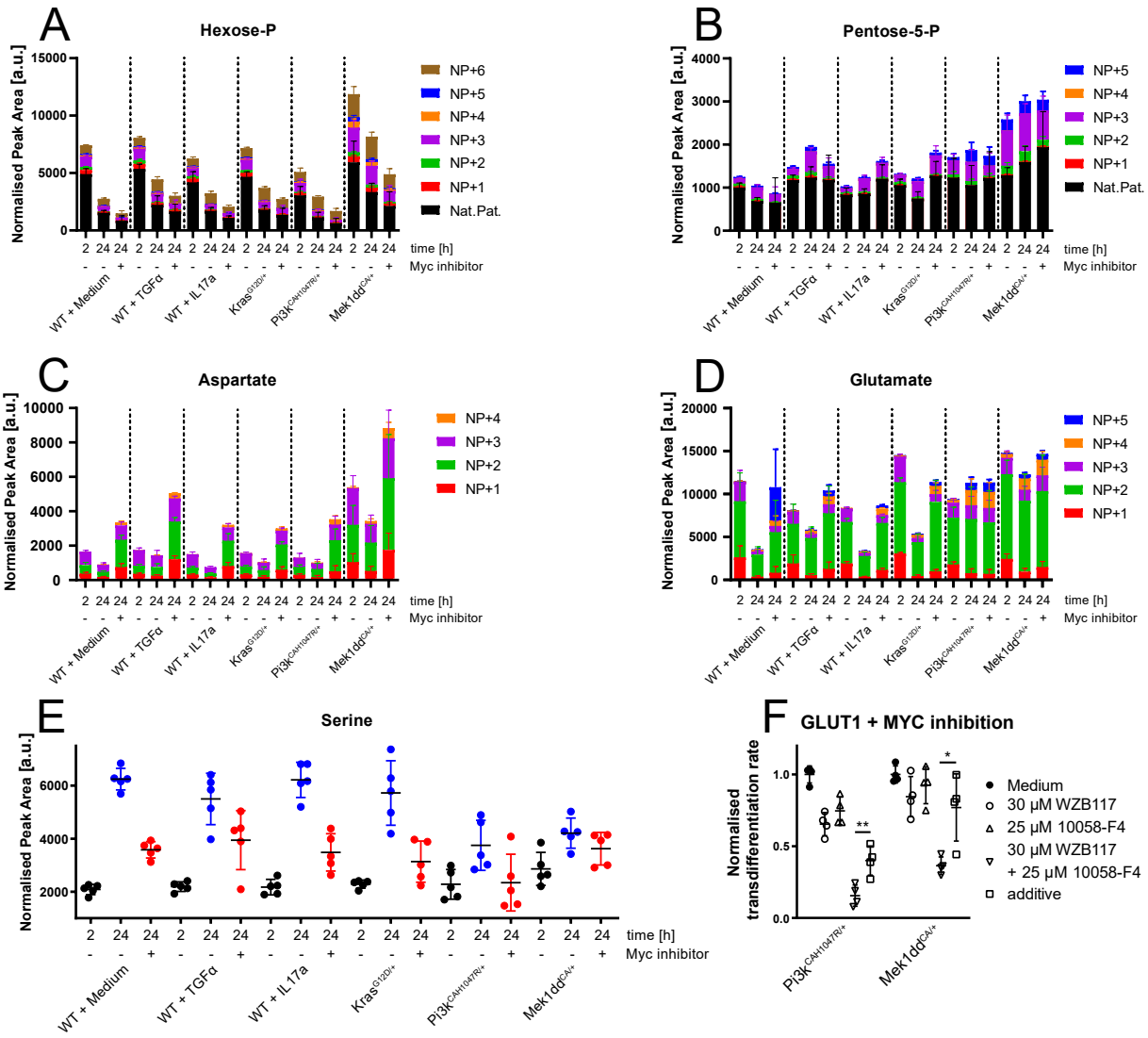

Figure 27: **Influence of MYC on metabolism. A-D.** Isotopologue distribution of hexose-P (**A**), pentose-5-P (**B**), aspartate (**C**) and glutamate (**D**) 2 h or 24 h after isolation. Cells were treated with ^{13}C-glucose for 2 h prior to harvesting. Inhibition of MYC using 50 µM 10058-F4 was present during the whole incubation time. **E.** Total amounts of serine 2 or 24 h after isolation of acinar cells with or without MYC inhibition by 50 µM 10058-F4. **F.** Normalised transdifferentiation rates after treatment with GLUT1 inhibitor WZB117, MYC inhibitor 10058-F4 or both. Mathematical addition of the effects of the single treatments is labelled as "additive". All values are displayed as mean ± SD. * = $p < 0.05$, ** = $p < 0.01$.

factor during differentiation processes as well as in metabolic reprogramming. In addition, FOXO1 is a target of AKT, thus of the PI3K signalling and the importance of PI3K signalling was already demonstrated in section 3.2. Upon phosphorylation, FOXO1 detaches from the DNA and is exported from the nucleus. In the pancreas, the subcellular localisation of FOXO1 is inversely correlated with the master transcription factor PDX1. To mimic

the effect of phosphorylation, a FOXO1-inhibitor was used (Figure 28A). For induced wild-type and KRAS$^{G12D/+}$-harbouring acinar cells, there was no significant effect of the three different FOXO1-inhibitor concentrations on the transdifferentiation rate. High concentrations of FOXO1-inhibitor resulted in a slight decrease of ADM formation in PI3K$^{CAH1047R/+}$- and MEK1DD$^{CA/+}$-harbouring acini. With MEK1DD$^{CA/+}$-induced ADM, this effect was already visible at intermediate concentrations of FOXO1-inhibitor. In contrast, the effect of FOXO1 inhibition on only medium-treated wild-type acinar cells was the opposite: Inhibition of FOXO1 resulted in an induction of ADM in wild-type acinar cells in a dose-dependent manner. At the highest concentration of the FOXO1-inhibitor, the transdifferentiation rate was similar to the TGFα-treatment.

FOXO1 gets phosphorylated and thereby inactivated by AKT, a downstream target of the PI3K. Therefore, it was tested if FOXO1 inhibition was sufficient to rescue ADM after PI3K-inhibition. To this end, KRAS$^{G12D/+}$-harbouring acinar cells were treated with either the PI3K-inhibitor or the highest concentration of FOXO1-inhibitor or the combination of both (Figure 28B). As demonstrated before, PI3K-inhibition led to a drastic reduction of ADM formation (see also Figure 9). The treatment with both inhibitors resulted in a minimal but statistically significant elevation of the transdifferentiation.

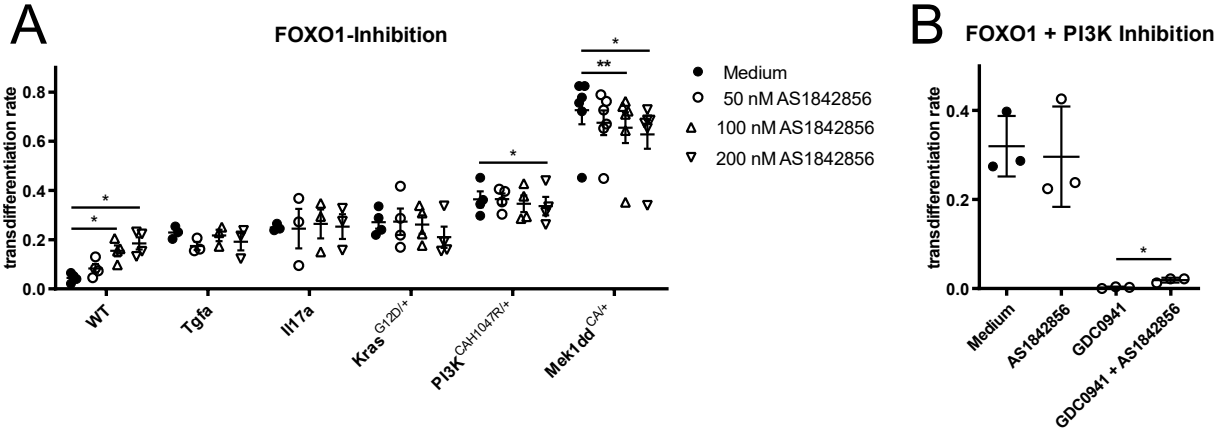

Figure 28: **FOXO inhibition promotes transdifferentiation in wild-type. A.** Transdifferentiation rates after treatement with various concentrations of the FOXO1-inhibitor AS1842856. **B.** Transdifferentiation rates after treatment with 200 nM AS1842856 (FOXO1-inhibitor), 1 µM GDC0941 (PI3K-inhibitor) or both. All values are displayed as mean ± SD. * = $p < 0.05$, ** = $p < 0.01$.

3.5 *In vivo* Validation

To validate the *in vitro* findings that have been described so far *in vivo*, the pancreatic tissue of 10-week-old mice was analysed. At first, the already described genotypes from sections 3.1 and 3.2 were investigated.

At 10 weeks of age the different oncogenes already led to alterations in the pancreas. $KRAS^{G12D/+}$-harbouring animals had mild edema and small areas of ADM lesions (Figure 29B). At the same time, large areas of acinar cells were morphologically unaffected and comparable to the time-matched wild-type control (Figure 29A). The oncogene $PI3K^{CAH1047R/+}$ caused stronger alterations (Figure 29C). There were still normal islets and acinar cells but to a lesser extent than in $KRAS^{G12D/+}$-harbouring animals. Still, the number of ADM lesions and edema area was increased. The strongest phenotype was seen with constitutively active MEK1 (Figure 29D). The lobular architecture of the pancreas was still preserved, but there were whole lobuli in which the acinar cells had transdifferentiated into ADM lesions. In addition, the edema became less pronounced compared to the other oncogene harbouring animals.

Knocking out *Egfr* in wild-type animals did not alter the morphology of pancreas (Figure 29E). Acinar cells as well as islets were comparable to the wild-type control. The same could be observed in animals lacking STAT3 activity (Figure 29G). As before, a normal morphology of the pancreas was observed. Also, the combination of both knock-outs did not show a phenotype (Figure 29I). When EGFR was deleted in $KRAS^{G12D/+}$-harbouring animals, the KRAS-phenotype was attenuated (Figure 29F). Acinar cells as well as islets displayed a normal phenotype. The lack of STAT3 activity in $KRAS^{G12D/+}$-harbouring animals had a similar phenotype (Figure 29H). The pancreas appeared morphologically normal including less or none ADM lesions. Also in the double-knock-out of *Egfr* and *Stat3* in $KRAS^{G12D/+}$-harbouring animals, the morphology was resembling the wild-type morphology (Figure 29J).

Besides oncogenic mutations, inflammation is a second cause of physiological ADM formation. To investigate this way of ADM induction, 10-week-old mice were challenged with an acute pancreatitis (Figure 30). As expected, wild-type pancreata displayed edema and ADM formation after pancreatitis (Figure 30A). There were still areas of acinar cells that did not undergo ADM. When $KRAS^{G12D/+}$-harbouring mice were challenged with pancreatitis, the ADM formation was more pronounced than in the wild-type controls (Figure 30B). In addition, the edema formation was stronger. In $PI3K^{CAH1047R/+}$-harbouring animals, there was

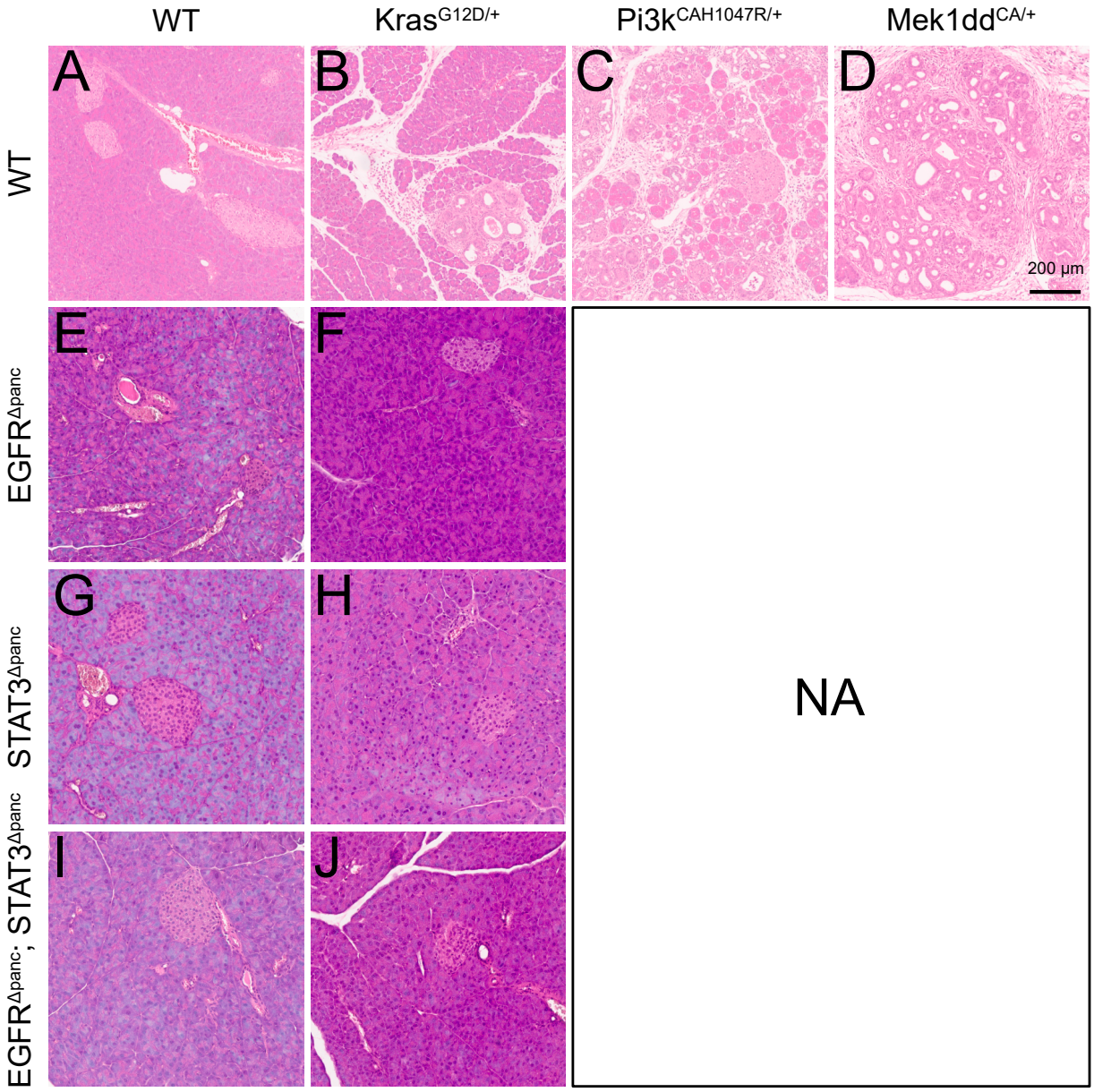

Figure 29: **Histology of pancreata at basal conditions. A-J.** H&E stainings of 10-week-old mice of various genotypes. The heading of of each column indicates the oncogene while the headings of the rows indicate additional knock-outs. The scale bar in **D** is representative for all images. NA marks genotypes which were not available.

an increased amount of ADM lesions in comparison to both basal conditions and pancreatitis in KRAS$^{G12D/+}$-harbouring animals (Figure 30C). In addition, some of the ADM lesions were not circular any more but seemed to be fused with neighbouring lesions. Also, there was edema within the lobuli. Oncogenic MEK led to a strong phenotype already at basal conditions. When these mice were subjected to pancreatitis the phenotype was even stronger

(Figure 30D). In addition to increased numbers of ADM lesions, there were PanIN lesions with this genotype. Another unique observation with oncogenic MEK was the composition of the non-acinar tissue. As with the other genotypes, there was an increase in the edema but there was also development of fibrosis.
The induction of pancreatitis in EGFR$^{\Delta panc}$ animals led to ADM formation that was weaker than in wild-type animals (Figure 30E). Still, there were sporadic ADM lesions but these were outnumbered by the areas of normal acinar tissue. Also, the edema formation was attenuated in comparison to wild-type animals. In contrast to this, the edema formation in animals lacking functional STAT3 was unaltered (Figure 30G). The number of ADM lesions was within the same range as for wild-type controls. The double knock-out was characterised by a strong impairment of the ADM formation after pancreatitis (Figure 30I). There were nearly no ADM lesions while the edema formation remained unaltered. When EGFR was deleted from KRAS$^{G12D/+}$-harbouring mice, the ADM and edema formation by pancreatitis were decreased (Figure 30F). The phenotype after EGFR deletion was more similar to wild-type than to KRAS$^{G12D/+}$-harbouring animals. In contrast to this, the deletion of functional STAT3 did not alter the ADM formation in KRAS$^{G12D/+}$-harbouring animals (Figure 30H). The amount of ADM lesions was comparable to STAT3 proficient mice. In addition, the edema formation was stronger compared to animals with functional STAT3. Interestingly, the ADM formation after pancreatitis in animals harbouring oncogenic KRAS but neither functional EGFR or STAT3 was rather comparable to the animals which were only lacking STAT3 (Figure 30J). While at the same time, the edema formation was closer to mice harbouring only KRAS$^{G12D/+}$ but no further mutations.

In order to quantitative the changes in the pancreas morphology at basal conditions and after inflammatory, the ADM and edema formation were measured (Figure 31). To this end, the ratio of the edema area to the whole pancreas area was calculated. For the ADM formation, the number of ADM lesions was assessed and given per mm^2 of edema-free pancreas area. As expected, the fraction of the edema area was increased in all genotypes after pancreatitis (Figure 31A). There were only two exceptions to be noted: Firstly, MEK1DD$^{CA/+}$-harbouring animals had a high ratio of edema already at basal conditions. This ratio was not further increased. Secondly, animals harbouring EGFR$^{\Delta panc}$ alone or in combination with oncogenic KRAS remained at their low ratio of edema even after pancreatitis. Analysing the number of ADM lesions in the tissue, again, an increase after pancreatitis was observed (Figure 31B). The two genotypes diverging from this pattern were EGFR$^{\Delta panc}$ in combination with either oncogenic KRAS or inactive STAT3. For KRAS$^{G12D/+}$- and EGFR$^{\Delta panc}$-harbouring animals

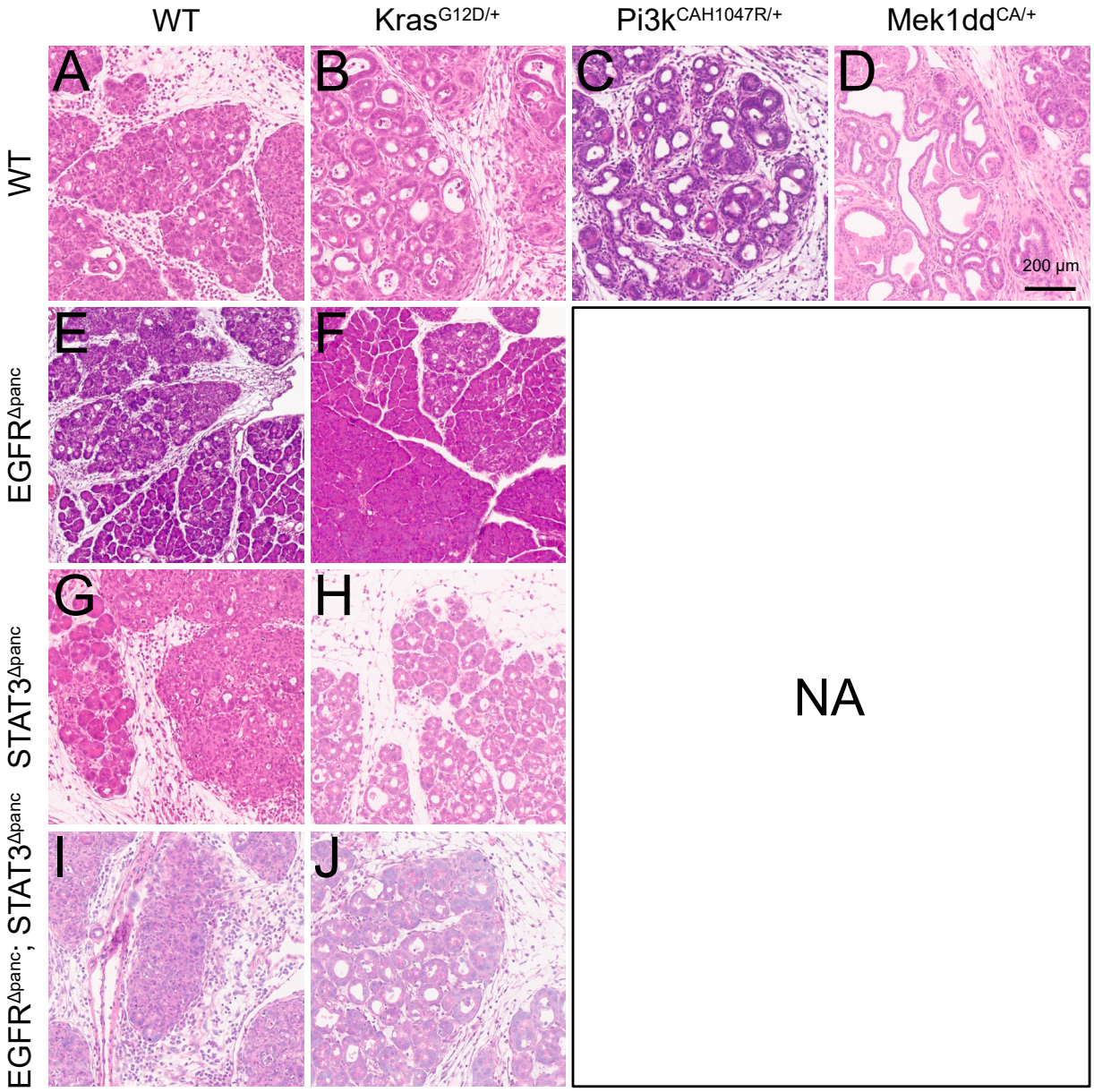

Figure 30: **Histology of pancreata after acute pancreatitis. A-J.** H&E stainings from 10-week-old mice of various genotypes after acute pancreatitis. The heading of of each column indicates the oncogene while the headings of the rows indicate additional knock-outs. The scale bar in **D** is representative for all images. NA marks genotypes which were not available.

the number of ADM lesions at basal condition was already low. After pancreatitis this number only merely increased. The same pattern could be observed for the double knock-out of EGFR and STAT3. The low basal ADM numbers remained at a low level after pancreatitis, apart from 2 out of 9 animals.

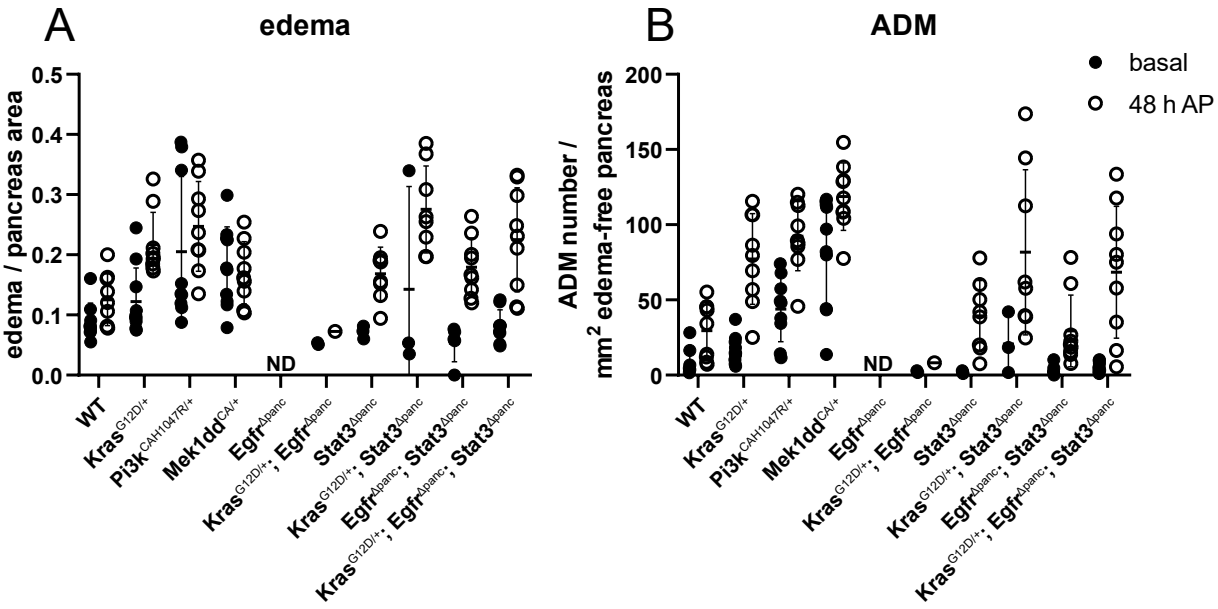

Figure 31: **Quantitative analysis of histological features after acute pancreatitis. A.** Ratio of edema area to pancreas area. **B.** Number of ADM lesions per edema-free pancreas area [mm^2]. The edema area calculated for **A** was subtracted from the pancreas area before determining the ratio. For each genotype control mice ("basal") and mice after pancreatitis ("48 h AP") were analysed. All values are displayed as mean ± SD. (ND = not determined)

To evaluate the correlation between the ADM formation *in vitro* and *in vivo*, the results of both approaches were plotted against each other (Figure 32). Firstly, the ADM formation in the tissue of 10-week-old animals without pancreatitis was compared to the transdifferentiation rates of unstimulated acinar cells (Figure 32A). By using a linear regression, it became visible that for most genotypes the ADM formation *in vivo* and *in vitro* followed the same pattern. The combination of oncogenic KRAS and knocked-out EGFR either with or without functional STAT3 showed the biggest differences between the *in vivo* and *in vitro* data. While $KRAS^{G12D/+}$-induced ADM formation was independent of EGFR *in vitro*, there was only a low number of ADM lesions in the tissue of 10-week-old animals.

Secondly, the ADM formation in the tissue of animals which underwent pancreatitis was compared to the transdifferentiation rates of stimulated acinar cells (Figure 32B). The stimulation *in vitro* was either achieved by active oncogenes or by the addition of TGFα or IL17a. For comparison, the following conditions were used: WT acinar cells with TGFα or IL17a stimulation; $EGFR^{\Delta panc}$ with IL17a stimulation; $STAT3^{\Delta panc}$ with TGFα stimulation; $EGFR^{\Delta panc}$; $STAT3^{\Delta panc}$ with TGFα or IL17a stimulation. As seen before with the basal conditions, the ADM formation *in vivo* and *in vitro* followed a similar trend for most genotypes. WT and $STAT3^{\Delta panc}$ animals had a slightly lower ADM formation after pancreatitis in comparison

to the transdifferentiation rates of isolated acinar cells. Animals with the combination of $KRAS^{G12D/+}$ and EGFR knock-out did not only have a low ADM formation at basal levels but also did not respond to the pancreatitis.

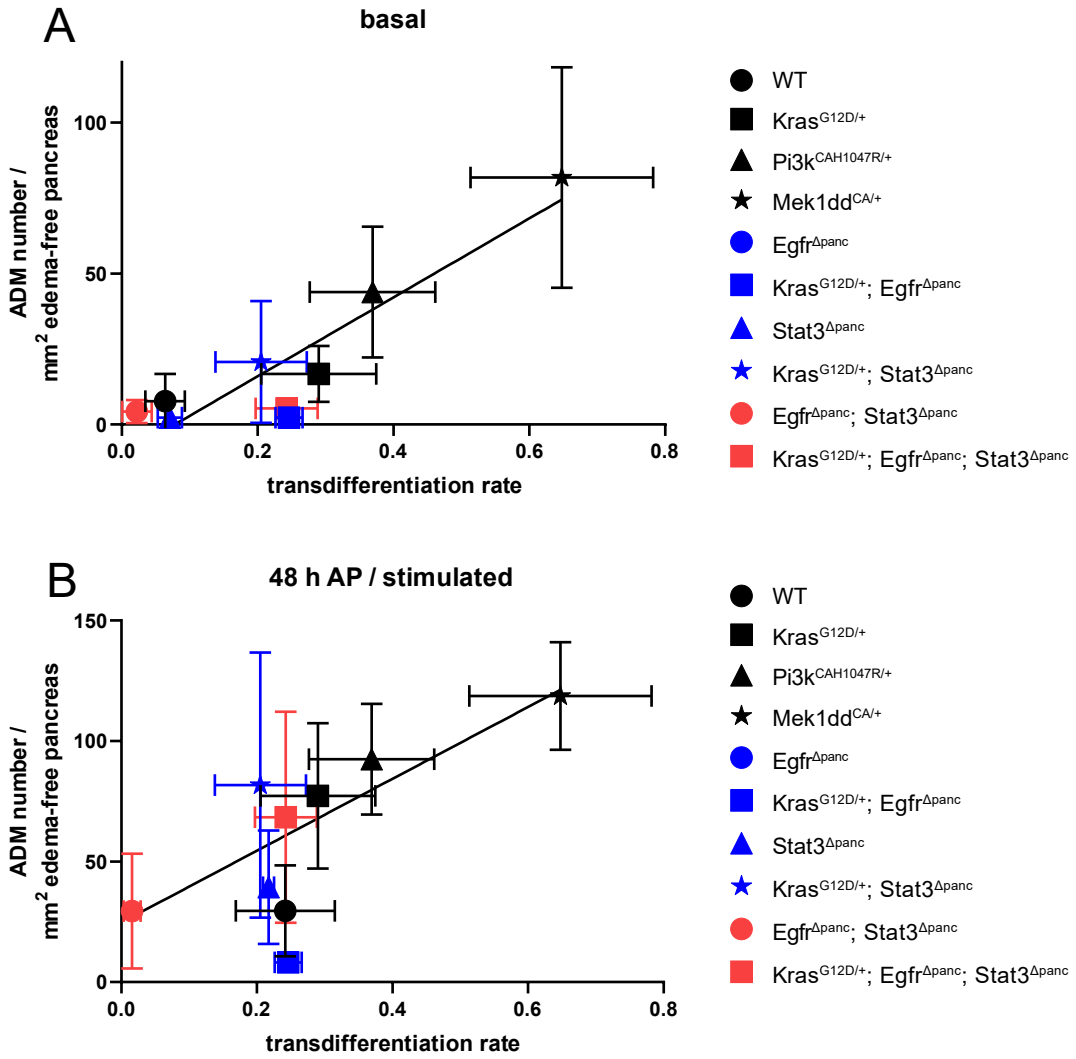

Figure 32: **Comparison of ADM induction *in vitro* and *in vivo*. A.** Transdifferentiation rates of isolated acinar cells plotted against number of ADM lesions per mm^2 edema-free pancreas of 10-week-old mice. *In vitro* transdifferentiation rates were derived from isolated acinar cells without further stimulation. **B.** Transdifferentiation rates of isolated acinar cells plotted against number of ADM lesions per mm^2 edema-free pancreas of mice after pancreatitis. *In vitro* transdifferentiation rates were derived from isolated acinar cells stimulated during culturing. Cells not harbouring an active oncogene were stimulated with either TGFα ($STAT3^{\Delta panc}$) or IL17a ($EGFR^{\Delta panc}$) or both (WT and $EGFR^{\Delta panc}$; $STAT3^{\Delta panc}$). All values are displayed as mean ± SD.

The second aspect of ADM that was found *in vitro*, was the increased importance of glycolysis

but also the need for a functional ETC. To test these findings *in vivo*, animals were treated with different inhibitors during the course of pancreatitis (Figure 33). To inhibit GLUT1, WZB117 was used, Rotenone was used as a complex I inhibitor of the ETC and DMSO as a solvent control. The animals were treated 24 h prior to and during the pancreatitis. For MEK1DD$^{CA/+}$-harbouring mice, the Rotenone-treatment was missing. As displayed in Figure 33A, induction of pancreatitis led to an increase in the edema area within the pancreas. None of the treatments (DMSO, Rotenone or WZB117) was followed by an alteration of the amount of edema. The number of ADM was increased by the induction of pancreatitis (Figure 33B). In wild-type animals, the number of ADM lesions after WZB117-treatment was slightly reduced while the other treatments had no effect. Still, the effect of WZB117 in wild-type animals was not significant. Animals harbouring KRAS$^{G12D/+}$ showed a visible but not significant reduction of ADM formation for all treatment groups including the DMSO control.
In contrast to this, Rotenone had a strong effect on PI3K$^{CAH1047R/+}$ animals. The amount of ADM after Rotenone but not after DMSO treatment was decreased. As for WZB117, there was no effect on this genotype. In MEK1DD$^{CA/+}$ mice, there was a reduction in ADM formation following the treatment with either DMSO or WZB117. The reduction by the inhibitor was stronger than in the DMSO control. Unfortunately, only the difference between the WZB117-treatment and the pancreatitis group but not between the WZB117-treatment and the DMSO group was significant.
Taken together, these observations show that the results of the *in vitro* experiments using different genetic alterations can be translated to a high degree into *in vivo* settings. The translation of inhibitor-based experiments into the *in vivo* systems was working to a much smaller extent.

In addition to the morphological analysis of the pancreatic tissue, the expression of key markers of metabolism were investigated. To this end, pancreatic tissue of 10-week-old mice either harbouring an active oncogene or wild-type animals was used. Tissue sections of these mice were stained for the glucose transporter GLUT1, the hexokinase HK1, the lactate dehydrogenase LDHA and a subunit of complex V of the ETC, ATP5D (Figure 34). Since ADM formation is sporadic at a 10-week timepoint, slides of oncogene harbouring mice contained ADM lesions as well as normal acinar tissue. Therefore, the staining intensities could be compared directly within a slide.
In wild-type animals, GLUT1 was strongly expressed in pancreatic islet cells (Figure 34A). The normal acinar cells were not stained for GLUT1. Both the other markers of glycolysis,

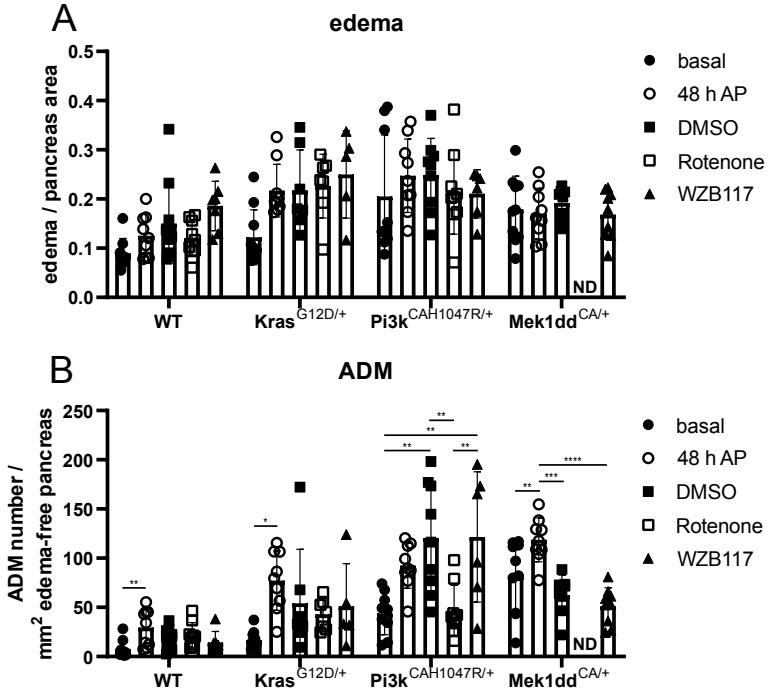

Figure 33: **Quantitative analysis of acute pancreatitis in combination with inhibitor treatment. A.** Ratio of edema area and pancreas area. **B.** Number of ADM lesions per edema-free pancreas area [mm^2]. The edema area calculated for **A** was subtracted from the pancreas are before determining the ration. For each genotype control mice ("basal") and mice undergoing pancreatitis ("48 h AP") were analysed. In addition, mice were treated with DMSO or the complex I inhibitor Rotenone or the GLUT1 inhibitor WZB117. All values are displayed as mean $\pm$ SD. (ND = not determined), * = $p < 0.05$, ** = $p < 0.01$, *** = $p < 0.001$, **** = $p < 0.0001$

HK1 and LDHA, were negative in wild-type pancreata, too (Figure 34B, C). The indicator of OxPhos ATP5D was expressed in the islet but not in the acinar cells (Figure 34D). In $KRAS^{G12D/+}$-harbouring animals, a strong staining for GLUT1 was observed within the ADM lesions (Figure 34E). The staining of the normal acinar cells was also stronger compared to the wild-type control but weaker than in the ADM lesions. In accordance with wild-type tissue, HK1 was also negative in normal acinar cells of $KRAS^{G12D/+}$ mice (Figure 34F). In contrast to this, ADM lesions were stained positive. In the LDHA staining, normal acinar cells as well as ADM lesions were stained (Figure 34G). The staining in the ADM lesions was slightly stronger. On the other hand, the staining for ATP5D was equally increased compared to wild-type animals (Figure 34H). Still, the increase was on a low level.
In $PI3K^{CAH1047R/+}$-harbouring mice a similar pattern was observed. While normal acinar cells remained negative, ADM lesions stained positive for GLUT1 and HK1 (Figure 34I, J). For LDHA, there was a strong but also homogeneous staining of acinar cells as well as ADM

lesions (Figure 34K). The staining for ATP5D revealed a small increase in the ADM lesions (Figure 34L). The staining of the normal acinar cells was within the range of the wild-type control. Also in MEK1DD$^{CA/+}$ animals, ADM lesions were positive for GLUT1 and HK1 while the normal acinar cells were negative (Figure 34M, N). Similar to oncogenic *Pi3k*, the staining for LDHA was strong and equal among ADM and acinar tissue (Figure 34O). In comparison to the wild-type control, ATP5D was mildly increased (Figure 34P). This increase was stronger in acinar cells than in ADM lesions.

To compare these findings to human ADM formation, tissue microarrays containing both normal tissue and ADM lesions were used. Normal acinar tissue was not stained for GLUT1 (Figure 35 A). Whereas, ADM lesions stained positive for GLUT1 (Figure 35D). A similar pattern was observed in the staining for HK1 (Figure 35B, E). Normal acinar tissue was negative and ADM lesions positive. For the ADM lesions, the staining was heterogeneous. They were all stained positive but to different extents. Analysing the LDHA staining, there was a mild staining in normal acinar tissue (Figure 35C). In the ADM samples, the staining was stronger in general (Figure 35F). But, there was also a gradient within the tissue with stronger staining in the ADM lesions and weaker in the surrounding tissue.

To have a more quantitative description, all IHCs were evaluated by the Institute of Pathology (TU Munich) (Figure 36). Quantification of the GLUT1 staining in murine tissue revealed an increased staining in ADM lesions compared to normal acinar tissue. (Figure 36A). This upregulation of GLUT1 was consistent across all oncogenes. For oncogenic MEK, the increase was not significant since there was already a moderately elevated staining for GLUT1 in the normal tissue. A similar pattern was observed in HK1 stainings (Figure 36B). For all genotypes, an increase in HK1 staining within the ADM lesions was detected. At the same time, there were no changes in the staining intensity of normal acinar cells in oncogenic mice compared to wild-type mice. In contrast to this, the staining for LDHA was already significantly increased in normal tissue of oncogenic mice (Figure 36C). Still, there was an increase in the ADM lesions; although this increase was not significant. The marker for OxPhos ATP5D mainly remained unchanged within all conditions (Figure 36D). There were some variations within single conditions like ADM lesions in PI3K$^{CAH1047R/+}$-harbouring mice but no global changes could be observed.
In the evaluation of the human staining, ADM lesions were subdivided into "early ADM" and "ADM". As for the murine samples, a gradual increase of GLUT1 staining was detected

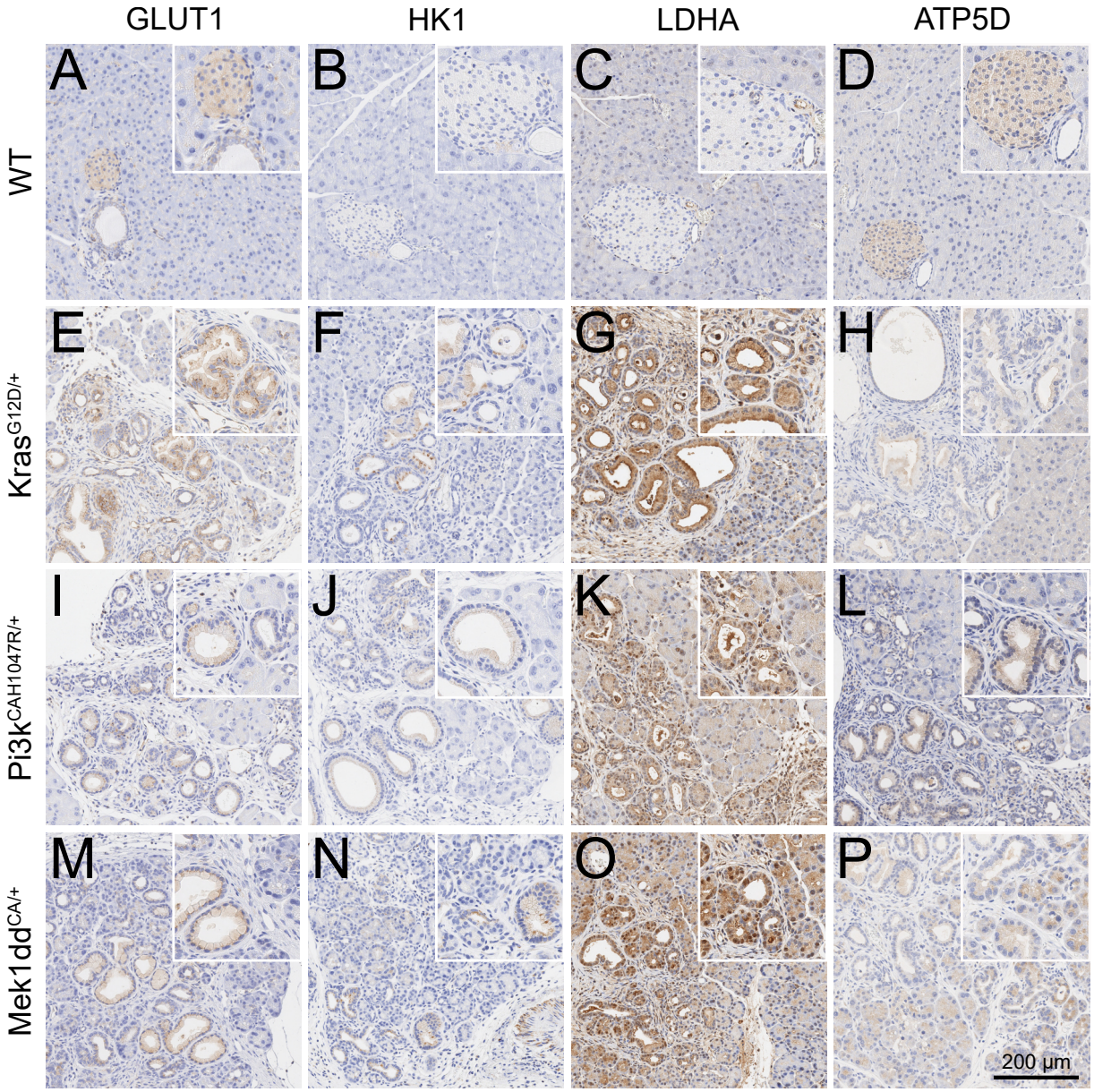

Figure 34: **Immunohistological staining of pancreata of 10-week-old mice.** Pancreata of wild-type mice or of mice harbouring active oncogenes were stained against GLUT1 (**A, E, I, M**), HK1 (**B, F, J, N**), LDHA (**C, G, K, O**) or ATP5D (**D, H, L, P**). The scale bar in **P** is representative for all images.

from normal tissue to ADM lesions (Figure 36E). Along the same line, there was a stepwise increase in the staining intensity of HK1 (Figure 36F). For LDHA, there was already a weak staining in normal acinar tissue (Figure 36G). The staining increased and reached its maximum already in early ADM lesions. The staining of ADM was comparable to early ADM.
In conclusion, the upregulation of glycolytic markers found in acinar explants was detected in

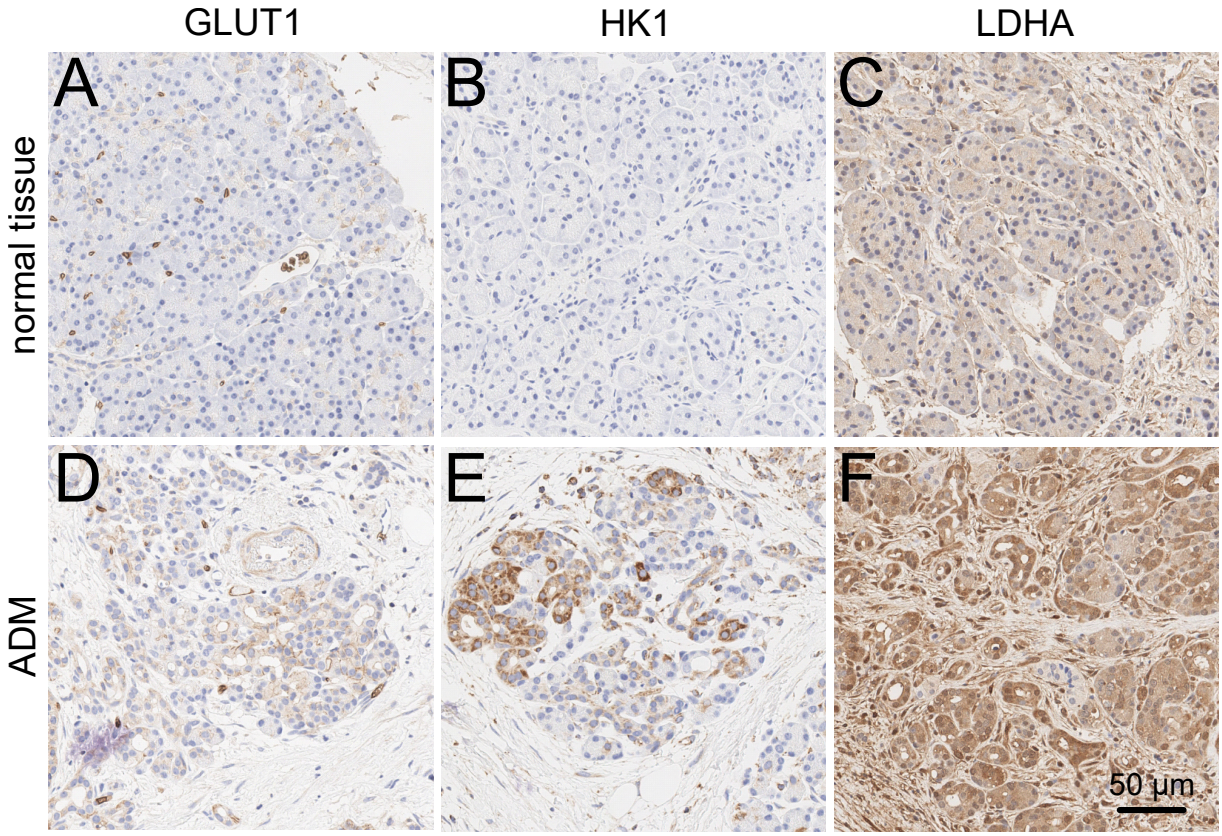

Figure 35: **Immunohistological staining of human pancreas.** Human tissue microarrays containing normal tissue and ADM lesions were stained against GLUT1 (**A, D**), HK1 (**B, E**) or LDHA (**C, F**).

murine and in human tissue as well.

To support the findings about the changed metabolism during ADM *in vivo*, the pancreatic metabolome of 10-week-old animals was acquired. For the analysis, tissue from the same wild-type and oncogene-harbouring animals as analysed before (Figures 29, 34) was used. The amounts of differently abundant metabolites were plotted against the number of ADM lesions found in the respective tissues (Figure 37). In accordance with the increased expression of GLUT1 during ADM, the amount of glucose within the tissue increased with the number of ADM lesions (Figure 37A). At the same time, the amount of succinate, a metabolite of the TCA cycle, decreased with higher ADM numbers (Figure 37B).
In addition to the central energy metabolism, the abundances of essential and non-essential amino acids were investigated. The amounts of the branched chain amino acids valine, leucine and isoleucine were all elevated with higher ADM numbers (Figure 37C-E). While the increase in the amount of leucine was rather small, isoleucine rose by a factor of 3 from

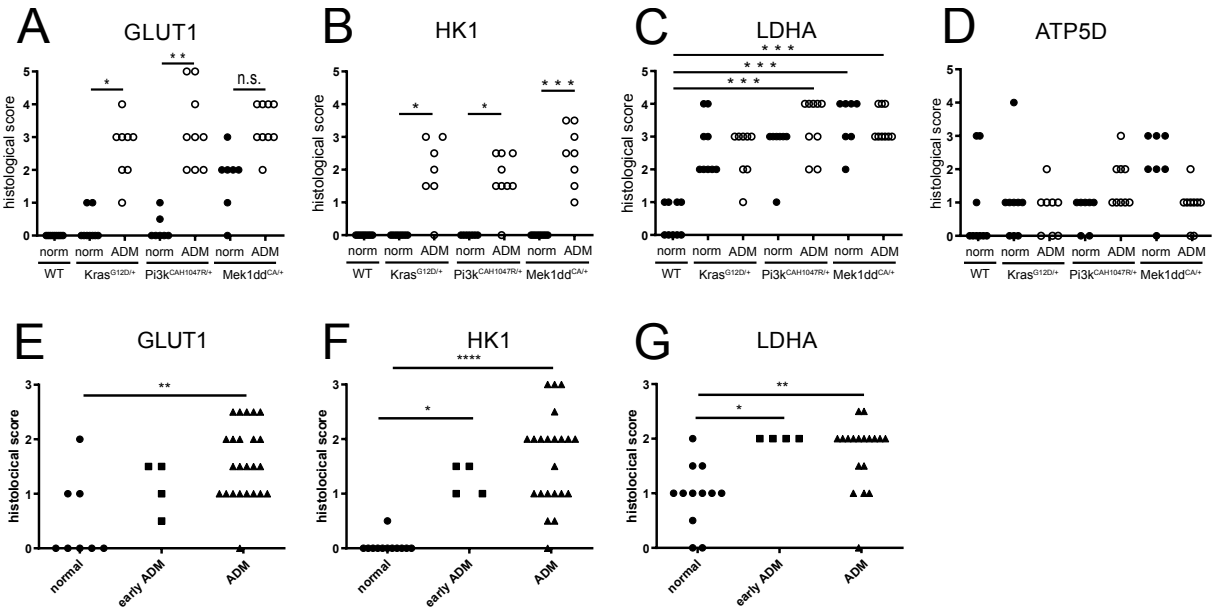

Figure 36: **Quantification of immunohistological staining. A-D.** Quantification of stainings against GLUT1 (**A**), HK1 (**B**), LDHA (**C**) and ATP5D (**D**) in murine tissue as displayed in Figure 34. **E-G.** Quantification of stainings against GLUT1 (**E**), HK1 (**F**) and LDHA (**G**) in human tissue as displayed in Figure 35. norm = normal tissue, n.s. = not significant, * = $p < 0.05$, ** = $p < 0.01$, *** = $p < 0.001$, **** = $p < 0.0001$.

wild-type to Mek1dd$^{CA/+}$-harbouring animals. Also, the essential amino acid phenylalanine increased with increasing numbers of ADM lesions in the tissue (Figure 37F). Similar to essential amino acids, the non-essential amino acids arginine and aspartate displayed a positive correlation with the ADM numbers (Figure 37G, H). In contrast to this, the amounts of glutamate decreases with higher rates of ADM formation in the tissue (Figure 37I). Among the assessed amino acids, this pattern was unique to glutamate.

In summary, the metabolome of the pancreatic tissues reflects the findings from the metabolome of the *in vitro* experiments.

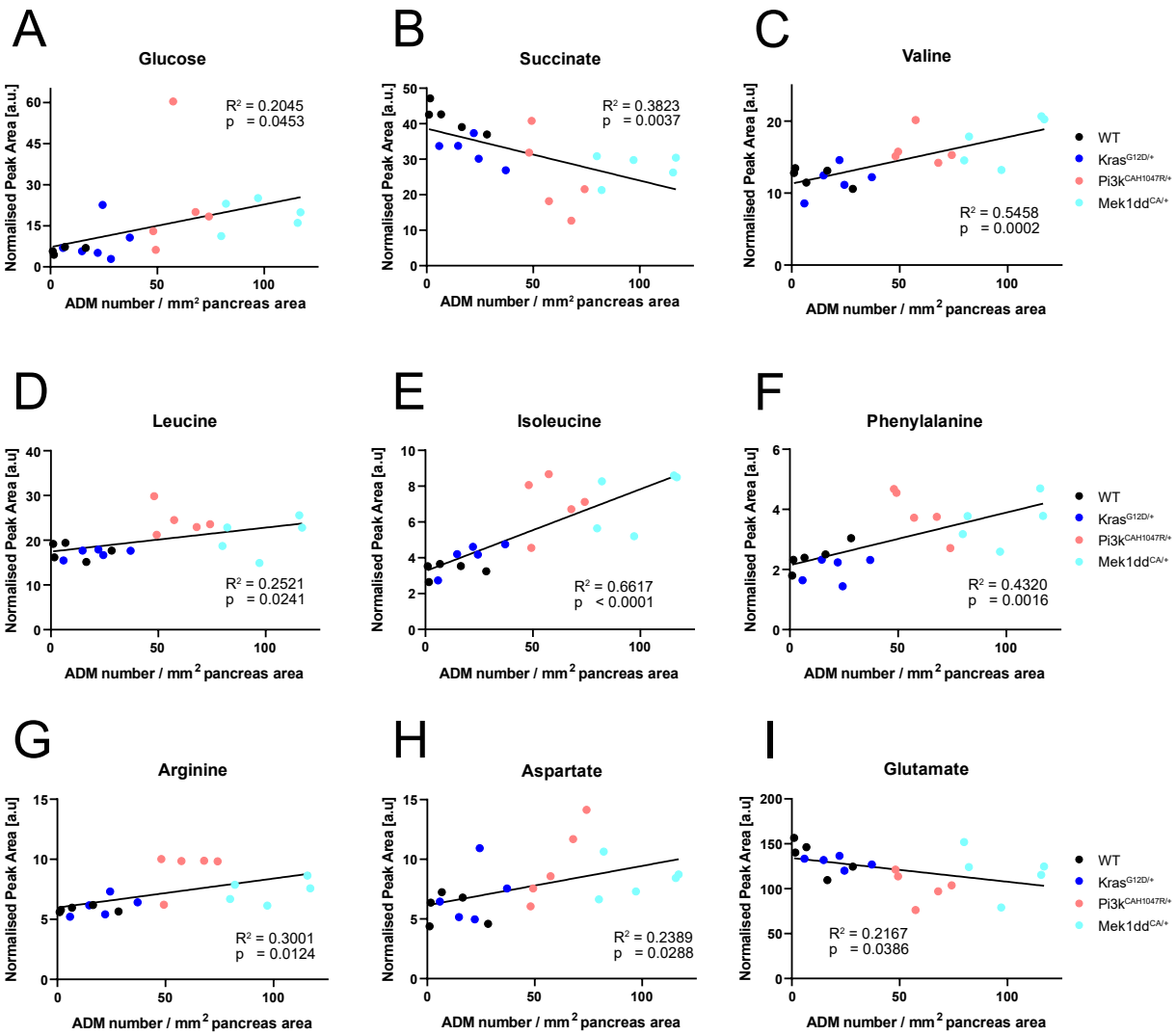

Figure 37: **Metabolic analysis by NMR of pancreatic tissue of 10-week-old mice.** Amounts of glucose (**A**), succinate (**B**), valine (**C**), leucine (**D**), isoleucine (**E**), phenylalanine (**F**), arginine (**G**), aspartate (**H**) and glutamate (**I**) in pancreatic tissue of 10-week-old mice. Metabolite amounts were plotted against the number of ADM lesions per mm^2 of edema-free pancreas in the respective animal.

4 Discussion

4.1 Signalling during ADM Formation

Acinar to ductal metaplasia (ADM) represents the first step during both regeneration after injury and initiation of tumour formation. In various studies, different inducers of ADM have been identified. Among these inducers, there are oncogenic KRAS and PI3K and ectopic expression of TGFα and IL17a [145][146][74][147]. Oncogenic MEK has not been studied in the context of ADM so far. In this study, all five inducers gave rise to ADM. Despite different transdifferentiation rates, the morphology as well as the transcriptional changes from an acinar identity to a ductal-like phenotype were consistent. TGFα- and KRAS-induced ADM share similarities on the levels of morphology, signalling and sensitivity towards inhibitors [146].In addition, KRAS-driven tumours display TGFα expression in the cancerous and normal tissue at the invasive front of the tumour [148].

IL17a exposed to acinar cells initiates ADM formation in contrast to IL6 and IL22. However, IL6 was suggested to play an important role in maintaining ADM and promoting PanIN progression since IL6 primes acinar cells towards a stronger reaction to a second inflammation [58][149]. IL22 which shares the down stream signal with IL6 has been reported to induce stemness in PDAC cells and is associated with a poor prognosis in patients [150][151]. Also, the expression of the IL22 receptor in the pancreas is stronger than in most other tissues [152]. IL22 has been shown to induce ADM under certain conditions at concentrations as used this thesis [153]. The main difference to the published protocol is the matrix. In this thesis, collagen was used a matrix and no IL22-induced ADM formation was observed. In contrast, when Matrigel® was used as extracellular matrix, IL22 seems to promote ADM. In addition, IL22 was reported to be elevated during pancreatitis and suggested to be important for tissue regeneration even in severe pancreatitis models [153][154][155].

During carcinogenesis, ADM lesions stain positive for the proliferation markers KI67 [156]. While in the context of inflammation, proliferation is needed to replenish the pool af acinar cells after pancreatitis [157]. Inhibition of proliferation had only minor to no effect on the transdifferentiation by the five inducers. Therefore, it was concluded that proliferation can be feature of ADM but is not essential. This is in line with reported findings that explanted acinar cells treated with EGF or TGFα show transdifferentiation but close to no proliferation *in vitro* [158][49]. In contrast, inhibition of protein synthesis blocked ADM formation. This was expected since ADM represents a fundamental change in the cell identity that requires the synthesis of new proteins like the ductal marker KRT19.

Both, PI3K and MEK represent KRAS effectors and are therefore likely to play a key role in

ADM development. Gain of function mutants of PI3K and MEK induced of ADM *in vitro* and *in vivo*. Inhibitors of PI3K and MEK blocked ADM formation regardless of its inducer. An important role of PI3K in ADM development has been proposed since pancreas specific ablation of PTEN, an inhibitor of PI3K, induced ADM formation *in vivo* [159]. PTEN deletion in an oncogenic *Kras* background further promoted ADM and PDAC development [156]. In additon, a constitutively active mutation of PI3K is sufficient to induce ADM formation and PDAC development independent of oncogenic *Kras* [74]. Also, the ADM induction via conditioned medium from macrophages is PI3K-depended [160]. Interestingly, inhibition of AKT, a downstream target of PI3K, was reported to induced more ADM lesions following acute pancreatitis [161].

MEK is an essential effector melocule in the KRAS pathway. The MEK inhibitor trametinib is currently evaluated in clinical trials [162][163]. The presented results show that constitutively active MEK is sufficient to induce ADM formation. Moreover, all five inducers rely on both PI3K and MEK. Thus, ADM induced by the PI3K gain of function mutant can be blocked by a MEK inhibitor and vice versa. So far, it has been reported that PI3K and MEK have similar effectors during ADM formation [164].

Several signalling pathways have been analysed in PDAC models and in specimens of patients with PDAC and shown to be deregulated, including STAT3, ERK, MTOR, AKT, NFχB and WNT/β-catenin [165][117]. For most of them, the role in ADM has not been investigated yet. To investigate the influence of these pathways, specific inhibitors were used on all five inducers. All five inducers were sensitive towards inhibition of mTOR, MYC and treatment with TGFβ. On the other hand, activation of the WNT signalling via inhibition of GSK3β led to a moderate inhibition of ADM which was similar in all inducers. In contrast to this, the inhibition of NFχB via IKK2 inhibition was followed by a strong inhibition of IL17a-induced ADM but only a mild inhibition of TGFα and KRAS and no changes in PI3K- and MEK-mediated ADM.

The strong effect of mTOR inhibtion via Rapamycin was in line with the results of the PI3K inhibition since mTOR is an effector molecule of PI3K. Additionally, mTOR was reported to have a crucial role in KRAS-driven tumourigenesis [166].

Inhibition of MYC leads to an upregulation of master transcription factors of acinar identity like PTF1A and MIST1 [167], while overexpression of MYC is sufficient to induce carcinogenesis in the pancreas [168]. Therefore, the observed inhibition of ADM is in accordance with previous results.

Regarding TGFβ and SMAD4, there are controversial discussion in the literature: For human acinar explants, TGFβ was shown to promote ADM [100]. In line with this, TGFβ secreted by

eosinophils worsens chronic pancreatitis in mice [169]. Both findings are opposing an ADM preventing role of TGFβ. On the other hand, a knock-out of SMAD4 and thereby a block of TGFβ signalling was shown to act synergistically with TGFα overexpression [170]. To fully resolve these contradictions a more detailed analysis is needed.
A potential role of GSK3β was already shown for TGFα- and KRAS-induced ADM [171]. In the same study, it was found that GSK3β activation increases MTOR signalling [171]. In addition, GSK3β was shown to activate STAT3 and NFκB [172][173]. Since all these three targets are activated by multiple pathways it can be speculated that the inhibition of GSK3β only leads to a partial reduction in the activity of these central signalling pathways. Thereby, the partial inhibition of ADM would be explained.
The result that NFκB inhibition attenuates Kras-mediated ADM formation has already been described [117]. Also, IL17a acts via NFκB [174]. PI3K- or MEK-induced ADM was not affected by inhibition of IKK2. Possibly a higher concentration of the inhibitor is needed for PI3K- and MEK-induced ADM as seen with MYC inhibition already. On the other hand, PI3K- and MEK-mediated ADM could be independent of NFκB. For EGFR signalling, which is upstream of PI3K and MEK, a positive feedback loop via NFκB was described [117]. It could be speculated that due to the ligand-independent activity of mutated PI3K or MEK this feedback loop is not needed.
In addition to the general pathways investigated so far, EGFR and STAT3 signalling were investigated since they are directly involved in the signalling of the two ligands used (TGFα and IL17a). The fact that EGFR inhibition, both genetically and pharmacologically, inhibited TGFα-induced ADM was expected since EGFR is the receptor for TGFα. On the other hand, STAT3 inhibition only had minor effects on TGFα-stimulated acinar cells. Since TGFα was reported to induce p-ERK and p-AKT but not p-STAT3, this result is in line with the literature, too [165]. The effect of the STAT3 inhibitor on TGFα-induced ADM is probably explained by the inhibitor's off-target effects on STAT1. The effect of the double inhibition reflected the results of the EGFR inhibition.
IL17a-induced ADM in turn was mainly unaffected by EGFR inhibition. Since IL17a signalling is reported to leave p-ERK levels unchanged this result is supported by previous work [174]. On the other hand, STAT3 inhibition was followed by a strong decrease of IL17a-mediated transdifferentiation because STAT3 is the main mediator of IL17a signalling [147]. Therefore, the results met the expectations. The result of inhibiting both EGFR and STAT3 was comparable to inhibiting STAT3 only.
KRAS-induced ADM formation was moderately reduced in all the genetic models or by EGFR inhibition. Only the STAT3 inhibitor had a strong effect. Again, the discrepancy

between genetical and pharmacological inhibition of STAT3 might be due to off-target effects of the inhibitor. The results of only moderate decrease in KRAS-induced ADM after EGFR inhibition is contradictory to previously published results. Transdifferentiation of $Kras^{G12D/+}$ acinar cells was shown to be sensitive towards both genetical and pharmacological inhibition of EGFR [48]. The knock-out as well as the EGFR inhibitor in the presented work are the same as in the literature. For STAT3 inhibition in $Kras^{G12D/+}$ animals the results are in line with previous reports. During pancreatitis in animals lacking STAT3 but harbouring oncogenic KRAS the ADM formation was reported to be reduced but not completely blocked [175].

PI3K- and MEK-mediated ADM formation was sensitive to the STAT3 inhibitor but not to EGFR inhibition. Since equivalent genetic models for these inhibitions are missing it is not possible to judge if the effect of the STAT3 inhibitor is due to its on- or off-target effect [176].

To compare the effects of EGFR and STAT3 inhibition *in vitro* with the *in vivo* situation, pancreata of 10-week-old mice with and without acute pancreatitis were investigated. Acute pancreatitis is an established way of inducing ADM *in vivo*. In caerulein-induced ADM, gene signatures of WNT, NOTCH and STAT3 signalling are enriched [177]. Most of these pathways have been investigated in the presented work *in vitro* before. Therefore, the pancreatits is a good model to test the presented *in vitro* findings.

Mainly, the results of the ADM formation in the tissues correlated well with the transdifferentiation rates of explanted acinar cells so that the *in vitro* results could be validated. The divergent genotypes were those harbouring oncogenic KRAS and the EGFR knock-out. Despite the results of transdifferentiation *in vitro*, there was no or only weak ADM formation *in vivo*. The hampered ADM formation following the EGFR knock-out is in line with reports of absent ADM and thus PDAC formation in animals harbouring oncogenic KRAS and an EGFR knock-out [178]. It can be speculated that either the stress during the isolation (enzymatic digestion and shear stress) or the culture conditions (bovine pituitary gland extract and fetal calf serum) provide additional stimuli to induce ADM formation in EGFR knock-out acini *in vitro*.

The reported decrease in ADM after pancreatitis in animals harbouring oncogenic KRAS and a STAT3 knock-out could be seen with some of the animals. It has to be noted though that the published data are observed at a later timepoint as the ones presented here (3 days vs 7 days) [175]. Additionally, the reduced ADM formation in this genotype without pancreatitis is well in line with published results [179].

The presented results lead to the following conclusions: ADM can be induced by a variety of different stimuli like cytokines and growth factors or oncogenes. Some ways of induction

are independent of each other as represented by IL17a-mediated ADM in EGFR knock-out animals and TGFα-mediated ADM in STAT3 knock-out animals. The idea of an additional EGFR-independent but NFχB-dependent way of ADM induction was also proposed by Liou *et al.* [180]. KRAS-induced ADM was shown to be positive for both p-STAT3 and p-ERK [175][181]. But at the same time, STAT3 signalling and ADM induction have been shown to be insensitive towards EGFR and MEK inhibition, further supporting the idea of independent ways of induction [179]. During acute pancreatits, ADM formation can be induced by IL17a. At the same time, depleting IL17a during pancreatitis does not fully block ADM [147]. Therefore, additional ways of ADM induction must exist. Despite the different ways of induction, the presented work provides strong evidence for a common downstream ADM program of the different inducers. This common program consists of the common sensitivities presented: PI3K, MEK and MYC activity as well as SMAD4 inactivity. Besides these investigated factors, additional research is needed to identify additional mediators and pathways involved.

4.2 Metabolic Changes during ADM Formation

Metabolic reprogramming is a hallmark of cancer [182]. Isolated wild-type acinar cells rely on both glycolysis and oxidative phosphorylation (OxPhos) [183]. External stimuli such as hypoxia increase the glycolytic capacity of acinar cells [184]. And even under normoxic conditions, OxPhos is reduced following stimulation with caerulein [185]. In this work, wild-type acinar cells stimulated with either TGFα or IL17a increase glycolysis and decrease OxPhos. These results are in line with the published stimulation by caerulein. A similar metabolic shift is seen in acini harbouring oncogenes which spontaneously undergo ADM.
Several levels of evidence indicate this metabolic switch from OxPhos to glycolysis. In the course of transdifferentiation the glucose transporter GLUT1 and lactate dehydrogenase (LDHA) were upregulated on RNA and protein level. In addition, GLUT1 expression co-localised with the expression of the ductal marker KRT19. Functionally, the uptake of glucose and the secretion of lactate correlated well with the transdifferentiation rate. At the same time, TCA cycle metabolites were downregulated. The same pattern was seen in an isotopic tracing experiment using fully labelled ^{13}C-glucose.
To validate these results *in vivo*, pancreata of 10-week-old mice were investigated. As with the acinar explants, both glucose and lactate increased with the number of ADM lesions in the tissue as seen by NMR analysis. In contrast to this, metabolites of the TCA cycle were decreasing. Additionally, the tissue was stained for the glycolytic markers GLUT1, HK1 and

LDHA. The upregulation of all these markers in ADM lesions confirmed the upregulation of glycolysis during the process of ADM. An identical pattern was seen in stainings of human tissue underlining the importance of this finding across species.
An upregulation of glycolysis has been described for cancer cells in response to KRAS mutations [110]. In addition, an upregulation of GLUT1, HK1, HK2 and LDHA was shown in cancer tissue [186][187]. Enzymes of the glycolysis have been proposed as prognostic markers. In pancreatic cancer, HK2 correlates with poor disease outcome [188], while for colorectal carcinoma, increased GLUT1 expression goes along with higher grades of dysplasia [189].
For some entities, there are reports of metabolic alterations during tumour development. In neoplastic lesions of the liver, an upregulation of HK was observed [190]. In preneoplastic rat renal basophilic cell lesions, there was an increased expression of GLUT1 compared to normal tissue [191]. For lung cancer, there is a study comparing metabolomes of early and late lesions to those of normal tissue [192]. It was seen that the degree of alterations in the metabolomes increase during the carcinogenesis. It has to be noted though that the "normal tissue" in this study was taken from cancer patients as well. Therefore, influences of the neighbouring tumour can not be fully excluded. This limitation applies to the presented *in vivo* metabolomes of the pancreas as well. For the *in vitro* metabolomes, this limitation does not apply. Despite the excessive studies of cancer metabolomes in the pancreas, metabolic changes in early lesions in the pancreas have not been described yet. Comparing the findings of this work with the work done in other cancer types, a similar development of a gradual increase in metabolic alterations as seen for lung cancer can be proposed. As seen by the experiments using inhibitors of glycolysis, this reprogramming of metabolism is not a bystander effect but essential for ADM development and tumour initiation.
Besides glucose, glutamine is another important fuel of the energy metabolism. Especially for pancreatic cancer, it was shown that glucose as a main source of energy is replaced by glutamine. This leads to a pronounced sensitivity towards glutaminolysis inhibition [193][115]. In order to enhance glutaminolysis, the required transporters and enzymes are upregulated [194]. Despite these findings for fully established cancer, there was no evidence for a glutamine dependency during ADM. Neither an upregulation of glutaminolysis-associated genes nor a sensitivity towards glutaminolysis inhibition was observed.
In addition to the upregulation of glycolysis, it was found that functional mitochondria are still needed for ADM formation. Since the attenuated transdifferentiation after inhibition of the electron transport chain at complex V could be rescued by uncoupling, ATP as the required resource from the mitochondrium can be excluded. In addition to ATP, the mitochondrium

supplies the cell with TCA cycle metabolites and redox equivalents [195]. It has already been shown that uncoupling can rescue an Oligomycin-induced decrease in NAD^+ [196]. Supplementation with nicotinamide (NAM) confirmed that the important function of the mitochondria is to provide redox equivalents in form of NAD^+. The supplementation with serine underlines the importance of NAD^+ for serine synthesis. Furthermore, the rescue by CCCP was sensitive towards serine synthesis inhibition. An impaired *de novo* synthesis of serine after ETC inhibition has already been described [197].

Serine itself has multiple functions within the cell. Apart from being a proteogenic amino acid, serine acts as a donor to both the folate cycle and the one-carbon metabolism [198]. The connection of the folate and the methionine cycle links serine to methylation of DNA and protein [199]. In addition, serine is part of heme and glutathione synthesis linking serine and ROS defence [200]. Within fully developed PDAC, serine was shown to be essential for tumour cell survival [201]. Tumour cells which are unable to synthesise serine by themselves are fully dependent on extracellular supplementation. The medium used for acinar cell culture did not contain serine. Therefore, the *in vitro* experiments were performed under serine-depleted conditions. Serine depletion in pancreatic and colorectal cancer cells was shown to induce redox and translational stress [201][202].

Another model proposed in the literature states that functional mitochondria are needed as a source of H_2O_2 during the course of ADM [117]. This was shown by either addition or scavenging of H_2O_2 to increase or decrease ADM, respectively. The necessity of H_2O_2 was shown for different ways of inducing ADM [203]. At first glance, this model appears contradictory to the serine model. But H_2O_2 has been shown to reduce the amount of NADH, thus increasing NAD^+ levels [204]. Therefore, both models proposing the importance of H_2O_2 or serine can be reconciled.

To test for the requirement of GLUT1 and complex I of the ETC *in vivo*, acute pancreatits was induced in the presence of matching inhibitors (WZB117 for GLUT1 and Rotenone for complex I). Since the edema formation was unaltered by the DMSO or inhibitor treatments, the induced inflammation was comparable. By Rotenone, only PI3K-mediated ADM formation was inhibited. In $Kras^{G12D/+}$-animals, both inhibitors led to ADM rates within the range of the DMSO control. For WZB117, MEK-induced transdifferentiation was decreased during acute pancreatitis. The decrease was only slightly stronger than in the DMSO control. Taking together these results indicate that the findings can be translated from the *in vitro* system *in vivo*. For a complete validation other inhibitors might be needed. In the literature, the complex I inhibitor Metformine was shown to reduce KRAS-induced ADM formation and tumour progression [205]. This result further supports the importance of mitochondrial

functionality.
Taking together these findings, the following model can be proposed: Besides altered signalling, ADM is characterised by a change in metabolism. Glycolysis is upregulated and serves as the main source of energy. Side branches of the glycolysis like the pentose-P-pathway are upregulated in addition. On the other hand, OxPhos is downregulated and dispensable as a provider of ATP. Still, OxPhos is needed to oxidise NADH to NAD^+ and NAD^+ in turn is needed for anabolic pathways like serine synthesis.

4.3 Interplay of Signalling and Metabolism

Several different interactions between cellular signalling and metabolism have been reported. Theses interactions have been demonstrated to work in both directions: For example, in natural killer cells, IL15 activates STAT3 which leads to a recruitment of GLUT1 to the cell membrane and therefore an increase in glycolysis [206]. On the other hand, increased amounts of acetyl-CoA or lactate were shown to increase histone acetylation [207] [208].
A master regulator integrating signalling and metabolism is the hypoxia induced factor 1 α (HIF1α). HIF1α is mainly activated via inhibited degradation and thereby stabilisation of the protein. Pharmacologically, this can be achieved by using $CoCl_2$ or deferoxamine to block the proline hydrolase (PHD) which is responsible for the degradation of HIF1α [209][210]. Notably, the effect of HIF1α stabilisation on ADM formation was heterogeneous: Either there was no effect, as seen with TGFα-stimulated wild-type or *Mek1dd*$^{CA/+}$-harbouring acini or there was an attenuation of ADM formation as seen in the other conditions. In addition, the effects of $CoCl_2$ and deferoxamine diverged in some cases as well.
The stabilisation of HIF1α was not expected to have inhibitory effects on ADM formation. HIF1α signalling leads to an increase in glycolysis and the importance of increased glycolysis has already been discussed in the previous section [211]. This increased glycolysis is facilitated by an increase of the transporters for glucose import and lactate export [212]. Accordingly, a knock-out of HIF1α is followed by a decrease of glycolysis [213]. In the pancreas, HIF1α is induced either by mutant KRAS or by hypoxia during acute pancreatitis [212][214]. An increase in HIF1α levels can be seen latest in PanIN1 [215]. Still, the HIF1α levels during ADM formation were only increased in two out of five ADM-inducing conditions. The result that especially deferoxamine inhibited ADM *in vitro* could be explained by its iron depleting mechanism. The depletion of iron can also interfere with enzymes of the TCA cycle which is also needed during ADM [210].

HIF1α is finely balanced with the activity of the AMP activated kinase (AMPK) [211]. AMPK activity is regulated by phosphorylation with pAMPK being the active form. Although there was no clear pattern in its phosphorylation, inhibition of AMPK led to a homogeneous inhibition of ADM formation. Therefore, AMPK activity must be essential for transdifferentiation. Since the expression of pAMPK was heterogeneous, the activity of AMPK could also be required in the beginning of ADM. ADM itself is energy demanding as seen in section 3.3. A high concentration of AMP indicative of ATP shortage is a known activator for AMPK [216]. Therefore, the need for AMPK activity can be explained. Still, AMPK activity alone is not sufficient. pAMPK is induced by the PHD-inhibitor CPI-613, but CPI-613 inhibited ADM (section 3.3) [217]. And in pancreatic tissue both AMPK and pAMPK are even reduced during pancreatitis, an ADM inducing condition [218].
pAMPK has several downstream targets. One of the most prominent one is the inactivation of acetyl-CoA carboxylase (ACC). Thereby, the *de novo* synthesis of fatty acids is inhibited [219]. But pAMPK can also be transcriptionally active if it binds pyruvate kinase isozyme M2 (PKM2). In this case, AMPK supports stemness of cancer cells [220]. To provide more nutrients, pAMPK increases autophagy [221]. Additionally, pAMPK inhibits mTOR and attenuates translation [222][223]. The inhibitory effect of pAMPK on mTOR underlines the complex regulation during ADM formation. Inhibition of either AMPK or mTOR prevented transdifferentiation. Therefore, a fine balance of these two master regulators must be found.
Besides the HIF1α-AMPK-axis the transcription factor MYC is not only a central regulator of cell signalling but also of the cellular metabolism. The impact of MYC on the signalling level has already been discussed above. MYC inhibition in acinar cells led to an increased consumption of glucose. At the same time, the metabolised glucose was unevenly distributed within the different metabolic pathways: While (glucose derived) pentose-5-P and serine were diminished the amounts of newly synthesised aspartate and glutamate increased. Aspartate and glutamate are mainly generated from TCA cycle intermediates. Since these effects were seen after MYC inhibition, MYC appears to direct glucose-derived metabolites to side branches of glycolysis instead of the TCA cycle.
In tumour cells, MYC was shown to increase glutamine metabolism. Specifically, glutaminolysis was upregulated providing metabolites for nucleotide synthesis [113]. In addition, several *in vivo* studies have found GLS to be upregulated in tumours as a consequence of MYC activity [224][225][226]. In contrast to this, ADM formation was unaffected by GLS inhibition and glutamine levels were independent of transdifferentiation rates. This discrepancy might be explained by a different biology of the ADM process compared to that of tumour growth. ADM is independent of proliferation (as seen by DNA synthesis inhibition) whereas tumour

progression is highly dependent on proliferation. Therefore, the demand for new nucleotides in cancer cells is considerably higher than in trandifferentiating acinar cells.
The observation that interleukin treatment, here IL17a, can change TCA cycle activity via MYC has already been described for IL4 and IL13 in cancer cells [227]. Again, the effect in ADM and tumour cells did not fully match. When looking at cancer stem cells the effect of MYC on metabolism becomes more comparable to ADM. Here, it was shown that MYC activity leads to an upregulation of glycolysis and a downregulation of OxPhos [96]. Since cancer stem cells represent a slowly proliferating cell population within the tumour, they share more commonalities with ADM than other cancer cells. Targeting MYC during ADM led to a even higher glucose consumption. This also explains why MYC inhibited acini were especially sensitive towards GLUT1 inhibition.
In addition to these transcription factors, FOXO1 was investigated. Although there was no effect of FOXO1 inhibition on stimulated acinar cells the transdifferentiation of medium-treated wild-type acini was increased. Until now, FOXO1 has mainly been investigated in β-cell of pancreatic islets [228]. It was found that FOXO1 and PDX1 have an inverse subcellular localisation [229]. Additionally, FOXO1 inhibits the translation of PDX1 [230]. Therefore, FOXO1 inhibition leads to a potential upregulation of PDX1. Persistent expression of PDX1 was shown to induce ADM [231]. Thus, PDX1 could be the mediator for the increased transdifferentiation of wild-type acini after FOXO1 inhibition.
Under physiological conditions, FOXO1 is expressed in ductal and centroacinar cells but is reduced during PDAC initiation [232]. In cancer stem cells, the expression is even further reduced [233]. Downstream of FOXO1 there is the long non-coding RNA LINCO1197. LINCO1197 inhibits β-catenin/WNT signalling [234]. By this FOXO1 inhibits β-catenin/WNT signalling. At the same time, inhibition of β-catenin/WNT signalling via a GSK3β inhibitor attenuated ADM formation in all five inducers. Therefore, FOXO1 activity opposes ADM formation. In the cell, FOXO1 gets phosphorylated by AKT and exported from the nucleus to inactivate it. Therefore, it was tested if FOXO1 inhibition could rescue the reduced ADM formation in $Kras^{G12D/+}$-harbouring acini after PI3K inhibition. The rescue effect was statistically significant but of a neglectable effect size. Therefore, it was concluded that FOXO1 is probably not the main target of PI3K/AKT signalling during ADM formation.
A second kinase targeting FOXO1 is AMPK [235] whose activity was found to be required for ADM formation in all inducers. Among the target genes of FOXO1, there are several enzymes of the central energy metabolism. In endothelial cells, activity of FOXO1 suppresses metabolic activity [236]. This metabolic regulation counteracts MYC activity. As part of the insulin response in hepatocytes, FOXO1 increases the capacity for glycogen production

in hepatocytes [237]. In further studies of hepatocytes, it was shown that FOXO1 balances gluconeogenesis, glycogen synthesis and glucose release [238]. In addition, there are also metabolic feedback loops since inhibition of glycolysis by 2-DG also leads to FOXO1 inhibition.

The investigated examples, HIF1α, AMPK, MYC and FOXO1 underline that there is a tight connection between the signalling and the metabolic changes during the process of ADM. While the effect of the signalling on the metabolism has been analysed to some extent already the inverse impact has only investigated in recent years.

4.4 Conclusion and Outlook

ADM formation occurs as the first step of tumour development as well as during pancreatitis. To cover the full spectrum of these different settings, not only oncogenic models of ADM like mutant KRAS were used but also inflammatory stimuli like TGFα. Throughout the investigation of the signalling, metabolic changes and their interplay, oncogenic and inflammatory ADM display similar requirements and vulnerabilities. Obviously, different stimuli need a variety of signalling pathways to initiate ADM. This became clear by the EGFR-dependency of TGFα-mediated ADM whereas IL17a signalling was independent of EGFR but dependent on STAT3. At the same time, after these initial steps all stimuli funnelled into a common ADM program. This program was mainly driven by activation of PI3K, MEK and MYC and was sensitive towards SMAD4 activation.

At the metabolic level, a common program towards increased glycolysis was observed. The remaining mitochondrial capacity was not important for ATP production but for sustaining the redox balance within the cell. This redox balance was shown to be important for serine synthesis. The shift towards glycolysis and anabolism was also reflected in the required activity and silencing of master regulators linking signalling and metabolism. So far there is no other study investigating ADM induced by a number and variety of stimuli as presented in this work. Therefore, the homogeneity of different ADM inductions is a unique aspect that has not been shown before. Additionally, the metabolic reprogramming formally known to be a tumour feature was not presented to take place already in the first step of pancreatic tumour development, namely ADM.

The presented results give new insight into the development of ADM. On the other hand, there are also new questions arising. Serine was found to be an important amino acid and metabolite needed during ADM. Several pathways like synthesis of proteins, membranes, nucleotides, methyl donors and glutathione are linked to serine metabolism. At the same time, it remains unclear in which of these pathways serine acts as the limiting factor. Isotopic tracing of ^{13}C-serine could help disentangling these complex networks in ADM.

Additionally, the connection between changes in signalling and metabolism need further analysis. To this end, target genes of AMPK and FOXO1 could be analysed. These would cover metabolic target genes which are actively upregulated (AMPK targets) and genes which are suppressed (former FOXO1 targets) during ADM. These target genes and not yet investigated central signalling pathways like hedgehog could serve as a base for a complementary screen to the one presented in this work. As a result, an even more comprehensive network of ADM formation could be developed.

Until now, a lot of effort was put into understanding common mechanisms of ADM develop-

ment during carcinogenesis and inflammation. A different perspective would be to investigate their differences. Inflammatory ADM recovers after the inflammation is resolved giving rise to new acinar cells whereas oncogenic ADM progresses into PanINs. An improved understanding, why ADM develops into one of the two directions could help preventing tumour development in high risk individuals or chronic pancreatitis patients.

During the presented work RNA samples were collected of stimulated wild-type and oncogenic acini *in vitro*. Additionally, RNA samples from pancreatic tissue of 10-weeks-old mice with and without active oncogenes either as control animals or after acute pancreatitis were acquired. So far, these samples have been analysed to find changes between normal acinar cells and ADM lesions. In addition, the expression profiles of these samples could be analysed for differences in oncogenic and inflammatory ADM.

To improve the resolution of the analysis, spatial transcriptomics can be applied. In this technique, cells from a FFPE slide are harvested and their transcriptome is acquired. In comparison to laser capture methods, spatial transcriptomics allows to analyse a whole FFPE slide instead of just selected areas. Since in spatial transcriptomics 4-5 cells are pooled the resolution is lower than in single cell transcriptomics. On the other hand, the additional spatial and thereby histological information is especially important when looking at rare cell populations like ADM in 10-week-old $Kras^{G12D}$-harbouring animals and the adjacent not yet transformed acini.

In a second approach, the well-established *in vitro* transdifferentiation can be further developed: So far, stimuli or inhibitors have been added from the beginning of the culture on. To study the impact of stimuli like TGFβ or inhibitors on established ADM, explanted acini can be cultured for 2 or 3 days and treated thereafter. This schedule would mimic an intervention after ADM has already formed.

To investigate the progression from ADM into PanINs the *in vitro* transdifferentiation can be modified in another way. The isolation of ductal cells or PanINs from the pancreas has already been described in the literature. Therefore, it could be tried to isolated acini, transdifferentiate them *in vitro* into ADM, explant them from the collagen gel and transfer them into ductal cell/PanIN culture conditions. Especially with strong oncogenes like MEK, it can be speculated that the ADM structures will progress further into PanIN cells. Of course, adjustments in the culture conditions may be needed. If this approach was successful it would be the first assay to monitor and manipulate PanIN development *in vitro*.

References

[1] T. Neuß, N. Wirges, M.-C. Chen, S. Usluer, R. Oellinger, S. Lier, M. Dudek, T. Madl, M. Jastroch, K. Steiger, W. Schmitz, H. Einwächter, and R. M. Schmid, "Acinar-ductal metaplasia in the pancreas requires a glycolytic switch and functional mitochondria," 2022.

[2] G. K. Gittes, "Developmental biology of the pancreas: a comprehensive review," *Developmental biology*, vol. 326, no. 1, pp. 4–35, 2009.

[3] W. F. Ganong and K. E. Barrett, *Ganong's Review of medical physiology*. A LANGE medical book, London: McGraw-Hill Medical, 23rd ed. ed., 2009.

[4] P. V. Röder, B. Wu, Y. Liu, and W. Han, "Pancreatic regulation of glucose homeostasis," *Experimental & molecular medicine*, vol. 48, p. e219, 2016.

[5] N. A. Campbell, J. B. Reece, A. Held, and J. Markl, eds., *Biologie*. Biologie, München: Pearson Studium, 6., aktualisierte aufl., [nachdr.] [2. dt. ausg. der amerikan.] ed., 2008.

[6] J. Keller and P. Layer, "Human pancreatic exocrine response to nutrients in health and disease," *Gut*, vol. 54 Suppl 6, no. Suppl 6, pp. vi1–vi28, 2005.

[7] L. C. Murtaugh and M. D. Keefe, "Regeneration and repair of the exocrine pancreas," *Annual review of physiology*, vol. 77, pp. 229–249, 2015.

[8] K. Alberti and P. Z. Zimmet, "Definition, diagnosis and classification of diabetes mellitus and its complications. part 1: diagnosis and classification of diabetes mellitus. provisional report of a who consultation," *Diabetic medicine : a journal of the British Diabetic Association*, vol. 15, no. 7, pp. 539–553, 1998.

[9] R. Pannala, J. B. Leirness, W. R. Bamlet, A. Basu, G. M. Petersen, and S. T. Chari, "Prevalence and clinical profile of pancreatic cancer-associated diabetes mellitus," *Gastroenterology*, vol. 134, no. 4, pp. 981–987, 2008.

[10] A. Sharma, T. C. Smyrk, M. J. Levy, M. A. Topazian, and S. T. Chari, "Fasting blood glucose levels provide estimate of duration and progression of pancreatic cancer before diagnosis," *Gastroenterology*, vol. 155, no. 2, pp. 490–500.e2, 2018.

[11] K. M. Chung, J. Singh, L. Lawres, K. J. Dorans, C. Garcia, D. B. Burkhardt, R. Robbins, A. Bhutkar, R. Cardone, X. Zhao, A. Babic, S. A. Vayrynen, A. Dias Costa, J. A. Nowak, D. T. Chang, R. F. Dunne, A. F. Hezel, A. C. Koong, J. J. Wilhelm, M. D.

Bellin, V. Nylander, A. L. Gloyn, M. I. McCarthy, R. G. Kibbey, S. Krishnaswamy, B. M. Wolpin, T. Jacks, C. S. Fuchs, and M. D. Muzumdar, "Endocrine-exocrine signaling drives obesity-associated pancreatic ductal adenocarcinoma," *Cell*, vol. 181, no. 4, pp. 832–847.e18, 2020.

[12] C.-M. Hu, S.-C. Tien, P.-K. Hsieh, Y.-M. Jeng, M.-C. Chang, Y.-T. Chang, Y.-J. Chen, Y.-J. Chen, E. Y.-H. P. Lee, and W.-H. Lee, "High glucose triggers nucleotide imbalance through o-glcnacylation of key enzymes and induces kras mutation in pancreatic cells," *Cell metabolism*, vol. 29, no. 6, pp. 1334–1349.e10, 2019.

[13] J. B. Ward, S. A. Jenkins, R. Sutton, and O. H. Petersen, "Is an elevated concentration of acinar cytosolic free ionised calcium the trigger for acute pancreatitis?," *The Lancet*, vol. 346, no. 8981, pp. 1016–1019, 1995.

[14] S. D. Leach, I. M. Modlin, G. A. Scheele, and F. S. Gorelick, "Intracellular activation of digestive zymogens in rat pancreatic acini. stimulation by high doses of cholecystokinin," *The Journal of clinical investigation*, vol. 87, no. 1, pp. 362–366, 1991.

[15] H. Neurath and K. A. Walsh, "Role of proteolytic enzymes in biological regulation (a review)," *Proceedings of the National Academy of Sciences of the United States of America*, vol. 73, no. 11, pp. 3825–3832, 1976.

[16] H. Witt, W. Luck, H. C. Hennies, M. Classen, A. Kage, U. Lass, O. Landt, and M. Becker, "Mutations in the gene encoding the serine protease inhibitor, kazal type 1 are associated with chronic pancreatitis," *Nature genetics*, vol. 25, no. 2, pp. 213–216, 2000.

[17] B. Krüger, E. Albrecht, and M. M. Lerch, "The role of intracellular calcium signaling in premature protease activation and the onset of pancreatitis," *The American Journal of Pathology*, vol. 157, no. 1, pp. 43–50, 2000.

[18] M. Raraty, J. Ward, G. Erdemli, C. Vaillant, J. P. Neoptolemos, R. Sutton, and O. H. Petersen, "Calcium-dependent enzyme activation and vacuole formation in the apical granular region of pancreatic acinar cells," *Proceedings of the National Academy of Sciences of the United States of America*, vol. 97, no. 24, pp. 13126–13131, 2000.

[19] J. Mayer, B. Rau, F. Gansauge, and H. G. Beger, "Inflammatory mediators in human acute pancreatitis: clinical and pathophysiological implications," *Gut*, vol. 47, no. 4, pp. 546–552, 2000.

[20] A. H. Lundberg, J. W. Eubanks, J. Henry, O. Sabek, M. Kotb, L. Gaber, A. Norby-

Teglund, and A. O. Gaber, “Trypsin stimulates production of cytokines from peritoneal macrophages in vitro and in vivo,” *Pancreas*, vol. 21, no. 1, pp. 41–51, 2000.

[21] O. Z. Ismail and V. Bhayana, “Lipase or amylase for the diagnosis of acute pancreatitis?,” *Clinical Biochemistry*, vol. 50, no. 18, pp. 1275–1280, 2017.

[22] C. Guerra, A. J. Schuhmacher, M. Cañamero, P. J. Grippo, L. Verdaguer, L. Pérez-Gallego, P. Dubus, E. P. Sandgren, and M. Barbacid, “Chronic pancreatitis is essential for induction of pancreatic ductal adenocarcinoma by k-ras oncogenes in adult mice,” *Cancer cell*, vol. 11, no. 3, pp. 291–302, 2007.

[23] S. Raimondi, A. B. Lowenfels, A. M. Morselli-Labate, P. Maisonneuve, and R. Pezzilli, “Pancreatic cancer in chronic pancreatitis; aetiology, incidence, and early detection,” *Best practice & research. Clinical gastroenterology*, vol. 24, no. 3, pp. 349–358, 2010.

[24] J. M. Braganza, S. H. Lee, R. F. McCloy, and M. J. McMahon, “Chronic pancreatitis,” *The Lancet*, vol. 377, no. 9772, pp. 1184–1197, 2011.

[25] A. S. Quante, C. Ming, M. Rottmann, J. Engel, S. Boeck, V. Heinemann, C. B. Westphalen, and K. Strauch, “Projections of cancer incidence and cancer-related deaths in germany by 2020 and 2030,” *Cancer Medicine*, vol. 5, no. 9, pp. 2649–2656, 2016.

[26] E. Dugnani, V. Sordi, S. Pellegrini, R. Chimienti, I. Marzinotto, V. Pasquale, D. Liberati, G. Balzano, C. Doglioni, M. Reni, A. Gandolfi, M. Falconi, V. Lampasona, and L. Piemonti, “Gene expression analysis of embryonic pancreas development master regulators and terminal cell fate markers in resected pancreatic cancer: A correlation with clinical outcome,” *Pancreatology : official journal of the International Association of Pancreatology (IAP) ... [et al.]*, vol. 18, no. 8, pp. 945–953, 2018.

[27] I. T. Virlos, I. M. Papazachariou, and R. C. N. Wiliamson, “Acinar cell carcinoma of the pancreas with and without endocrine differentiation,” *HPB : the official journal of the International Hepato Pancreato Biliary Association*, vol. 4, no. 2, pp. 87–90, 2002.

[28] G. Phan, “Surgical experience with pancreatic and peripancreatic neuroendocrine tumors: review of 125 patients,” *Journal of gastrointestinal surgery : official journal of the Society for Surgery of the Alimentary Tract*, vol. 2, no. 5, pp. 473–482, 1998.

[29] D. S. Longnecker, H. Shinozuka, and A. Dekker, “Focal acinar cell dysplasia in human pancreas,” *Cancer*, vol. 45, no. 3, pp. 534–540, 1980.

[30] A. D. Singhi, E. J. Koay, S. T. Chari, and A. Maitra, “Early detection of pancreatic

cancer: Opportunities and challenges," *Gastroenterology*, vol. 156, no. 7, pp. 2024–2040, 2019.

[31] C. Shi and R. H. Hruban, "Intraductal papillary mucinous neoplasm," *Human pathology*, vol. 43, no. 1, pp. 1–16, 2012.

[32] L. D. Wood, M. B. Yurgelun, and M. G. Goggins, "Genetics of familial and sporadic pancreatic cancer," *Gastroenterology*, vol. 156, no. 7, pp. 2041–2055, 2019.

[33] C. Almoguera, D. Shibata, K. Forrester, J. Martin, N. Arnheim, and M. Perucho, "Most human carcinomas of the exocrine pancreas contain mutant c-k-ras genes," *Cell*, vol. 53, no. 4, pp. 549–554, 1988.

[34] K. de Bosscher, C. S. Hill, and F. J. Nicolás, "Molecular and functional consequences of smad4 c-terminal missense mutations in colorectal tumour cells," *The Biochemical journal*, vol. 379, no. Pt 1, pp. 209–216, 2004.

[35] R. F. Hwang, E. M. Gordon, W. F. Anderson, and D. Parekh, "Gene therapy for primary and metastatic pancreatic cancer with intraperitoneal retroviral vector bearing the wild-type p53 gene," *Surgery*, vol. 124, no. 2, pp. 143–50; discussion 150–1, 1998.

[36] C. Caldas, S. A. Hahn, L. T. da Costa, M. S. Redston, M. Schutte, A. B. Seymour, C. L. Weinstein, R. H. Hruban, C. J. Yeo, and S. E. Kern, "Frequent somatic mutations and homozygous deletions of the p16 (mts1) gene in pancreatic adenocarcinoma," *Nature genetics*, vol. 8, no. 1, pp. 27–32, 1994.

[37] K. Lekka, E. Tzitzi, A. Giakoustidis, V. Papadopoulos, and D. Giakoustidis, "Contemporary management of borderline resectable pancreatic ductal adenocarcinoma," *Annals of hepato-biliary-pancreatic surgery*, vol. 23, no. 2, pp. 97–108, 2019.

[38] V. Chin, A. Nagrial, K. Sjoquist, C. A. O'Connor, L. Chantrill, A. V. Biankin, R. J. Scholten, and D. Yip, "Chemotherapy and radiotherapy for advanced pancreatic cancer," *The Cochrane database of systematic reviews*, vol. 3, p. CD011044, 2018.

[39] D. D. von Hoff, T. Ervin, F. P. Arena, E. G. Chiorean, J. Infante, M. Moore, T. Seay, S. A. Tjulandin, W. W. Ma, M. N. Saleh, M. Harris, M. Reni, S. Dowden, D. Laheru, N. Bahary, R. K. Ramanathan, J. Tabernero, M. Hidalgo, D. Goldstein, E. van Cutsem, X. Wei, J. Iglesias, and M. F. Renschler, "Increased survival in pancreatic cancer with nab-paclitaxel plus gemcitabine," *The New England journal of medicine*, vol. 369, no. 18, pp. 1691–1703, 2013.

[40] M. J. Pishvaian, R. J. Bender, D. Halverson, L. Rahib, A. E. Hendifar, S. Mikhail, V. Chung, V. J. Picozzi, D. Sohal, E. M. Blais, K. Mason, E. E. Lyons, L. M. Matrisian, J. R. Brody, S. Madhavan, and E. F. Petricoin, "Molecular profiling of patients with pancreatic cancer: Initial results from the know your tumor initiative," *Clinical cancer research : an official journal of the American Association for Cancer Research*, vol. 24, no. 20, pp. 5018–5027, 2018.

[41] H. L. Hondow, S. B. Fox, G. Mitchell, R. J. Scott, V. Beshay, S. Q. Wong, and A. Dobrovic, "A high-throughput protocol for mutation scanning of the brca1 and brca2 genes," *BMC Cancer*, vol. 11, p. 265, 2011.

[42] H. F. Vasen, N. A. Gruis, R. R. Frants, P. A. van der Velden, E. T. Hille, and W. Bergman, "Risk of developing pancreatic cancer in families with familial atypical multiple mole melanoma associated with a specific 19 deletion of p16 (p16-leiden)," *International journal of cancer*, vol. 87, no. 6, pp. 809–811, 2000.

[43] R. L. S. Mesman, F. M. G. R. Calléja, G. Hendriks, B. Morolli, B. Misovic, P. Devilee, C. J. van Asperen, H. Vrieling, and M. P. G. Vreeswijk, "The functional impact of variants of uncertain significance in brca2," *Genetics in medicine : official journal of the American College of Medical Genetics*, vol. 21, no. 2, pp. 293–302, 2019.

[44] A. B. Lowenfels, P. Maisonneuve, E. P. DiMagno, Y. Elitsur, L. K. Gates, J. Perrault, and D. C. Whitcomb, "Hereditary pancreatitis and the risk of pancreatic cancer. international hereditary pancreatitis study group," *Journal of the National Cancer Institute*, vol. 89, no. 6, pp. 442–446, 1997.

[45] K. Tamura, J. Yu, T. Hata, M. Suenaga, K. Shindo, T. Abe, A. MacGregor-Das, M. Borges, C. L. Wolfgang, M. J. Weiss, J. He, M. I. Canto, G. M. Petersen, S. Gallinger, S. Syngal, R. E. Brand, A. Rustgi, S. H. Olson, E. Stoffel, M. L. Cote, G. Zogopoulos, J. B. Potash, F. S. Goes, R. W. McCombie, P. P. Zandi, M. Pirooznia, M. Kramer, J. Parla, J. R. Eshleman, N. J. Roberts, R. H. Hruban, A. P. Klein, and M. Goggins, "Mutations in the pancreatic secretory enzymes cpa1 and cpb1 are associated with pancreatic cancer," *Proceedings of the National Academy of Sciences of the United States of America*, vol. 115, no. 18, pp. 4767–4772, 2018.

[46] V. FENDRICH, F. ESNI, M. V. R. Garay, G. FELDMANN, N. HABBE, J. N. Jensen, Y. DOR, D. STOFFERS, J. Jensen, S. D. Leach, and A. Maitra, "Hedgehog signaling is required for effective regeneration of exocrine pancreas," *Gastroenterology*, vol. 135, no. 2, pp. 621–631, 2008.

[47] B. Kong, P. Bruns, N. A. Behler, L. Chang, A. M. Schlitter, J. Cao, A. Gewies, J. Ruland, S. Fritzsche, N. Valkovskaya, Z. Jian, I. Regel, S. Raulefs, M. Irmler, J. Beckers, H. Friess, M. Erkan, N. S. Mueller, S. Roth, T. Hackert, I. Esposito, F. J. Theis, J. Kleeff, and C. W. Michalski, "Dynamic landscape of pancreatic carcinogenesis reveals early molecular networks of malignancy," *Gut*, vol. 67, no. 1, pp. 146–156, 2018.

[48] C. M. Ardito, B. M. Grüner, K. K. Takeuchi, C. Lubeseder-Martellato, N. Teichmann, P. K. Mazur, K. E. Delgiorno, E. S. Carpenter, C. J. Halbrook, J. C. Hall, D. Pal, T. Briel, A. Herner, M. Trajkovic-Arsic, B. Sipos, G.-Y. Liou, P. Storz, N. R. Murray, D. W. Threadgill, M. Sibilia, M. K. Washington, C. L. Wilson, R. M. Schmid, E. W. Raines, H. C. Crawford, and J. T. Siveke, "Egf receptor is required for kras-induced pancreatic tumorigenesis," *Cancer cell*, vol. 22, no. 3, pp. 304–317, 2012.

[49] A. L. Means, I. M. Meszoely, K. Suzuki, Y. Miyamoto, A. K. Rustgi, R. J. Coffey, C. V. E. Wright, D. A. Stoffers, and S. D. Leach, "Pancreatic epithelial plasticity mediated by acinar cell transdifferentiation and generation of nestin-positive intermediates," *Development (Cambridge, England)*, vol. 132, no. 16, pp. 3767–3776, 2005.

[50] K. Hedegger, H. Algül, M. Lesina, A. Blutke, R. M. Schmid, M. R. Schneider, and M. Dahlhoff, "Unraveling erbb network dynamics upon betacellulin signaling in pancreatic ductal adenocarcinoma in mice," *Molecular oncology*, vol. 14, no. 8, pp. 1653–1669, 2020.

[51] C. Schneeweis, M. Wirth, D. Saur, M. Reichert, and G. Schneider, "Oncogenic kras and the egfr loop in pancreatic carcinogenesis-a connection to licensing nodes," *Small GTPases*, vol. 9, no. 6, pp. 457–464, 2018.

[52] V. Asati, D. K. Mahapatra, and S. K. Bharti, "Pi3k/akt/mtor and ras/raf/mek/erk signaling pathways inhibitors as anticancer agents: Structural and pharmacological perspectives," *European journal of medicinal chemistry*, vol. 109, pp. 314–341, 2016.

[53] Z. Yao, S. L. Painter, W. C. Fanslow, D. Ulrich, B. M. Macduff, M. K. Spriggs, and R. J. Armitage, "Human il-17: a novel cytokine derived from t cells," *Journal of immunology (Baltimore, Md. : 1950)*, vol. 155, no. 12, pp. 5483–5486, 1995.

[54] S. Vlachos, A. K. Tsaroucha, G. Konstantoudakis, F. Papachristou, G. Trypsianis, D. Schizas, G. Vaos, and C. Simopoulos, "Serum profiles of m30, m65 and interleukin-17 compared with c-reactive protein in patients with mild and severe acute pancreatitis," *Journal of hepato-biliary-pancreatic sciences*, vol. 21, no. 12, pp. 911–918, 2014.

[55] M. Leppkes, C. Maueröder, S. Hirth, S. Nowecki, C. Günther, U. Billmeier, S. Paulus, M. Biermann, L. E. Munoz, M. Hoffmann, D. Wildner, A. L. Croxford, A. Waisman, K. Mowen, D. E. Jenne, V. Krenn, J. Mayerle, M. M. Lerch, G. Schett, S. Wirtz, M. F. Neurath, M. Herrmann, and C. Becker, "Externalized decondensed neutrophil chromatin occludes pancreatic ducts and drives pancreatitis," *Nature communications*, vol. 7, p. 10973, 2016.

[56] C. Loncle, L. Bonjoch, E. Folch-Puy, M. B. Lopez-Millan, S. Lac, M. I. Molejon, E. Chuluyan, P. Cordelier, P. Dubus, G. Lomberk, R. Urrutia, D. Closa, and J. L. Iovanna, "Il17 functions through the novel reg3β-jak2-stat3 inflammatory pathway to promote the transition from chronic pancreatitis to pancreatic cancer," *Cancer research*, vol. 75, no. 22, pp. 4852–4862, 2015.

[57] T. Sakurai, D. Yoshiga, W. Ariyoshi, T. Okinaga, H. Kiyomiya, J. Furuta, I. Yoshioka, K. Tominaga, and T. Nishihara, "Essential role of mitogen-activated protein kinases in il-17a-induced mmp-3 expression in human synovial sarcoma cells," *BMC Research Notes*, vol. 9, p. 68, 2016.

[58] M. Lesina, M. U. Kurkowski, K. Ludes, S. Rose-John, M. Treiber, G. Klöppel, A. Yoshimura, W. Reindl, B. Sipos, S. Akira, R. M. Schmid, and H. Algül, "Stat3/socs3 activation by il-6 transsignaling promotes progression of pancreatic intraepithelial neoplasia and development of pancreatic cancer," *Cancer cell*, vol. 19, no. 4, pp. 456–469, 2011.

[59] C. M. Horvath, "The jak-stat pathway stimulated by interleukin 6," *Science's STKE : signal transduction knowledge environment*, vol. 2004, no. 260, p. tr9, 2004.

[60] H. Algül, M. Treiber, M. Lesina, H. Nakhai, D. Saur, F. Geisler, A. Pfeifer, S. Paxian, and R. M. Schmid, "Pancreas-specific rela/p65 truncation increases susceptibility of acini to inflammation-associated cell death following cerulein pancreatitis," *The Journal of clinical investigation*, vol. 117, no. 6, pp. 1490–1501, 2007.

[61] I. Gukovsky, A. S. Gukovskaya, T. A. Blinman, V. Zaninovic, and S. J. Pandol, "Early nf-kappab activation is associated with hormone-induced pancreatitis," *The American journal of physiology*, vol. 275, no. 6, pp. G1402–14, 1998.

[62] L. Zhu, T. Tran, J. M. Rukstalis, P. Sun, B. Damsz, and S. F. Konieczny, "Inhibition of mist1 homodimer formation induces pancreatic acinar-to-ductal metaplasia," *Molecular and Cellular Biology*, vol. 24, no. 7, pp. 2673–2681, 2004.

[63] C. L. Pin, J. M. Rukstalis, C. Johnson, and S. F. Konieczny, "The bhlh transcription factor mist1 is required to maintain exocrine pancreas cell organization and acinar cell identity," *The Journal of Cell Biology*, vol. 155, no. 4, pp. 519–530, 2001.

[64] A. S. Kowalik, C. L. Johnson, S. A. Chadi, J. Y. Weston, E. N. Fazio, and C. L. Pin, "Mice lacking the transcription factor mist1 exhibit an altered stress response and increased sensitivity to caerulein-induced pancreatitis," *American journal of physiology. Gastrointestinal and liver physiology*, vol. 292, no. 4, pp. G1123–32, 2007.

[65] G. Shi, L. Zhu, Y. Sun, R. Bettencourt, B. Damsz, R. H. Hruban, and S. F. Konieczny, "Loss of the acinar-restricted transcription factor mist1 accelerates kras-induced pancreatic intraepithelial neoplasia," *Gastroenterology*, vol. 136, no. 4, pp. 1368–1378, 2009.

[66] L. Zhu, G. Shi, C. M. Schmidt, R. H. Hruban, and S. F. Konieczny, "Acinar cells contribute to the molecular heterogeneity of pancreatic intraepithelial neoplasia," *The American Journal of Pathology*, vol. 171, no. 1, pp. 263–273, 2007.

[67] A. Papageorge, D. Lowy, and E. M. Scolnick, "Comparative biochemical properties of p21 ras molecules coded for by viral and cellular ras genes," *Journal of Virology*, vol. 44, no. 2, pp. 509–519, 1982.

[68] J. K. Voice, R. L. Klemke, A. Le, and J. H. Jackson, "Four human ras homologs differ in their abilities to activate raf-1, induce transformation, and stimulate cell motility," *The Journal of biological chemistry*, vol. 274, no. 24, pp. 17164–17170, 1999.

[69] M. P. Quinlan, S. E. Quatela, M. R. Philips, and J. Settleman, "Activated kras, but not hras or nras, may initiate tumors of endodermal origin via stem cell expansion," *Molecular and Cellular Biology*, vol. 28, no. 8, pp. 2659–2674, 2008.

[70] L. Zhang, T. Ma, J. Brozick, K. Babalola, R. Budiu, G. Tseng, and A. M. Vlad, "Effects of kras activation and pten deletion alone or in combination on muc1 biology and epithelial-to-mesenchymal transition in ovarian cancer," *Oncogene*, vol. 35, no. 38, pp. 5010–5020, 2016.

[71] M. Kanda, H. Matthaei, J. Wu, S.-M. Hong, J. Yu, M. Borges, R. H. Hruban, A. Maitra, K. Kinzler, B. Vogelstein, and M. Goggins, "Presence of somatic mutations in most early-stage pancreatic intraepithelial neoplasia," *Gastroenterology*, vol. 142, no. 4, pp. 730–733.e9, 2012.

[72] S. R. Hingorani, E. F. Petricoin, A. Maitra, V. Rajapakse, C. King, M. A. Jacobetz,

S. Ross, T. P. Conrads, T. D. Veenstra, B. A. Hitt, Y. Kawaguchi, D. Johann, L. A. Liotta, H. C. Crawford, M. E. Putt, T. Jacks, C. V. Wright, R. H. Hruban, A. M. Lowy, and D. A. Tuveson, "Preinvasive and invasive ductal pancreatic cancer and its early detection in the mouse: Cancer cell, 4(6), 437-450," 2003.

[73] A. J. Aguirre, N. Bardeesy, M. Sinha, L. Lopez, D. A. Tuveson, J. Horner, M. S. Redston, and R. A. DePinho, "Activated kras and ink4a/arf deficiency cooperate to produce metastatic pancreatic ductal adenocarcinoma," *Genes & development*, vol. 17, no. 24, pp. 3112–3126, 2003.

[74] S. Eser, N. Reiff, M. Messer, B. Seidler, K. Gottschalk, M. Dobler, M. Hieber, A. Arbeiter, S. Klein, B. Kong, C. W. Michalski, Am Schlitter, I. Esposito, A. J. Kind, L. Rad, A. E. Schnieke, M. Baccarini, Alessi, R. Rad, R. M. Schmid, G. Schneider, and D. Saur, "Selective requirement of pi3k/pdk1 signaling for kras oncogene-driven pancreatic cell plasticity and cancer," *Cancer cell*, vol. 23, no. 3, 2013.

[75] J. A. Engelman, L. Chen, X. Tan, K. Crosby, A. R. Guimaraes, R. Upadhyay, M. Maira, K. McNamara, S. A. Perera, Y. Song, L. R. Chirieac, R. Kaur, A. Lightbown, J. Simendinger, T. Li, R. F. Padera, C. García-Echeverría, R. Weissleder, U. Mahmood, L. C. Cantley, and K.-K. Wong, "Effective use of pi3k and mek inhibitors to treat mutant kras g12d and pik3ca h1047r murine lung cancers," *Nature medicine*, vol. 14, no. 12, pp. 1351–1356, 2008.

[76] J. R. Adams, K. Xu, J. C. Liu, N. M. R. Agamez, A. J. Loch, R. G. Wong, W. Wang, K. L. Wright, T. F. Lane, E. Zacksenhaus, and S. E. Egan, "Cooperation between pik3ca and p53 mutations in mouse mammary tumor formation," *Cancer research*, vol. 71, no. 7, pp. 2706–2717, 2011.

[77] K.-H. Lim and C. M. Counter, "Reduction in the requirement of oncogenic ras signaling to activation of pi3k/akt pathway during tumor maintenance," *Cancer cell*, vol. 8, no. 5, pp. 381–392, 2005.

[78] T. Asano, Y. Yao, J. Zhu, D. Li, J. L. Abbruzzese, and S. A. G. Reddy, "The pi 3-kinase/akt signaling pathway is activated due to aberrant pten expression and targets transcription factors nf-kappab and c-myc in pancreatic cancer cells," *Oncogene*, vol. 23, no. 53, pp. 8571–8580, 2004.

[79] M. Serrano, G. J. Hannon, and D. Beach, "A new regulatory motif in cell-cycle control

causing specific inhibition of cyclin d/cdk4," *Nature*, vol. 366, no. 6456, pp. 704–707, 1993.

[80] R. E. Wilentz, J. Geradts, R. Maynard, G. J. Offerhaus, M. Kang, M. Goggins, C. J. Yeo, S. E. Kern, and R. H. Hruban, "Inactivation of the p16 (ink4a) tumor-suppressor gene in pancreatic duct lesions: loss of intranuclear expression," *Cancer research*, vol. 58, no. 20, pp. 4740–4744, 1998.

[81] A. Maitra, N. V. Adsay, P. Argani, C. Iacobuzio-Donahue, A. de Marzo, J. L. Cameron, C. J. Yeo, and R. H. Hruban, "Multicomponent analysis of the pancreatic adenocarcinoma progression model using a pancreatic intraepithelial neoplasia tissue microarray," *Modern pathology : an official journal of the United States and Canadian Academy of Pathology, Inc*, vol. 16, no. 9, pp. 902–912, 2003.

[82] E. Rozenblum, M. Schutte, M. Goggins, S. A. Hahn, S. Panzer, M. Zahurak, S. N. Goodman, T. A. Sohn, R. H. Hruban, C. J. Yeo, and S. E. Kern, "Tumor-suppressive pathways in pancreatic carcinoma," *Cancer research*, vol. 57, no. 9, pp. 1731–1734, 1997.

[83] M. Schutte, R. H. Hruban, J. Geradts, R. Maynard, W. Hilgers, S. K. Rabindran, C. A. Moskaluk, S. A. Hahn, I. Schwarte-Waldhoff, W. Schmiegel, S. B. Baylin, S. E. Kern, and J. G. Herman, "Abrogation of the rb/p16 tumor-suppressive pathway in virtually all pancreatic carcinomas," *Cancer research*, vol. 57, no. 15, pp. 3126–3130, 1997.

[84] M. S. Redston, C. Caldas, A. B. Seymour, R. H. Hruban, L. da Costa, C. J. Yeo, and S. E. Kern, "p53 mutations in pancreatic carcinoma and evidence of common involvement of homocopolymer tracts in dna microdeletions," *Cancer research*, vol. 54, no. 11, pp. 3025–3033, 1994.

[85] C. Vennin, P. Mélénec, R. Rouet, M. Nobis, A. S. Cazet, K. J. Murphy, D. Herrmann, D. A. Reed, M. C. Lucas, S. C. Warren, Z. Elgundi, M. Pinese, G. Kalna, D. Roden, M. Samuel, A. Zaratzian, S. T. Grey, A. Da Silva, W. Leung, S. Mathivanan, Y. Wang, A. W. Braithwaite, D. Christ, A. Benda, A. Parkin, P. A. Phillips, J. M. Whitelock, A. J. Gill, O. J. Sansom, D. R. Croucher, B. L. Parker, M. Pajic, J. P. Morton, T. R. Cox, and P. Timpson, "Caf hierarchy driven by pancreatic cancer cell p53-status creates a pro-metastatic and chemoresistant environment via perlecan," *Nature communications*, vol. 10, no. 1, p. 3637, 2019.

[86] T. Kamijo, F. Zindy, M. F. Roussel, D. E. Quelle, J. R. Downing, R. A. Ashmun,

G. Grosveld, and C. J. Sherr, "Tumor suppression at the mouse ink4a locus mediated by the alternative reading frame product p19 arf," *Cell*, vol. 91, no. 5, pp. 649–659, 1997.

[87] S. R. Hingorani, L. Wang, A. S. Multani, C. Combs, T. B. Deramaudt, R. H. Hruban, A. K. Rustgi, S. Chang, and D. A. Tuveson, "Trp53r172h and krasg12d cooperate to promote chromosomal instability and widely metastatic pancreatic ductal adenocarcinoma in mice," *Cancer cell*, vol. 7, no. 5, pp. 469–483, 2005.

[88] M. Tada, K. Furuuchi, M. Kaneda, J. Matsumoto, M. Takahashi, A. Hirai, Y. Mitsumoto, R. D. Iggo, and T. Moriuchi, "Inactivate the remaining p53 allele or the alternate p73? preferential selection of the arg72 polymorphism in cancers with recessive p53 mutants but not transdominant mutants," *Carcinogenesis*, vol. 22, no. 3, pp. 515–517, 2001.

[89] C. Y. Lin, J. Lovén, P. B. Rahl, R. M. Paranal, C. B. Burge, J. E. Bradner, T. I. Lee, and R. A. Young, "Transcriptional amplification in tumor cells with elevated c-myc," *Cell*, vol. 151, no. 1, pp. 56–67, 2012.

[90] M. Saborowski, A. Saborowski, J. P. Morris, B. Bosbach, L. E. Dow, J. Pelletier, D. S. Klimstra, and S. W. Lowe, "A modular and flexible esc-based mouse model of pancreatic cancer," *Genes & development*, vol. 28, no. 1, pp. 85–97, 2014.

[91] X. Chen, H. Xu, P. Yuan, F. Fang, M. Huss, V. B. Vega, E. Wong, Y. L. Orlov, W. Zhang, J. Jiang, Y.-H. Loh, H. C. Yeo, Z. X. Yeo, V. Narang, K. R. Govindarajan, B. Leong, A. Shahab, Y. Ruan, G. Bourque, W.-K. Sung, N. D. Clarke, C.-L. Wei, and H.-H. Ng, "Integration of external signaling pathways with the core transcriptional network in embryonic stem cells," *Cell*, vol. 133, no. 6, pp. 1106–1117, 2008.

[92] K. I. Zeller, X. Zhao, C. W. H. Lee, K. P. Chiu, F. Yao, J. T. Yustein, H. S. Ooi, Y. L. Orlov, A. Shahab, H. C. Yong, Y. Fu, Z. Weng, V. A. Kuznetsov, W.-K. Sung, Y. Ruan, C. V. Dang, and C.-L. Wei, "Global mapping of c-myc binding sites and target gene networks in human b cells," *Proceedings of the National Academy of Sciences of the United States of America*, vol. 103, no. 47, pp. 17834–17839, 2006.

[93] S. Walz, F. Lorenzin, J. Morton, K. E. Wiese, B. von Eyss, S. Herold, L. Rycak, H. Dumay-Odelot, S. Karim, M. Bartkuhn, F. Roels, T. Wüstefeld, M. Fischer, M. Teichmann, L. Zender, C.-L. Wei, O. Sansom, E. Wolf, and M. Eilers, "Activation and repression by oncogenic myc shape tumour-specific gene expression profiles," *Nature*, vol. 511, no. 7510, pp. 483–487, 2014.

[94] A. V. Vaseva, D. R. Blake, T. S. K. Gilbert, S. Ng, G. Hostetter, S. H. Azam, I. Ozkan-Dagliyan, P. Gautam, K. L. Bryant, K. H. Pearce, L. E. Herring, H. Han, L. M. Graves, A. K. Witkiewicz, E. S. Knudsen, C. V. Pecot, N. Rashid, P. J. Houghton, K. Wennerberg, A. D. Cox, and C. J. Der, "Kras suppression-induced degradation of myc is antagonized by a mek5-erk5 compensatory mechanism," *Cancer cell*, vol. 34, no. 5, pp. 807–822.e7, 2018.

[95] D. R. Blake, A. V. Vaseva, R. G. Hodge, M. P. Kline, T. S. K. Gilbert, V. Tyagi, D. Huang, G. C. Whiten, J. E. Larson, X. Wang, K. H. Pearce, L. E. Herring, L. M. Graves, S. V. Frye, M. J. Emanuele, A. D. Cox, and C. J. Der, "Application of a myc degradation screen identifies sensitivity to cdk9 inhibitors in kras-mutant pancreatic cancer," *Science signaling*, vol. 12, no. 590, 2019.

[96] P. Sancho, E. Burgos-Ramos, A. Tavera, T. Bou Kheir, P. Jagust, M. Schoenhals, D. Barneda, K. Sellers, R. Campos-Olivas, O. Graña, C. R. Viera, M. Yuneva, B. Sainz, and C. Heeschen, "Myc/pgc-1α balance determines the metabolic phenotype and plasticity of pancreatic cancer stem cells," *Cell metabolism*, vol. 22, no. 4, pp. 590–605, 2015.

[97] K. Kojima, S. M. Vickers, N. V. Adsay, N. C. Jhala, H.-G. Kim, T. R. Schoeb, W. E. Grizzle, and C. A. Klug, "Inactivation of smad4 accelerates kras(g12d)-mediated pancreatic neoplasia," *Cancer research*, vol. 67, no. 17, pp. 8121–8130, 2007.

[98] C. Liang, J. Xu, Q. Meng, B. Zhang, J. Liu, J. Hua, Y. Zhang, S. Shi, and X. Yu, "Tgfb1-induced autophagy affects the pattern of pancreatic cancer progression in distinct ways depending on smad4 status," *Autophagy*, vol. 16, no. 3, pp. 486–500, 2020.

[99] T. Yamaguchi, S. Ikehara, Y. Akimoto, H. Nakanishi, M. Kume, K. Yamamoto, O. Ohara, and Y. Ikehara, "Tgf-β signaling promotes tube-structure-forming growth in pancreatic duct adenocarcinoma," *Scientific Reports*, vol. 9, no. 1, p. 11247, 2019.

[100] J. Liu, N. Akanuma, C. Liu, A. Naji, G. A. Halff, W. K. Washburn, L. Sun, and P. Wang, "Tgf-β1 promotes acinar to ductal metaplasia of human pancreatic acinar cells," *Scientific reports*, vol. 6, p. 30904, 2016.

[101] J. Kim, W. R. Bamlet, A. L. Oberg, K. G. Chaffee, G. Donahue, X.-J. Cao, S. Chari, B. A. Garcia, G. M. Petersen, and K. S. Zaret, "Detection of early pancreatic ductal adenocarcinoma with thrombospondin-2 and ca19-9 blood markers," *Science translational medicine*, vol. 9, no. 398, 2017.

[102] S. Ali, C. Cohen, J. V. Little, J. H. Sequeira, M. B. Mosunjac, and M. T. Siddiqui, "The utility of smad4 as a diagnostic immunohistochemical marker for pancreatic adenocarcinoma, and its expression in other solid tumors," *Diagnostic cytopathology*, vol. 35, no. 10, pp. 644–648, 2007.

[103] O. Warburg, "The metabolism of carcinoma cells," *The Journal of Cancer Research*, vol. 9, no. 1, pp. 148–163, 1925.

[104] O. Warburg, F. Wind, and E. Negelein, "The metabolism of tumors in the body," *The Journal of General Physiology*, vol. 8, no. 6, pp. 519–530, 1927.

[105] S. Dai, Y. Peng, Y. Zhu, D. Xu, F. Zhu, W. Xu, Q. Chen, X. Zhu, T. Liu, C. Hou, J. Wu, and Y. Miao, "Glycolysis promotes the progression of pancreatic cancer and reduces cancer cell sensitivity to gemcitabine," *Biomedicine & pharmacotherapy = Biomedecine & pharmacotherapie*, vol. 121, p. 109521, 2020.

[106] F. Demircioglu, J. Wang, J. Candido, A. S. H. Costa, P. Casado, B. de Luxan Delgado, L. E. Reynolds, J. Gomez-Escudero, E. Newport, V. Rajeeve, A.-M. Baker, M. Roy-Luzarraga, T. A. Graham, J. Foster, Y. Wang, J. J. Campbell, R. Singh, P. Zhang, T. J. Schall, F. R. Balkwill, J. Sosabowski, P. R. Cutillas, C. Frezza, P. Sancho, and K. Hodivala-Dilke, "Cancer associated fibroblast fak regulates malignant cell metabolism," *Nature communications*, vol. 11, no. 1, p. 1290, 2020.

[107] A. Viale, P. Pettazzoni, C. A. Lyssiotis, H. Ying, N. Sánchez, M. Marchesini, A. Carugo, T. Green, S. Seth, V. Giuliani, M. Kost-Alimova, F. Muller, S. Colla, L. Nezi, G. Genovese, A. K. Deem, A. Kapoor, W. Yao, E. Brunetto, Y. Kang, M. Yuan, J. M. Asara, Y. A. Wang, T. P. Heffernan, A. C. Kimmelman, H. Wang, J. B. Fleming, L. C. Cantley, R. A. DePinho, and G. F. Draetta, "Oncogene ablation-resistant pancreatic cancer cells depend on mitochondrial function," *Nature*, vol. 514, no. 7524, pp. 628–632, 2014.

[108] S. Valle, S. Alcalá, L. Martin-Hijano, P. Cabezas-Sáinz, D. Navarro, E. R. Muñoz, L. Yuste, K. Tiwary, K. Walter, L. Ruiz-Cañas, M. Alonso-Nocelo, J. A. Rubiolo, E. González-Arnay, C. Heeschen, L. Garcia-Bermejo, P. C. Hermann, L. Sánchez, P. Sancho, M. Á. Fernández-Moreno, and B. Sainz, "Exploiting oxidative phosphorylation to promote the stem and immunoevasive properties of pancreatic cancer stem cells," *Nature Communications*, vol. 11, no. 1, p. 5265, 2020.

[109] T. D. Pollard, W. C. Earnshaw, and J. Lippincott-Schwartz, *Cell biology: Das Original*

mit Übersetzungshilfen. Easy reading, Heidelberg: Spektrum Akad. Verl., 2. aufl. ed., 2007.

[110] H. Ying, A. C. Kimmelman, C. A. Lyssiotis, S. Hua, G. C. Chu, E. Fletcher-Sananikone, J. W. Locasale, J. Son, H. Zhang, J. L. Coloff, H. Yan, W. Wang, S. Chen, A. Viale, H. Zheng, J.-h. Paik, C. Lim, A. R. Guimaraes, E. S. Martin, J. Chang, A. F. Hezel, S. R. Perry, J. Hu, B. Gan, Y. Xiao, J. M. Asara, R. Weissleder, Y. A. Wang, L. Chin, L. C. Cantley, and R. A. DePinho, "Oncogenic kras maintains pancreatic tumors through regulation of anabolic glucose metabolism," *Cell*, vol. 149, no. 3, pp. 656–670, 2012.

[111] N. Santana-Codina, A. A. Roeth, Y. Zhang, A. Yang, O. Mashadova, J. M. Asara, X. Wang, R. T. Bronson, C. A. Lyssiotis, H. Ying, and A. C. Kimmelman, "Oncogenic kras supports pancreatic cancer through regulation of nucleotide synthesis," *Nature communications*, vol. 9, no. 1, p. 4945, 2018.

[112] K. E. Wellen, C. Lu, A. Mancuso, J. M. S. Lemons, M. Ryczko, J. W. Dennis, J. D. Rabinowitz, H. A. Coller, and C. B. Thompson, "The hexosamine biosynthetic pathway couples growth factor-induced glutamine uptake to glucose metabolism," *Genes & development*, vol. 24, no. 24, pp. 2784–2799, 2010.

[113] D. R. Wise, R. J. DeBerardinis, A. Mancuso, N. Sayed, X.-Y. Zhang, H. K. Pfeiffer, I. Nissim, E. Daikhin, M. Yudkoff, S. B. McMahon, and C. B. Thompson, "Myc regulates a transcriptional program that stimulates mitochondrial glutaminolysis and leads to glutamine addiction," *Proceedings of the National Academy of Sciences of the United States of America*, vol. 105, no. 48, pp. 18782–18787, 2008.

[114] P. Gao, I. Tchernyshyov, T.-C. Chang, Y.-S. Lee, K. Kita, T. Ochi, K. I. Zeller, A. M. de Marzo, J. E. van Eyk, J. T. Mendell, and C. V. Dang, "c-myc suppression of mir-23a/b enhances mitochondrial glutaminase expression and glutamine metabolism," *Nature*, vol. 458, no. 7239, pp. 762–765, 2009.

[115] J. Son, C. A. Lyssiotis, H. Ying, X. Wang, S. Hua, M. Ligorio, R. M. Perera, C. R. Ferrone, E. Mullarky, N. Shyh-Chang, Y. Kang, J. B. Fleming, N. Bardeesy, J. M. Asara, M. C. Haigis, R. A. DePinho, L. C. Cantley, and A. C. Kimmelman, "Glutamine supports pancreatic cancer growth through a kras-regulated metabolic pathway," *Nature*, vol. 496, no. 7443, pp. 101–105, 2013.

[116] F. Weinberg, R. Hamanaka, W. W. Wheaton, S. Weinberg, J. Joseph, M. Lopez, B. Kalyanaraman, G. M. Mutlu, G. R. S. Budinger, and N. S. Chandel, "Mitochondrial

metabolism and ros generation are essential for kras-mediated tumorigenicity," *Proceedings of the National Academy of Sciences of the United States of America*, vol. 107, no. 19, pp. 8788–8793, 2010.

[117] G.-Y. Liou, H. Döppler, K. E. Delgiorno, L. Zhang, M. Leitges, H. C. Crawford, M. P. Murphy, and P. Storz, "Mutant kras-induced mitochondrial oxidative stress in acinar cells upregulates egfr signaling to drive formation of pancreatic precancerous lesions," *Cell reports*, vol. 14, no. 10, pp. 2325–2336, 2016.

[118] C. Li, Y. Zhang, J. Liu, R. Kang, D. J. Klionsky, and D. Tang, "Mitochondrial dna stress triggers autophagy-dependent ferroptotic death," *Autophagy*, vol. 17, no. 4, pp. 948–960, 2021.

[119] E. C. Cheung, G. M. DeNicola, C. Nixon, K. Blyth, C. F. Labuschagne, D. A. Tuveson, and K. H. Vousden, "Dynamic ros control by tigar regulates the initiation and progression of pancreatic cancer," *Cancer cell*, vol. 37, no. 2, pp. 168–182.e4, 2020.

[120] M. A. Badgley, D. M. Kremer, H. C. Maurer, K. E. Delgiorno, H.-J. Lee, V. Purohit, I. R. Sagalovskiy, A. Ma, J. Kapilian, C. E. M. Firl, A. R. Decker, S. A. Sastra, C. F. Palermo, L. R. Andrade, P. Sajjakulnukit, Li Zhang, Z. P. Tolstyka, T. Hirschhorn, C. Lamb, T. Liu, W. Gu, E. S. Seeley, E. Stone, G. Georgiou, U. Manor, A. Iuga, G. M. Wahl, B. R. Stockwell, C. A. Lyssiotis, and K. P. Olive, "Cysteine depletion induces pancreatic tumor ferroptosis in mice," *Science (New York, N.Y.)*, vol. 368, no. 6486, pp. 85–89, 2020.

[121] M. Wagner, H. LUHRS, G. KLOPPEL, G. Adler, and R. SCHMID, "Malignant transformation of duct-like cells originating from acini in transforming growth factor α transgenic mice," *Gastroenterology*, vol. 115, no. 5, pp. 1254–1262, 1998.

[122] M. Wagner, F. R. Greten, C. K. Weber, S. Koschnick, T. Mattfeldt, W. Deppert, H. Kern, G. Adler, and R. M. Schmid, "A murine tumor progression model for pancreatic cancer recapitulating the genetic alterations of the human disease," *Genes & development*, vol. 15, no. 3, pp. 286–293, 2001.

[123] K. Izeradjene, C. Combs, M. Best, A. Gopinathan, A. Wagner, W. M. Grady, C.-X. Deng, R. H. Hruban, N. V. Adsay, D. A. Tuveson, and S. R. Hingorani, "Kras(g12d) and smad4/dpc4 haploinsufficiency cooperate to induce mucinous cystic neoplasms and invasive adenocarcinoma of the pancreas," *Cancer cell*, vol. 11, no. 3, pp. 229–243, 2007.

[124] N. Bardeesy, K.-H. Cheng, J. H. Berger, G. C. Chu, J. Pahler, P. Olson, A. F. Hezel, J. Horner, G. Y. Lauwers, D. Hanahan, and R. A. DePinho, "Smad4 is dispensable for normal pancreas development yet critical in progression and tumor biology of pancreas cancer," *Genes & development*, vol. 20, no. 22, pp. 3130–3146, 2006.

[125] M. Lampel and H. F. Kern, "Acute interstitial pancreatitis in the rat induced by excessive doses of a pancreatic secretagogue," *Virchows Archiv. A, Pathological anatomy and histology*, vol. 373, no. 2, pp. 97–117, 1977.

[126] S. Sato, H. A. Stark, J. Martinez, M. A. Beaven, R. T. Jensen, and J. D. Gardner, "Receptor occupation, calcium mobilization, and amylase release in pancreatic acini: effect of cck-jmv-180," *The American journal of physiology*, vol. 257, no. 2 Pt 1, pp. G202–9, 1989.

[127] E. Archer-Lahlou, C. Escrieut, P. Clerc, J. Martinez, L. Moroder, C. Logsdon, A. Kopin, C. Seva, M. Dufresne, L. Pradayrol, B. Maigret, and D. Fourmy, "Molecular mechanism underlying partial and full agonism mediated by the human cholecystokinin-1 receptor," *The Journal of biological chemistry*, vol. 280, no. 11, pp. 10664–10674, 2005.

[128] J. Mayerle, M. Sendler, and M. M. Lerch, *The pancreapedia: Secretagogue (Caerulein) induced pancreatitis in rodents*. 2013.

[129] J. H. Yu, J. W. Lim, W. Namkung, H. Kim, and K. H. Kim, "Suppression of cerulein-induced cytokine expression by antioxidants in pancreatic acinar cells," *Laboratory investigation; a journal of technical methods and pathology*, vol. 82, no. 10, pp. 1359–1368, 2002.

[130] D. I. Heath, A. Cruickshank, M. Gudgeon, A. Jehanli, A. Shenkin, and C. W. Imrie, "Role of interleukin-6 in mediating the acute phase protein response and potential as an early means of severity assessment in acute pancreatitis," *Gut*, vol. 34, no. 1, pp. 41–45, 1993.

[131] S. A. Mookerjee, A. A. Gerencser, D. G. Nicholls, and M. D. Brand, "Quantifying intracellular rates of glycolytic and oxidative atp production and consumption using extracellular flux measurements," *The Journal of biological chemistry*, vol. 292, no. 17, pp. 7189–7207, 2017.

[132] S. Mueller, T. Engleitner, R. Maresch, M. Zukowska, S. Lange, T. Kaltenbacher, B. Konukiewitz, R. Öllinger, M. Zwiebel, A. Strong, H.-Y. Yen, R. Banerjee, S. Louzada, B. Fu, B. Seidler, J. Götzfried, K. Schuck, Z. Hassan, A. Arbeiter,

N. Schönhuber, S. Klein, C. Veltkamp, M. Friedrich, L. Rad, M. Barenboim, C. Ziegenhain, J. Hess, O. M. Dovey, S. Eser, S. Parekh, F. Constantino-Casas, J. de La Rosa, M. I. Sierra, M. Fraga, J. Mayerle, G. Klöppel, J. Cadiñanos, P. Liu, G. Vassiliou, W. Weichert, K. Steiger, W. Enard, R. M. Schmid, F. Yang, K. Unger, G. Schneider, I. Varela, A. Bradley, D. Saur, and R. Rad, "Evolutionary routes and kras dosage define pancreatic cancer phenotypes," *Nature*, vol. 554, no. 7690, pp. 62–68, 2018.

[133] A. Vignoli, V. Ghini, G. Meoni, C. Licari, P. G. Takis, L. Tenori, P. Turano, and C. Luchinat, "High-throughput metabolomics by 1d nmr," *Angewandte Chemie (International ed. in English)*, vol. 58, no. 4, pp. 968–994, 2019.

[134] L. Streese, A. M. Springer, A. Deiseroth, J. Carrard, D. Infanger, C. Schmaderer, A. Schmidt-Trucksäss, T. Madl, and H. Hanssen, "Metabolic profiling links cardiovascular risk and vascular end organ damage," *Atherosclerosis*, vol. 331, pp. 45–53, 2021.

[135] D. Metzger and P. Chambon, "Site- and time-specific gene targeting in the mouse," *Methods*, vol. 24, no. 1, pp. 71–80, 2001.

[136] H. Nakhai, S. Sel, J. Favor, L. Mendoza-Torres, F. Paulsen, G. I. W. Duncker, and R. M. Schmid, "Ptf1a is essential for the differentiation of gabaergic and glycinergic amacrine cells and horizontal cells in the mouse retina," *Development (Cambridge, England)*, vol. 134, no. 6, pp. 1151–1160, 2007.

[137] L. Srinivasan, Y. Sasaki, D. P. Calado, B. Zhang, J. H. Paik, R. A. DePinho, J. L. Kutok, J. F. Kearney, K. L. Otipoby, and K. Rajewsky, "Pi3 kinase signals bcr-dependent mature b cell survival," *Cell*, vol. 139, no. 3, pp. 573–586, 2009.

[138] A. Natarajan, B. Wagner, and M. Sibilia, "The egf receptor is required for efficient liver regeneration," *Proceedings of the National Academy of Sciences of the United States of America*, vol. 104, no. 43, pp. 17081–17086, 2007.

[139] S. Sano, S. Itami, K. Takeda, M. Tarutani, Y. Yamaguchi, H. Miura, K. Yoshikawa, S. Akira, and J. Takeda, "Keratinocyte-specific ablation of stat3 exhibits impaired skin remodeling, but does not affect skin morphogenesis," *The EMBO journal*, vol. 18, no. 17, 1999.

[140] Ignacio Moreno de Alboran, Rónán C O'Hagan, Frank Gärtner, Barbara Malynn, Laurie Davidson, Robert Rickert, Klaus Rajewsky, Ronald A DePinho, and Frederick W

Alt, “Analysis of c-myc function in normal cells via conditional gene-targeted mutation,” *Immunity*, vol. 14, no. 1, pp. 45–55, 2001.

[141] J. N. Jensen, E. Cameron, M. V. R. Garay, T. W. Starkey, R. Gianani, and J. Jensen, “Recapitulation of elements of embryonic development in adult mouse pancreatic regeneration,” *Gastroenterology*, vol. 128, no. 3, pp. 728–741, 2005.

[142] J. Schindelin, I. Arganda-Carreras, E. Frise, V. Kaynig, M. Longair, T. Pietzsch, S. Preibisch, C. Rueden, S. Saalfeld, B. Schmid, J.-Y. Tinevez, D. J. White, V. Hartenstein, K. Eliceiri, P. Tomancak, and A. Cardona, “Fiji: an open-source platform for biological-image analysis,” *Nature Methods*, vol. 9, no. 7, pp. 676–682, 2012.

[143] R Core Team, *R: A Language and Environment for Statistical Computing*. R Foundation for Statistical Computing, Vienna, Austria, 2020.

[144] Bioconductor, “Deseq2,” 2020-10-17T14:44:34.000Z.

[145] Y. Miyamoto, A. Maitra, B. Ghosh, U. Zechner, P. Argani, C. A. Iacobuzio-Donahue, V. Sriuranpong, T. Iso, I. M. Meszoely, M. S. Wolfe, R. H. Hruban, D. W. Ball, R. M. Schmid, and S. D. Leach, “Notch mediates tgfα-induced changes in epithelial differentiation during pancreatic tumorigenesis,” *Cancer cell*, vol. 3, no. 6, pp. 565–576, 2003.

[146] M. L. Scotti, K. E. Smith, A. M. Butler, S. R. Calcagno, H. C. Crawford, M. Leitges, A. P. Fields, and N. R. Murray, “Protein kinase c iota regulates pancreatic acinar-to-ductal metaplasia,” *PLoS ONE*, vol. 7, no. 2, p. e30509, 2012.

[147] F. McAllister, J. M. Bailey, J. Alsina, C. J. Nirschl, R. Sharma, H. Fan, Y. Rattigan, J. C. Roeser, R. H. Lankapalli, H. Zhang, E. M. Jaffee, C. G. Drake, F. Housseau, A. Maitra, J. K. Kolls, C. L. Sears, D. M. Pardoll, and S. D. Leach, “Oncogenic kras activates a hematopoietic-to-epithelial il-17 signaling axis in preinvasive pancreatic neoplasia,” *Cancer cell*, vol. 25, no. 5, pp. 621–637, 2014.

[148] S. Kibe, K. Ohuchida, Y. Ando, S. Takesue, H. Nakayama, T. Abe, S. Endo, K. Koikawa, T. Okumura, C. Iwamoto, K. Shindo, T. Moriyama, K. Nakata, Y. Miyasaka, M. Shimamoto, T. Ohtsuka, K. Mizumoto, Y. Oda, and M. Nakamura, “Cancer-associated acinar-to-ductal metaplasia within the invasive front of pancreatic cancer contributes to local invasion,” *Cancer letters*, vol. 444, pp. 70–81, 2019.

[149] E. Del Poggetto, I.-L. Ho, C. Balestrieri, E.-Y. Yen, S. Zhang, F. Citron, R. Shah, D. Corti, G. R. Diaferia, C.-Y. Li, S. Loponte, F. Carbone, Y. Hayakawa, G. Valenti, S. Jiang, L. Sapio, H. Jiang, P. Dey, S. Gao, A. K. Deem, S. Rose-John, W. Yao,

H. Ying, A. D. Rhim, G. Genovese, T. P. Heffernan, A. Maitra, T. C. Wang, L. Wang, G. F. Draetta, A. Carugo, G. Natoli, and A. Viale, "Epithelial memory of inflammation limits tissue damage while promoting pancreatic tumorigenesis," *Science (New York, N.Y.)*, vol. 373, no. 6561, p. eabj0486, 2021.

[150] W. He, J. Wu, J. Shi, Y.-M. Huo, W. Dai, J. Geng, P. Lu, M.-W. Yang, Y. Fang, W. Wang, Z.-G. Zhang, A. Habtezion, Y.-W. Sun, and J. Xue, "Il22ra1/stat3 signaling promotes stemness and tumorigenicity in pancreatic cancer," *Cancer research*, vol. 78, no. 12, pp. 3293–3305, 2018.

[151] Z. Wen, Q. Liao, J. Zhao, Y. Hu, L. You, Z. Lu, C. Jia, Y. Wei, and Y. Zhao, "High expression of interleukin-22 and its receptor predicts poor prognosis in pancreatic ductal adenocarcinoma," *Annals of surgical oncology*, vol. 21, no. 1, pp. 125–132, 2014.

[152] S. Aggarwal, M. H. Xie, M. Maruoka, J. Foster, and A. L. Gurney, "Acinar cells of the pancreas are a target of interleukin-22," *Journal of interferon & cytokine research : the official journal of the International Society for Interferon and Cytokine Research*, vol. 21, no. 12, pp. 1047–1053, 2001.

[153] M. Perusina Lanfranca, Y. Zhang, A. Girgis, S. Kasselman, J. Lazarus, I. Kryczek, L. Delrosario, A. Rhim, L. Koneva, M. Sartor, L. Sun, C. Halbrook, H. Nathan, J. Shi, H. C. Crawford, M. Di Pasca Magliano, W. Zou, and T. L. Frankel, "Interleukin 22 signaling regulates acinar cell plasticity to promote pancreatic tumor development in mice," *Gastroenterology*, vol. 158, no. 5, pp. 1417–1432.e11, 2020.

[154] R. A. Saxton, L. T. Henneberg, M. Calafiore, L. Su, K. M. Jude, A. M. Hanash, and K. C. Garcia, "The tissue protective functions of interleukin-22 can be decoupled from pro-inflammatory actions through structure-based design," *Immunity*, vol. 54, no. 4, pp. 660–672.e9, 2021.

[155] J. Bai, J. Bai, and M. Yang, "Interleukin-22 attenuates acute pancreatitis-associated intestinal mucosa injury in mice via stat3 activation," *Gut and Liver*, vol. 15, no. 5, pp. 771–781, 2021.

[156] R. Hill, J. H. Calvopina, C. Kim, Y. Wang, D. W. Dawson, T. R. Donahue, S. Dry, and H. Wu, "Pten loss accelerates krasg12d-induced pancreatic cancer development," *Cancer research*, vol. 70, no. 18, pp. 7114–7124, 2010.

[157] B. M. Desai, J. Oliver-Krasinski, D. D. de Leon, C. Farzad, N. Hong, S. D. Leach, and D. A. Stoffers, "Preexisting pancreatic acinar cells contribute to acinar cell, but

not islet beta cell, regeneration," *The Journal of clinical investigation*, vol. 117, no. 4, pp. 971–977, 2007.

[158] N. Sphyris, C. D. Logsdon, and D. J. Harrison, "Improved retention of zymogen granules in cultured murine pancreatic acinar cells and induction of acinar-ductal transdifferentiation in vitro," *Pancreas*, vol. 30, no. 2, pp. 148–157, 2005.

[159] B. Z. Stanger, B. Stiles, G. Y. Lauwers, N. Bardeesy, M. Mendoza, Y. Wang, A. Greenwood, K.-H. Cheng, M. McLaughlin, D. Brown, R. A. DePinho, H. Wu, D. A. Melton, and Y. DOR, "Pten constrains centroacinar cell expansion and malignant transformation in the pancreas," *Cancer cell*, vol. 8, no. 3, pp. 185–195, 2005.

[160] X. Huang, X. Li, Q. Ma, Q. Xu, W. Duan, J. Lei, L. Zhang, and Z. Wu, "Chronic alcohol exposure exacerbates inflammation and triggers pancreatic acinar-to-ductal metaplasia through pi3k/akt/ikk," *International journal of molecular medicine*, vol. 35, no. 3, pp. 653–663, 2015.

[161] R. Chen, T. Hornemann, S. Štefanić, E. M. Schraner, R. Zuellig, T. Reding, E. Malagola, D. C. Henstridge, A. P. Hills, R. Graf, and S. Sonda, "Serine administration as a novel prophylactic approach to reduce the severity of acute pancreatitis during diabetes in mice," *Diabetologia*, vol. 63, no. 9, pp. 1885–1899, 2020.

[162] J. R. Infante, B. G. Somer, J. O. Park, C.-P. Li, M. E. Scheulen, S. M. Kasubhai, D.-Y. Oh, Y. Liu, S. Redhu, K. Steplewski, and N. Le, "A randomised, double-blind, placebo-controlled trial of trametinib, an oral mek inhibitor, in combination with gemcitabine for patients with untreated metastatic adenocarcinoma of the pancreas," *European journal of cancer (Oxford, England : 1990)*, vol. 50, no. 12, pp. 2072–2081, 2014.

[163] G. Shi, D. DiRenzo, C. Qu, D. Barney, D. Miley, and S. F. Konieczny, "Maintenance of acinar cell organization is critical to preventing kras-induced acinar-ductal metaplasia," *Oncogene*, vol. 32, no. 15, pp. 1950–1958, 2013.

[164] P. He, J. W. Yang, V. W. Yang, and A. B. Bialkowska, "Krüppel-like factor 5, increased in pancreatic ductal adenocarcinoma, promotes proliferation, acinar-to-ductal metaplasia, pancreatic intraepithelial neoplasia, and tumor growth in mice," *Gastroenterology*, vol. 154, no. 5, pp. 1494–1508.e13, 2018.

[165] J. Shen, D. P. Ha, G. Zhu, D. F. Rangel, A. Kobielak, P. S. Gill, S. Groshen, L. Dubeau, and A. S. Lee, "Grp78 haploinsufficiency suppresses acinar-to-ductal metaplasia, signaling, and mutant kras-driven pancreatic tumorigenesis in mice," *Proceedings of the*

National Academy of Sciences of the United States of America, vol. 114, no. 20, pp. E4020–E4029, 2017.

[166] Y. Zhao, B. Schoeps, D. Yao, Z. Zhang, K. Schuck, V. Tissen, C. Jäger, A. M. Schlitter, R. van der Kammen, C. Ludwig, J. G. D'Haese, S. Raulefs, N. Maeritz, S. Shen, X. Zou, A. Krüger, J. Kleeff, C. W. Michalski, H. Friess, M. Innocenti, and B. Kong, "mtorc1 and mtorc2 converge on the arp2/3 complex to promote krasg12d-induced acinar-to-ductal metaplasia and early pancreatic carcinogenesis," *Gastroenterology*, vol. 160, no. 5, pp. 1755–1770.e17, 2021.

[167] C. Tekin, B. P. Scicluna, S. C. Lodestijn, K. Shi, M. F. Bijlsma, and C. A. Spek, "Protease-activated receptor 1 drives and maintains ductal cell fates in the premalignant pancreas and ductal adenocarcinoma," *Molecular oncology*, vol. 15, no. 11, pp. 3091–3108, 2021.

[168] P. J. Grippo and E. P. Sandgren, "Acinar-to-ductal metaplasia accompanies c-myc-induced exocrine pancreatic cancer progression in transgenic rodents," *International journal of cancer*, vol. 131, no. 5, pp. 1243–1248, 2012.

[169] H. K. Kandikattu, M. Manohar, A. K. Verma, S. Kumar, C. S. Yadavalli, S. Upparahalli Venkateshaiah, and A. Mishra, "Macrophages-induced il-18-mediated eosinophilia promotes characteristics of pancreatic malignancy," *Life Science Alliance*, vol. 4, no. 8, 2021.

[170] D. Garcia-Carracedo, C.-C. Yu, N. Akhavan, S. A. Fine, F. Schönleben, N. Maehara, D. C. Karg, C. Xie, W. Qiu, R. L. Fine, H. E. Remotti, and G. H. Su, "Smad4 loss synergizes with tgfα overexpression in promoting pancreatic metaplasia, panin development, and fibrosis," *PLoS ONE*, vol. 10, no. 3, p. e0120851, 2015.

[171] Li Ding, G.-Y. Liou, D. M. Schmitt, P. Storz, J.-S. Zhang, and D. D. Billadeau, "Glycogen synthase kinase-3β ablation limits pancreatitis-induced acinar-to-ductal metaplasia," *The Journal of pathology*, vol. 243, no. 1, pp. 65–77, 2017.

[172] A. V. Ougolkov, M. E. Fernandez-Zapico, D. N. Savoy, R. A. Urrutia, and D. D. Billadeau, "Glycogen synthase kinase-3beta participates in nuclear factor kappab-mediated gene transcription and cell survival in pancreatic cancer cells," *Cancer research*, vol. 65, no. 6, pp. 2076–2081, 2005.

[173] S. Baumgart, N.-M. Chen, J.-S. Zhang, D. D. Billadeau, I. N. Gaisina, A. P. Kozikowski, S. K. Singh, D. Fink, P. Ströbel, C. Klindt, L. Zhang, W. R. Bamlet, A. Koenig, E. Hes-

smann, T. M. Gress, V. Ellenrieder, and A. Neesse, "Gsk-3β governs inflammation-induced nfatc2 signaling hubs to promote pancreatic cancer progression," *Molecular cancer therapeutics*, vol. 15, no. 3, pp. 491–502, 2016.

[174] Y. Zhang, M. Zoltan, E. Riquelme, H. Xu, I. Sahin, S. Castro-Pando, M. F. Montiel, K. Chang, Z. Jiang, J. Ling, S. Gupta, W. Horne, M. Pruski, H. Wang, S.-C. Sun, G. Lozano, P. Chiao, A. Maitra, S. D. Leach, J. K. Kolls, E. Vilar, T. C. Wang, J. M. Bailey, and F. McAllister, "Immune cell production of interleukin 17 induces stem cell features of pancreatic intraepithelial neoplasia cells," *Gastroenterology*, vol. 155, no. 1, pp. 210–223.e3, 2018.

[175] A. Fukuda, S. C. Wang, J. P. Morris, A. E. Folias, A. Liou, G. E. Kim, S. Akira, K. M. Boucher, M. A. Firpo, S. J. Mulvihill, and M. Hebrok, "Stat3 and mmp7 contribute to pancreatic ductal adenocarcinoma initiation and progression," *Cancer cell*, vol. 19, no. 4, pp. 441–455, 2011.

[176] K. Siddiquee, S. Zhang, W. C. Guida, M. A. Blaskovich, B. Greedy, H. R. Lawrence, M. L. R. Yip, R. Jove, M. M. McLaughlin, N. J. Lawrence, S. M. Sebti, and J. Turkson, "Selective chemical probe inhibitor of stat3, identified through structure-based virtual screening, induces antitumor activity," *Proceedings of the National Academy of Sciences of the United States of America*, vol. 104, no. 18, pp. 7391–7396, 2007.

[177] R. Gruber, R. Panayiotou, E. Nye, B. Spencer-Dene, G. Stamp, and A. Behrens, "Yap1 and taz control pancreatic cancer initiation in mice by direct up-regulation of jak-stat3 signaling," *Gastroenterology*, vol. 151, no. 3, pp. 526–539, 2016.

[178] C. Navas, I. Hernández-Porras, A. J. Schuhmacher, M. Sibilia, C. Guerra, and M. Barbacid, "Egf receptor signaling is essential for k-ras oncogene-driven pancreatic ductal adenocarcinoma," *Cancer cell*, vol. 22, no. 3, pp. 318–330, 2012.

[179] R. B. Corcoran, G. Contino, V. Deshpande, A. Tzatsos, C. Conrad, C. H. Benes, D. E. Levy, J. Settleman, J. A. Engelman, and N. Bardeesy, "Stat3 plays a critical role in kras-induced pancreatic tumorigenesis," *Cancer research*, vol. 71, no. 14, pp. 5020–5029, 2011.

[180] G.-Y. Liou, H. Döppler, B. Necela, M. Krishna, H. C. Crawford, M. Raimondo, and P. Storz, "Macrophage-secreted cytokines drive pancreatic acinar-to-ductal metaplasia through nf-κb and mmps," *The Journal of Cell Biology*, vol. 202, no. 3, pp. 563–577, 2013.

[181] K. Ebine, C. R. Chow, B. T. DeCant, H. Z. Hattaway, P. J. Grippo, K. Kumar, and H. G. Munshi, "Slug inhibits pancreatic cancer initiation by blocking kras-induced acinar-ductal metaplasia," *Scientific Reports*, vol. 6, p. 29133, 2016.

[182] D. Hanahan and R. A. Weinberg, "The hallmarks of cancer," *Cell*, vol. 100, no. 1, pp. 57–70, 2000.

[183] S. G. Voronina, S. L. Barrow, A. W. M. Simpson, O. V. Gerasimenko, G. Da Silva Xavier, G. A. Rutter, O. H. Petersen, and A. V. Tepikin, "Dynamic changes in cytosolic and mitochondrial atp levels in pancreatic acinar cells," *Gastroenterology*, vol. 138, no. 5, pp. 1976–1987, 2010.

[184] H. Bauduin, M. Colin, and J. E. Dumont, "Energy sources for protein synthesis and enzymatic secretion in rat pancreas in vitro," *Biochimica et Biophysica Acta (BBA) - Nucleic Acids and Protein Synthesis*, vol. 174, no. 2, pp. 722–733, 1969.

[185] W. Halangk, R. Matthias, L. Schild, F. Meyer, H. U. Schulz, and H. Lippert, "Effect of supramaximal cerulein stimulation on mitochondrial energy metabolism in rat pancreas," *Pancreas*, vol. 16, no. 1, pp. 88–95, 1998.

[186] A. V. Pinho, A. Mawson, A. Gill, M. Arshi, M. Warmerdam, M. Giry-Laterriere, N. Eling, T. Lie, E. Kuster, S. Camargo, A. V. Biankin, J. Wu, and I. Rooman, "Sirtuin 1 stimulates the proliferation and the expression of glycolysis genes in pancreatic neoplastic lesions," *Oncotarget*, vol. 7, no. 46, pp. 74768–74778, 2016.

[187] Y. Rong, W. Wu, X. Ni, T. Kuang, D. Jin, D. Wang, and W. Lou, "Lactate dehydrogenase a is overexpressed in pancreatic cancer and promotes the growth of pancreatic cancer cells," *Tumour biology : the journal of the International Society for Oncodevelopmental Biology and Medicine*, vol. 34, no. 3, pp. 1523–1530, 2013.

[188] M. Anderson, R. Marayati, R. Moffitt, and J. J. Yeh, "Hexokinase 2 promotes tumor growth and metastasis by regulating lactate production in pancreatic cancer," *Oncotarget*, vol. 8, no. 34, pp. 56081–56094, 2017.

[189] M. Sakashita, N. Aoyama, R. Minami, S. Maekawa, K. Kuroda, D. Shirasaka, T. Ichihara, Y. Kuroda, S. Maeda, and M. Kasuga, "Glut1 expression in t1 and t2 stage colorectal carcinomas," *European Journal of Cancer*, vol. 37, no. 2, pp. 204–209, 2001.

[190] D. Mayer, F. Klimek, A. Rempel, and P. Bannasch, "Hexokinase expression in liver preneoplasia and neoplasia," *Biochemical Society transactions*, vol. 25, no. 1, pp. 122–127, 1997.

[191] Y. S. Ahn, H. Zerban, and P. Bannasch, "Expression of glucose transporter isoforms (glut1, glut2) and activities of hexokinase, pyruvate kinase, and malic enzyme in preneoplastic and neoplastic rat renal basophilic cell lesions," *Virchows Archiv. B, Cell pathology including molecular pathology*, vol. 63, no. 6, pp. 351–357, 1993.

[192] M. Nie, K. Yao, X. Zhu, N. Chen, N. Xiao, Y. Wang, B. Peng, L. Yao, P. Li, P. Zhang, and Z. Hu, "Evolutionary metabolic landscape from preneoplasia to invasive lung adenocarcinoma," *Nature Communications*, vol. 12, no. 1, p. 6479, 2021.

[193] D. E. Biancur, J. A. Paulo, B. Małachowska, M. Del Quiles Rey, C. M. Sousa, X. Wang, A. S. W. Sohn, G. C. Chu, S. P. Gygi, J. W. Harper, W. Fendler, J. D. Mancias, and A. C. Kimmelman, "Compensatory metabolic networks in pancreatic cancers upon perturbation of glutamine metabolism," *Nature Communications*, vol. 8, p. 15965, 2017.

[194] Y. D. Bhutia and V. Ganapathy, "Glutamine transporters in mammalian cells and their functions in physiology and cancer," *Biochimica et biophysica acta*, vol. 1863, no. 10, pp. 2531–2539, 2016.

[195] L. Yang, J. C. Garcia Canaveras, Z. Chen, L. Wang, L. Liang, C. Jang, J. A. Mayr, Z. Zhang, J. M. Ghergurovich, Le Zhan, S. Joshi, Z. Hu, M. R. McReynolds, X. Su, E. White, R. J. Morscher, and J. D. Rabinowitz, "Serine catabolism feeds nadh when respiration is impaired," *Cell metabolism*, vol. 31, no. 4, pp. 809–821.e6, 2020.

[196] A. Luengo, Z. Li, D. Y. Gui, L. B. Sullivan, M. Zagorulya, B. T. Do, R. Ferreira, A. Naamati, A. Ali, C. A. Lewis, C. J. Thomas, S. Spranger, N. J. Matheson, and M. G. Vander Heiden, "Increased demand for nad+ relative to atp drives aerobic glycolysis," *Molecular cell*, vol. 81, no. 4, pp. 691–707.e6, 2021.

[197] F. F. Diehl, C. A. Lewis, B. P. Fiske, and M. G. Vander Heiden, "Cellular redox state constrains serine synthesis and nucleotide production to impact cell proliferation," *Nature metabolism*, vol. 1, no. 9, pp. 861–867, 2019.

[198] M. E. Pacold, K. R. Brimacombe, S. H. Chan, J. M. Rohde, C. A. Lewis, L. J. Y. M. Swier, R. Possemato, W. W. Chen, L. B. Sullivan, B. P. Fiske, S. Cho, E. Freinkman, K. Birsoy, M. Abu-Remaileh, Y. D. Shaul, C. M. Liu, M. Zhou, M. J. Koh, H. Chung, S. M. Davidson, A. Luengo, A. Q. Wang, X. Xu, A. Yasgar, Li Liu, G. Rai, K. D. Westover, M. G. Vander Heiden, M. Shen, N. S. Gray, M. B. Boxer, and D. M. Sabatini, "A phgdh inhibitor reveals coordination of serine synthesis and one-carbon unit fate," *Nature chemical biology*, vol. 12, no. 6, pp. 452–458, 2016.

[199] X. Gao and J. W. Locasale, "Serine metabolism links tumor suppression to the epigenetic landscape," *Cell metabolism*, vol. 24, no. 6, pp. 777–779, 2016.

[200] S. Vandekeere, C. Dubois, J. Kalucka, M. R. Sullivan, M. García-Caballero, J. Goveia, R. Chen, F. F. Diehl, L. Bar-Lev, J. Souffreau, A. Pircher, S. Kumar, S. Vinckier, Y. Hirabayashi, S. Furuya, L. Schoonjans, G. Eelen, B. Ghesquière, E. Keshet, X. Li, M. G. Vander Heiden, M. Dewerchin, and P. Carmeliet, "Serine synthesis via phgdh is essential for heme production in endothelial cells," *Cell metabolism*, vol. 28, no. 4, pp. 573–587.e13, 2018.

[201] R. S. Banh, D. E. Biancur, K. Yamamoto, A. S. W. Sohn, B. Walters, M. Kuljanin, A. Gikandi, H. Wang, J. D. Mancias, R. J. Schneider, M. E. Pacold, and A. C. Kimmelman, "Neurons release serine to support mrna translation in pancreatic cancer," *Cell*, vol. 183, no. 5, pp. 1202–1218.e25, 2020.

[202] M. Tajan, M. Hennequart, E. C. Cheung, F. Zani, A. K. Hock, N. Legrave, O. D. K. Maddocks, R. A. Ridgway, D. Athineos, A. Suárez-Bonnet, R. L. Ludwig, L. Novellasdemunt, N. Angelis, V. S. W. Li, G. Vlachogiannis, N. Valeri, N. Mainolfi, V. Suri, A. Friedman, M. Manfredi, K. Blyth, O. J. Sansom, and K. H. Vousden, "Serine synthesis pathway inhibition cooperates with dietary serine and glycine limitation for cancer therapy," *Nature Communications*, vol. 12, no. 1, p. 366, 2021.

[203] H. R. Döppler, G.-Y. Liou, and P. Storz, "Generation of hydrogen peroxide and downstream protein kinase d1 signaling is a common feature of inducers of pancreatic acinar-to-ductal metaplasia," *Antioxidants (Basel, Switzerland)*, vol. 11, no. 1, 2022.

[204] A. C. Nulton-Persson and L. I. Szweda, "Modulation of mitochondrial function by hydrogen peroxide," *The Journal of biological chemistry*, vol. 276, no. 26, pp. 23357–23361, 2001.

[205] K. Chen, W. Qian, Z. Jiang, L. Cheng, J. Li, L. Sun, C. Zhou, L. Gao, M. Lei, B. Yan, J. Cao, W. Duan, and Q. Ma, "Metformin suppresses cancer initiation and progression in genetic mouse models of pancreatic cancer," *Molecular Cancer*, vol. 16, no. 1, p. 131, 2017.

[206] A. Coulibaly, S. Y. Velásquez, N. Kassner, J. Schulte, M. V. Barbarossa, and H. A. Lindner, "Stat3 governs the hif-1α response in il-15 primed human nk cells," *Scientific Reports*, vol. 11, no. 1, p. 7023, 2021.

[207] A. Carrer, S. Trefely, S. Zhao, S. L. Campbell, R. J. Norgard, K. C. Schultz, S. Sidoli,

J. L. D. Parris, H. C. Affronti, S. Sivanand, S. Egolf, Y. Sela, M. Trizzino, A. Gardini, B. A. Garcia, N. W. Snyder, B. Z. Stanger, and K. E. Wellen, "Acetyl-coa metabolism supports multistep pancreatic tumorigenesis," *Cancer discovery*, vol. 9, no. 3, pp. 416–435, 2019.

[208] T. Latham, L. Mackay, D. Sproul, M. Karim, J. Culley, D. J. Harrison, L. Hayward, P. Langridge-Smith, N. Gilbert, and B. H. Ramsahoye, "Lactate, a product of glycolytic metabolism, inhibits histone deacetylase activity and promotes changes in gene expression," *Nucleic Acids Research*, vol. 40, no. 11, pp. 4794–4803, 2012.

[209] M. A. Selak, S. M. Armour, E. D. MacKenzie, H. Boulahbel, D. G. Watson, K. D. Mansfield, Y. Pan, M. C. Simon, C. B. Thompson, and E. Gottlieb, "Succinate links tca cycle dysfunction to oncogenesis by inhibiting hif-alpha prolyl hydroxylase," *Cancer cell*, vol. 7, no. 1, pp. 77–85, 2005.

[210] W.-H. Tong, C. Sourbier, G. Kovtunovych, S. Y. Jeong, M. Vira, M. Ghosh, V. V. Romero, R. Sougrat, S. Vaulont, B. Viollet, Y.-S. Kim, S. Lee, J. Trepel, R. Srinivasan, G. Bratslavsky, Y. Yang, W. M. Linehan, and T. A. Rouault, "The glycolytic shift in fumarate-hydratase-deficient kidney cancer lowers ampk levels, increases anabolic propensities and lowers cellular iron levels," *Cancer cell*, vol. 20, no. 3, pp. 315–327, 2011.

[211] P. Esteves, C. Pecqueur, C. Ransy, C. Esnous, V. Lenoir, F. Bouillaud, A.-L. Bulteau, A. Lombès, C. Prip-Buus, D. Ricquier, and M.-C. Alves-Guerra, "Mitochondrial retrograde signaling mediated by ucp2 inhibits cancer cell proliferation and tumorigenesis," *Cancer research*, vol. 74, no. 14, pp. 3971–3982, 2014.

[212] P. C. McDonald, S. C. Chafe, W. S. Brown, S. Saberi, M. Swayampakula, G. Venkateswaran, O. Nemirovsky, J. A. Gillespie, J. M. Karasinska, S. E. Kalloger, C. T. Supuran, D. F. Schaeffer, A. Bashashati, S. P. Shah, J. T. Topham, D. T. Yapp, J. Li, D. J. Renouf, B. Z. Stanger, and S. Dedhar, "Regulation of ph by carbonic anhydrase 9 mediates survival of pancreatic cancer cells with activated kras in response to hypoxia," *Gastroenterology*, vol. 157, no. 3, pp. 823–837, 2019.

[213] M. Maruggi, F. I. Layng, R. Lemos, G. Garcia, B. P. James, M. Sevilla, F. Soldevilla, B. J. Baaten, P. R. de Jong, M. Y. Koh, and G. Powis, "Absence of hif1a leads to glycogen accumulation and an inflammatory response that enables pancreatic tumor growth," *Cancer research*, vol. 79, no. 22, pp. 5839–5848, 2019.

[214] M.-J. Park, S. Iyer, X. Xue, J. Bragazzi Cunha, S. Gu, D. Moons, S. W. Pipe, J. A. Williams, D. M. Simeone, Y. M. Shah, and M. B. Omary, "Hif1-alpha regulates acinar cell function and response to injury in mouse pancreas," *Gastroenterology*, vol. 154, no. 6, pp. 1630–1634.e3, 2018.

[215] K. E. Lee, M. Spata, L. J. Bayne, E. L. Buza, A. C. Durham, D. Allman, R. H. Vonderheide, and M. C. Simon, "Hif1a deletion reveals pro-neoplastic function of b cells in pancreatic neoplasia," *Cancer discovery*, vol. 6, no. 3, pp. 256–269, 2016.

[216] L. Antonucci, J. B. Fagman, J. Y. Kim, J. Todoric, I. Gukovsky, M. Mackey, M. H. Ellisman, and M. Karin, "Basal autophagy maintains pancreatic acinar cell homeostasis and protein synthesis and prevents er stress," *Proceedings of the National Academy of Sciences of the United States of America*, vol. 112, no. 45, pp. E6166–74, 2015.

[217] L. Gao, Z. Xu, Z. Huang, Y. Tang, D. Yang, J. Huang, L. He, M. Liu, Z. Chen, and Y. Teng, "Cpi-613 rewires lipid metabolism to enhance pancreatic cancer apoptosis via the ampk-acc signaling," *Journal of experimental & clinical cancer research : CR*, vol. 39, no. 1, p. 73, 2020.

[218] F. Al-Hashem, M. Abd Ellatif, A. M. ShamsEldeen, S. S. Kamar, B. Al-Ani, and M. A. Haidara, "Vitamin e protects against the modulation of tnf-α-ampk axis and inhibits pancreas injury in a rat model of l-arginine-induced acute necrotising pancreatitis," *Archives of physiology and biochemistry*, pp. 1–9, 2020.

[219] Q. Xu, N. Wu, X. Li, C. Guo, C. Li, B. Jiang, H. Wang, and D. Shi, "Inhibition of ptp1b blocks pancreatic cancer progression by targeting the pkm2/ampk/mtoc1 pathway," *Cell Death & Disease*, vol. 10, no. 12, p. 874, 2019.

[220] Y.-C. Yang, M.-H. Chien, H.-Y. Liu, Y.-C. Chang, C.-K. Chen, W.-J. Lee, T.-C. Kuo, M. Hsiao, K.-T. Hua, and T.-Y. Cheng, "Nuclear translocation of pkm2/ampk complex sustains cancer stem cell populations under glucose restriction stress," *Cancer letters*, vol. 421, pp. 28–40, 2018.

[221] S. Jia, X. Xu, S. Zhou, Y. Chen, G. Ding, and L. Cao, "Fisetin induces autophagy in pancreatic cancer cells via endoplasmic reticulum stress- and mitochondrial stress-dependent pathways," *Cell Death & Disease*, vol. 10, no. 2, p. 142, 2019.

[222] C. Xu, Y. Wang, Q. Tu, Z. Zhang, M. Chen, J. Mwangi, Y. Li, Y. Jin, X. Zhao, and R. Lai, "Targeting surface nucleolin induces autophagy-dependent cell death in pancreatic cancer via ampk activation," *Oncogene*, vol. 38, no. 11, pp. 1832–1844, 2019.

[223] R. Wang and W. Hu, "Asprosin promotes β-cell apoptosis by inhibiting the autophagy of β-cell via ampk-mtor pathway," *Journal of cellular physiology*, vol. 236, no. 1, pp. 215–221, 2021.

[224] M. O. Yuneva, T. W. M. Fan, T. D. Allen, R. M. Higashi, D. V. Ferraris, T. Tsukamoto, J. M. Matés, F. J. Alonso, C. Wang, Y. Seo, X. Chen, and J. M. Bishop, "The metabolic profile of tumors depends on both the responsible genetic lesion and tissue type," *Cell metabolism*, vol. 15, no. 2, pp. 157–170, 2012.

[225] Y. Xiang, Z. E. Stine, J. Xia, Y. Lu, R. S. O'Connor, B. J. Altman, A. L. Hsieh, A. M. Gouw, A. G. Thomas, P. Gao, L. Sun, L. Song, B. Yan, B. S. Slusher, J. Zhuo, L. L. Ooi, C. G. L. Lee, A. Mancuso, A. S. McCallion, A. Le, M. C. Milone, S. Rayport, D. W. Felsher, and C. V. Dang, "Targeted inhibition of tumor-specific glutaminase diminishes cell-autonomous tumorigenesis," *The Journal of clinical investigation*, vol. 125, no. 6, pp. 2293–2306, 2015.

[226] E. H. Shroff, L. S. Eberlin, V. M. Dang, A. M. Gouw, M. Gabay, S. J. Adam, D. I. Bellovin, P. T. Tran, W. M. Philbrick, A. Garcia-Ocana, S. C. Casey, Y. Li, C. V. Dang, R. N. Zare, and D. W. Felsher, "Myc oncogene overexpression drives renal cell carcinoma in a mouse model through glutamine metabolism," *Proceedings of the National Academy of Sciences of the United States of America*, vol. 112, no. 21, pp. 6539–6544, 2015.

[227] P. Dey, J. Li, J. Zhang, S. Chaurasiya, A. Strom, H. Wang, W.-T. Liao, F. Cavallaro, P. Denz, V. Bernard, E.-Y. Yen, G. Genovese, P. Gulhati, J. Liu, D. Chakravarti, P. Deng, T. Zhang, F. Carbone, Q. Chang, H. Ying, X. Shang, D. J. Spring, B. Ghosh, N. Putluri, A. Maitra, Y. A. Wang, and R. A. DePinho, "Oncogenic kras-driven metabolic reprogramming in pancreatic cancer cells utilizes cytokines from the tumor microenvironment," *Cancer discovery*, vol. 10, no. 4, pp. 608–625, 2020.

[228] F. Cinti, R. Bouchi, J. Y. Kim-Muller, Y. Ohmura, P. R. Sandoval, M. Masini, L. Marselli, M. Suleiman, L. E. Ratner, P. Marchetti, and D. Accili, "Evidence of β-cell dedifferentiation in human type 2 diabetes," *The Journal of clinical endocrinology and metabolism*, vol. 101, no. 3, pp. 1044–1054, 2016.

[229] M. Kobayashi, O. Kikuchi, T. Sasaki, H.-J. Kim, H. Yokota-Hashimoto, Y.-S. Lee, K. Amano, T. Kitazumi, V. Y. Susanti, Y. I. Kitamura, and T. Kitamura, "Foxo1 as a double-edged sword in the pancreas: analysis of pancreas- and β-cell-specific foxo1

knockout mice," *American journal of physiology. Endocrinology and metabolism*, vol. 302, no. 5, pp. E603–13, 2012.

[230] O. Kikuchi, M. Kobayashi, K. Amano, T. Sasaki, T. Kitazumi, H.-J. Kim, Y.-S. Lee, H. Yokota-Hashimoto, Y.-I. Kitamura, and T. Kitamura, "Foxo1 gain of function in the pancreas causes glucose intolerance, polycystic pancreas, and islet hypervascularization," *PLoS ONE*, vol. 7, no. 2, p. e32249, 2012.

[231] T. Miyatsuka, H. Kaneto, T. Shiraiwa, T.-a. Matsuoka, K. Yamamoto, K. Kato, Y. Nakamura, S. Akira, K. Takeda, Y. Kajimoto, Y. Yamasaki, E. P. Sandgren, Y. Kawaguchi, C. V. E. Wright, and Y. Fujitani, "Persistent expression of pdx-1 in the pancreas causes acinar-to-ductal metaplasia through stat3 activation," *Genes & development*, vol. 20, no. 11, pp. 1435–1440, 2006.

[232] W. Al-Zoughbi, S. Schauer, M. Pichler, and G. Hoefler, "Early loss of forkhead transcription factor, o subgroup, member 1 protein in the development of pancreatic ductal adenocarcinoma," *Pathobiology*, vol. 85, no. 5-6, pp. 342–347, 2018.

[233] W. Song, Q. Li, L. Wang, W. Huang, and L. Wang, "Foxo1-negative cells are cancer stem-like cells in pancreatic ductal adenocarcinoma," *Scientific Reports*, vol. 5, p. 10081, 2015.

[234] J. Ling, F. Wang, C. Liu, X. Dong, Y. Xue, X. Jia, W. Song, and Q. Li, "Foxo1-regulated lncrna linc01197 inhibits pancreatic adenocarcinoma cell proliferation by restraining wnt/β-catenin signaling," *Journal of experimental & clinical cancer research : CR*, vol. 38, no. 1, p. 179, 2019.

[235] C. Cantó, Z. Gerhart-Hines, J. N. Feige, M. Lagouge, L. Noriega, J. C. Milne, P. J. Elliott, P. Puigserver, and J. Auwerx, "Ampk regulates energy expenditure by modulating nad+ metabolism and sirt1 activity," *Nature*, vol. 458, no. 7241, pp. 1056–1060, 2009.

[236] K. Wilhelm, K. Happel, G. Eelen, S. Schoors, M. F. Oellerich, R. Lim, B. Zimmermann, I. M. Aspalter, C. A. Franco, T. Boettger, T. Braun, M. Fruttiger, K. Rajewsky, C. Keller, J. C. Brüning, H. Gerhardt, P. Carmeliet, and M. Potente, "Foxo1 couples metabolic activity and growth state in the vascular endothelium," *Nature*, vol. 529, no. 7585, pp. 216–220, 2016.

[237] J. Altomonte, A. Richter, S. Harbaran, J. Suriawinata, J. Nakae, S. N. Thung, M. Meseck, D. Accili, and H. Dong, "Inhibition of foxo1 function is associated with im-

proved fasting glycemia in diabetic mice," *American journal of physiology. Endocrinology and metabolism*, vol. 285, no. 4, pp. E718–28, 2003.

[238] F. Langlet, R. A. Haeusler, D. Lindén, E. Ericson, T. Norris, A. Johansson, J. R. Cook, K. Aizawa, L. Wang, C. Buettner, and D. Accili, "Selective inhibition of foxo1 activator/repressor balance modulates hepatic glucose handling," *Cell*, vol. 171, no. 4, pp. 824–835.e18, 2017.

Acknowledgements

First of all, I would like to thank my first supervisor **Prof Roland M Schmid** for giving me the opportunity to work in his group. Thank you for a lot of support, guidance and enthusiasm throughout these years. It was your lab where I learned most of my scientific skills and the importance of both passion and focus in research.

I also want to thank my second supervisor **Prof Angelika Schnieke**. Thank you for taking over the second supervision and critically following my data during our meetings. In addition, I would like to thank you for giving me the chance of trying to transfer the isolation skills I gained from mice to your pig model.

Henrik Einwächter, I have to thank for being my mentor and supporting me whenever it was needed. You trusted me and my work very early so that I became an independent researcher. At the same time, there was always room for critical discussions about my own results and those from literature. And, thank you for making my data evaluation skills R-ational and EXCELent.

A big thank you goes out to our former Postdoc **Mariana Rickmann**. I started in this lab having no idea about the pancreas, mouse work and all our genotypes and you took the time to explain to me whatever I asked. The foundation of what I learned in this lab was built by you.

Thank you, **Min-Chun Chen**, for joining the acinar project and continuing it. I had a good time sharing the project and my previous results with you. I'm sure that the loose ends I'm leaving behind are in good hands.

To my fellow PhD collegues **Sankaranarayanan Ramasubramanian, Chao Wu, Bailing Li, Leeanne Mundle, Judit Desztics, Ali Altaee**: We all faced and shared times of fun, motivation, depression and devastation. The helpful team spirit and good atmosphere made me enjoy the good times and helped me during the bad ones.

Melanie Höcker, I owe thank to you for having my back if it came to paper work and

documentation in regards to mouse work. Thanks for taking turns in treating mice in the night! Additionally, there was always time to share complains, sorrows and successes with you.

The team of technicians, **Anja Motz, Mathilde Neuhofer, Anke Bettenbrock**, did a great job in organising the lab and providing helping hands. In addition, I got a lot of help with my mice in times of holidays or a broken wrist, and quite some FFPE blocks have neither been cut nor stained by myself.

Andrea Stroppiana, thank you for a lot of explanations about documentation in the mouse room. Also, I enjoyed our exchange and discussions about Terry Pratchett.

Sophie Levantovsky was the first intern that I was supervising on my own. Thank you for this good experience. You managed to acquire a lot of data within this short time and provided me with a good start of a new aspect of my thesis. Additionally, your feedback helped me to improve my supervision skills.

From the neighbouring group (AG Quante), **Jonas Ingermann** was always there as a constant support. Ranging from scientific advice and discussions, via politics and mockery to fooling around I knew where I could find someone to talk to. Thank you for having a critical look at my data and listening to my thoughts, ideas and hypotheses.

The Quante Ladies, **Akanksha Anand, Theresa Baumeister**, were always there to share experience, insides, ideas, data, books and recepies. Thank you for the good time, the uncounted meetings on the roof terrace or in cell culture and the kind words during hard times.

From AG Algül, **Kivanç Görgülü** definitely deserves gratefulness. Being termed once the walking PubMed, he was always happy to help with literature and discuss data and hypotheses. Additionally, it was fun to joke around with you.

Besides random meetings in the mouse room, **Ludwig Kübelsbeck** helped me in balancing myself. Whenever I felt too good and everything was running too perfectly fine I could be

certain of a grounding but kindly delivered defeat at the kicker table.

Lina Staufer, thank you for a lot of mental and moral support. I knew where I could find someone to discuss data and developments within and beyond the scope of thesis.

Thanks to all the people from the **Gastrolabor II** for creating a stimulating and friendly environment where I always felt welcome. I really enjoyed the common lunches in the kitchen as well as all the small and big celebrations.

Thank you **Leeanne**, **Min-Chun**, **Akanksha**, **Kivanç**, **Alex** and **Burkard** for proofreading parts of the thesis!

The best cooperation partner that I worked with was **Werner Schmitz** who did the ^{13}C measurements. Bringing a lot of enthusiasm and tons of knowledge made me leave every meeting completely overwhelmed with information but in a good mood.

Svenja Lier became my personal MYCologist supporting me with inhibitors, antibodies and tons of ideas concerning the role of MYC in ADM.

Thanks to my parents **Karin** and **Burkard** and my brother **Steffen** for all the mental support, all the good words and the common joy when things worked out.

And finally, a big thank you to my beloved wife **Alex**. You have been enduring all my trains of thoughts, my good and my stupid ideas, my complaints and so much more. And still, you supported me and helped me to find my way through ImagesJ macros. You had my back when too many things piled up and you cheered me up when Murphy's law was the only constant in the lab. Thank you for reminding me every now and then of the life outside of the lab.